ANL-7561

Argonne National Laboratory

REACTOR DEVELOPMENT PROGRAM PROGRESS REPORT

March 1969

The facilities of Argonne National Laboratory are owned by the United States Government. Under the terms of a contract (W-31-109-Eng-38) between the U. S. Atomic Energy Commission, Argonne Universities Association and The University of Chicago, the University employs the staff and operates the Laboratory in accordance with policies and programs formulated, approved and reviewed by the Association.

MEMBERS OF ARGONNE UNIVERSITIES ASSOCIATION

The University of Arizona
Carnegie-Mellon University
Case Western Reserve University
The University of Chicago
University of Cincinnati
Illinois Institute of Technology
University of Illinois
Indiana University
Iowa State University
The University of Iowa
Kansas State University
The University of Kansas
Loyola University
Marquette University
Michigan State University
The University of Michigan
University of Minnesota
University of Missouri
Northwestern University
University of Notre Dame
The Ohio State University
Ohio University
The Pennsylvania State University
Purdue University
Saint Louis University
Southern Illinois University
University of Texas
Washington University
Wayne State University
The University of Wisconsin

Printed in the United States of America
Available from
Clearinghouse for Federal Scientific and Technical Information
National Bureau of Standards, U. S. Department of Commerce
Springfield, Virginia 22151
Price: Printed Copy $3.00; Microfiche $0.65

ANL-7561
Reactor Technology

ARGONNE NATIONAL LABORATORY
9700 South Cass Avenue
Argonne, Illinois 60439

REACTOR DEVELOPMENT PROGRAM PROGRESS REPORT

March 1969

Robert B. Duffield, Laboratory Director
Stephen Lawroski, Associate Laboratory Director

Division	Director
Chemical Engineering	R. C. Vogel
EBR-II Project	M. Levenson
Metallurgy	M. V. Nevitt
Reactor Engineering	L. J. Koch
Reactor Physics	R. Avery

Report coordinated by
A. Glassner and A. D. Rossin

Issued April 22, 1969

FOREWORD

The Reactor Development Program Progress Report, issued monthly,* is intended to be a means of reporting those items of significant technical progress which have occurred in both the specific reactor projects and the general engineering research and development programs. The report is organized in accordance with budget activities in a way which, it is hoped, gives the clearest, most logical overall view of progress. Since the intent is to report only items of significant progress, not all activities are reported each month. In order to issue this report as soon as possible after the end of the month editorial work must necessarily be limited. Also, since this is an informal progress report, the results and data presented should be understood to be preliminary and subject to change unless otherwise stated.

The issuance of these reports is not intended to constitute publication in any sense of the word. Final results either will be submitted for publication in regular professional journals or will be published in the form of ANL topical reports.

The last six reports issued in this series are:

September 1968	ANL-7500
October 1968	ANL-7513
November 1968	ANL-7518
December 1968	ANL-7527
January 1969	ANL-7548
February 1969	ANL-7553

* The April 1969 Reactor Development Program Progress Report is to be combined with the May 1969 report. This material will appear as one volume and will be issued at the scheduled time for release of the May 1969 report.

REACTOR DEVELOPMENT PROGRAM

Highlights of Project Activities for March 1969

EBR-II

The reactor was started on March 3, for Run 33A, after having been shut down since January 2 for scheduled modifications and maintenance. No abnormal ^{133}Xe or ^{135}Xe activity levels were observed in the cover gas. Between startup and March 15, the reactor was operated for 458 MWd, raising its cumulative operational total to 23,223 MWd. Four experimental subassemblies containing experiments which had not been previously irradiated were loaded into the reactor grid before Run 33A.

All hot-line production activities in the argon cell of the FCF have been phased out. Preparation of ingots of 95 w/o U (64 w/o ^{235}U)-5 w/o fissium for Mark-II fuel alloy was started in the alloy-preparation furnace of the FCF cold line. The equipment in the cold line has been modified for fabrication and inspection of Mark-II fuel elements. The acceptance rate of vendor-produced Mark-IA driver-fuel elements continues to be greater than 95%. Over 5000 of these elements were received between February 15 and March 15, bringing the total received through March 15 to 11,736.

Under a new task, several concepts of a facility for testing and evaluating instruments in the core of EBR-II are being developed and studied. As now planned, the facility would occupy a thimble in one of the control-rod positions of the reactor.

ZPR-3

Measurements with Assembly I of the FTR Resumed Phase B Critical Experiments continue. Small-sample central worths of U-235, U-238, Pu-239, B-10, Ta, Fe, Cr, Ni, Na, and Li-6 were obtained, and radial reaction-rate traverses with B-10, U-238, and Pu-239 were made. A second determination of the temperature coefficient of this reactor (Assembly 56B) was made and, combined with an earlier measurement, gave a value of $-(2.41 \pm 0.03)$ Ih/°C. Core and blanket drawers were exchanged at several locations near the core edge to evaluate the worth of core drawers relative to reflector material at these locations. Even- and odd-numbered drawers, loaded differently, showed different specific fissile-mass worths at equal radii; similar evidence of the two-drawer cell structure appears in the periodicity shown in U-238 and B-10 radial reaction-rate traverses in this assembly.

ZPR-6 and -9

Acceptance testing of the new duct work and filter plenum chambers for the reactor cell-exhaust systems and confinement shell-exhaust system is in progress. Measurement of leakage rate of the steel confinement shell both under positive and negative pressures have been started. Upon the completion of these measurements, testing of the fans and the emergency steam turbine and air balancing of the new air-exhaust systems will complete the modifications required to adapt these facilities to plutonium operation.

The annual interlock checkout of the reactor control circuitry for both reactors is in progress. It is anticipated that the reactors will be ready for loading about the end of April. The operating instructions for the facilities have been submitted to AEC-CH for review.

The new fuel-storage vault has been accepted by the Laboratory.

ZPPR

Approval for the operation of ZPPR was received on March 27, 1969 and operation began on that date.

TABLE OF CONTENTS

TABLE OF CONTENTS

TABLE OF CONTENTS

I. LIQUID METAL FAST BREEDER REACTORS--CIVILIAN

A. Fuel Development--LMFBR

1. Oxide

a. Fuel Studies

(i) Fuel Element Performance (L. A. Neimark, W. F. Murphy, and E. J. Petkus)

Last Reported: ANL-7553, pp. 1-2 (Feb 1969).

(a) Void Deployment (Group O-3). Three fuel elements have been vibratorily compacted with angular Dynapak fuel particles, but difficulties have been experienced in loading the fourth element with the mixed-oxide fuel. This element is to have a smear density of 79 ± 1%. Bridging in the fuel column is believed to be responsible for the slow feeding of the fine fuel particles.

The specifications of the irradiation capsules for Group O-3 fuel elements have been prepared. Tubing and material for the end plugs are on hand, and fabrication of capsule parts will start as soon as the specifications are approved.

(b) Analysis of Fuel-element Swelling (Groups O-4 and O-5). The objectives and test matrices of capsules for Groups O-4 and O-5 were reviewed with AEC-RDT personnel in a meeting at ANL on February 25, 1969. The principal objective of the fuel-element performance analysis that forms the basis for these irradiations is to determine how fuel-element dimensional changes are controlled by the swelling and yielding of the cladding. Such yielding is due to the combined stresses that result from released fission gas, fuel swelling, and mechanical interactions between the fuel and cladding. The variables in these experiments are the plenum-to-fuel ratio as well as the smear density and the oxygen-to-metal ratio of the fuel. The test matrix and the design of the experiment are being refined by analysis of fuel-element performance by means of the SWELL-2 behavior code. The results will, in turn, be used to verify and refine the behavior models for fuel and cladding used in the code.

(ii) Fuel Swelling Studies (L. A. Neimark and L. C. Michels)

Not reported previously.

A technique for thinning oxide specimens for transmission electron microscopy has been developed. This technique will be employed

to investigate the behavior of fission-gas bubbles in specimens of $(U,Pu)O_2$ obtained from EBR-II fuel-element irradiation tests and in specimens of oxides from future irradiations.

The technique is a modified version of that reported by Manley.* In the modified version small pieces of UO_2 (approximately 0.060 in. in diameter by 0.020 in. thick) are mounted in an epoxy resin by using a method similar to that previously described for mounting carbide specimens (see Progress Report for December 1968, ANL-7527, p. 99). The composite disk-shape specimen (approximately 0.125 in. in diameter) is ground on both sides to a thickness of about 0.005 in. The central region of the UO_2 is then prethinned on both sides of the specimen by using a jet of airborne abrasive until perforation occurs. A chemical polish at a temperature of 120°C is used for final thinning and for removing any disturbed material. Satisfactory sections of UO_2 have been prepared with this technique. Minor difficulties involving differential thermal expansion between the UO_2 specimen and the epoxy as well as some degree of chemical attack and thermal decomposition of the epoxy during the chemical-polishing step have been encountered. An attempt will be made to eliminate these minor difficulties while work to perfect the technique continues.

B. Physics Development--LMFBR

1. Theoretical Reactor Physics

a. Fast Critical Experiments--Theoretical Support (R. B. Nicholson)

Last Reported: ANL-7553, p. 7 (Feb 1969).

The integration scheme to determine the resonance J-function in the present MC^2 code involves two 16-point Gauss-Legendre quadratures over the ranges 0 to $20/\xi$ and $20/\xi$ to $200/\xi$; an asymptotic formula must then be used to evaluate the remainder in the interval $200/\xi$ to ∞. Although the accuracy is satisfactory, we have found that comparable and also satisfactory accuracy can be obtained with two four-point Gauss-Legendre quadratures and no remainder. This is accomplished by choosing a more nearly optimum upper limit for the first integral and making the transformation $x = 1/y$ in the second integral, which then easily covers the complete range to $x = \infty$ with no remainder. The limit of integration is chosen to be the greater of the two formulas

$$x_1 = \sqrt{(1+\beta)/\beta}$$

*Manley, A. J., J. Nucl. Mater. 15, 143-145 (1965); 27, 216-224 (1968).

and

$$x_1 = (2/\xi)[\ln(1+0.66\xi/\beta) + 1.9]^{1/2}.$$

This procedure reduces the computer time for calculation of the J-function by nearly a factor of four.

2. Experimental Reactor Physics

a. Fast Critical Experiments--Experimental Support (Idaho)

(i) Neutron Spectrometry (W. G. Davey)

Last Reported: ANL-7548, p. 12 (Jan 1969).

(a) High Count-rate Electronics. The high count-rate electronics system for the proton-recoil spectrometer has been completed and is being tested. A block diagram of the system is shown in Fig. I.B.1.

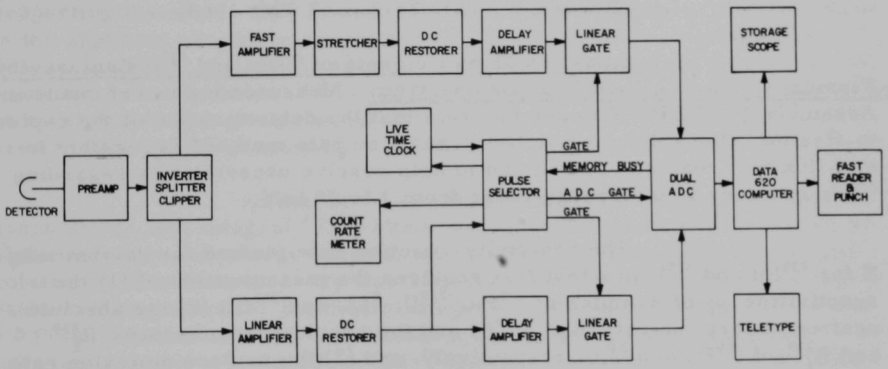

Fig. I.B.1. Block Diagram for High Count-rate Electronics System

Two essential features are the charge-sensitive preamplifier* which is matched to a pole-zero-compensated linear amplifier and DC restorer for overload protection,** and the pulse selector which inspects the output pulses of the linear amplifier and rejects pileup events, overload pulses, and pulses that occur when the baseline is displaced.

The linear gates are controlled by the pulse selector and operate in conjunction with the ADC coincidence gate. These gates

*Larson, J. M., A Wide-band Charge-sensitive Preamplifier for Proton-recoil Proportional Counting, ANL-7517.

**Larson, J. M., and Powell, J. E., Spectrum Distortion from Amplifier Overloads in Proton-recoil Proportional Counting, to be published in Nucl. Instruments and Methods.

open only after the pulse selector has determined that a pulse is free from distortion. Delaying amplifiers precede the linear gates to provide coincidence timing.

The live-time clock is controlled by the pulse selector and ADC computer busy signal, and remains off both for the duration of a distorted pulse and while the ADC's and computer are busy converting and storing an undistorted pulse.

The system has been tested in ZPR-3 at maximum counting rates of 35,000 cps. Preliminary results were encouraging, but more testing will be necessary before complete confidence can be placed in the system.

b. Fast Critical Experiments--Experimental Support

(i) Reaction Rates Related to Fuel Cycles (R. Gold)

Last Reported: ANL-7513, p. 7 (Oct 1968).

(a) Low-flux Measurements of ^{239}Pu and ^{235}U Capture-to-Fission Ratios in a Fast Reactor Spectrum. Measurements were made in Assembly 24 of ZPR-9 to demonstrate that the determination of the capture-to-fission ratio α by the reactivity-reaction rate method* is feasible in low-flux fast reactor spectra and to help resolve uncertainties regarding ^{239}Pu α values in the energy range from 1 to 10 keV.

The reactivity-reaction rate method for determining $\overline{\alpha}$ for ^{239}Pu and ^{235}U in a fast flux requires the measurement of (1) the reactivities ρ_i of samples of ^{239}Pu, ^{235}U, ^{6}Li, and ^{252}Cf; (2) the absolute neutron absorption rate R_a, of ^{6}Li and the absolute fission rates R_f^{239} and R_f^{235} of ^{239}Pu and ^{235}U, respectively, and (3) the neutron emission rate S from spontaneous fission in the ^{252}Cf sample. When the results are normalized to a common power level,

$$(1+\overline{\alpha}) = \frac{R_a(A)\{(\rho/R_f)[1 - (\rho_s/\rho)] - (\overline{\nu}/S)\rho(Cf)W_f/W_f(Cf)\}\ W_a(A)/W_a}{\rho(A)\{1 - [\rho_s(A)/\rho(A)]\}}.$$

The calculated factors $[1 - (\rho_s/\rho)]$ and $\{1 - [\rho_s(A)/\rho(A)]\}$ correct for the scattering contribution to the measured reactivity in the fissile samples and the absorber A, respectively. These correction terms differed from unity by less than 1%. The factor $W_f/W_f(Cf)$ accounts for the difference

*Redman, W. C., and Bretscher, M. M., Direct Determination of Uranium-235 Capture-to-Fission Ratio in a Zero Power Reactor, Nucl. Sci. Eng. 27, 34 (1967); Low Flux Measurement of U-235 Epi-cadmium Capture-to-Fission Ratio, ibid. 31, 247 (1968).

between the average neutron importance for the sample's spectrum of fission neutrons for the sample and that for spontaneous fission of ^{252}Cf. Similarly, $W_a(A)/W_a$ corrects for the difference in the average neutron importance for absorption in the ^{6}Li absorber as compared with absorption in the fissile materials. For the conditions existing in these measurements, $W_f/W_f(Cf)$ and $W_a(A)/W_a$ differ from unity by 1 to 3%. Except for the effective number of neutrons emitted per fission, $\bar{\nu}$, all the remaining terms in the above equation are measured quantities.

The neutron absorption rate in ^{6}Li was found by extracting the tritium produced by the $^{6}Li(n,\alpha)^{3}H$ reaction in the irradiated sample and determining its activity by liquid scintillation-counting techniques. Fission rates were measured radiochemically by a procedure* involving the recovery of the fission product ^{99}Mo from the irradiated sample and absolute beta counting. A fine autorod mechanism was used to measure the reactivities of the various samples. In the case of the ^{252}Cf source the measured reactivity consisted of two parts. The first was the reactivity resulting from neutron-induced reactions in ^{252}Cf and its supporting material. The second part, $\rho(Cf)$ which appears in the equation, is the apparent reactivity associated with the emission of spontaneous-fission neutrons. Since this varies inversely as the neutron flux while the first part is independent of flux, $\rho(Cf)$ was found by measuring the reactivity at several different power levels. The manganese bath technique** was used to determine the strength S of the californium source.

Assembly 24 of ZPR-9 was designed to give a soft spectrum so that integral ^{239}Pu-alpha measurements would be sensitive to alpha values in the energy range from 1 to 10 keV. For this core the calculated median fission energy was 13 keV. The ^{239}Pu capture-to-fission ratio was measured for plutonium sample thicknesses of 0.005, 0.015, and 0.030 in. Similarly, 0.005-, and 0.020-, and 0.040-in.-thick enriched uranium samples were used for the ^{235}U-alpha measurements. A preliminary analysis of the data, corrected to zero thickness, yielded $\bar{\alpha}^{239} = 0.513 \pm 0.039$ and $\bar{\alpha}^{235} = 0.329 \pm 0.028$. Calculations based on ENDF/B cross-section data gave $\bar{\alpha}^{239} = 0.352$ and $\bar{\alpha}^{235} = 0.346$. When the Oak Ridge† and United Kingdom†† differential data $\alpha(E)^{239}$ were used, the calculated values of $\bar{\alpha}^{239}$ were 0.438 and 0.556, respectively.

---

*Armani, R. J., "Absolute Determination of Fission Rates in U-235 and U-238 and Capture Rates in U-238 by Radiochemical Techniques," Reactor Physics Division Annual Report, July 1, 1965 to June 30, 1966, ANL-7210, p. 304 (1967).

**De Volpi, A., Porges, K. G., and Armani, R. J., "Absolute Calibration of Fission Neutron Source Strength Relying Upon An Improved Manganese Bath Technique and Absolute Beta-Gamma Coincidence Counting," Symposium on Standardization of Radionuclides, pp. 717-727 (IAEA, Vienna, 1967).

† De Saussure, G., et al., "Measurement of the Neutron Capture and Fission Cross Sections and of Their Ratio Alpha for U^{233}, U^{235} and Pu^{239}," Nuclear Data for Reactors, Vol. 2, pp. 233-249 (IAEA, Vienna, 1967).

†† Schomberg, M. G., Sowerby, M. G., and Evans, F. W., "New Methods of Measuring Alpha(E) for Pu^{239}," Symposium on Fast Reactor Physics and Related Safety Problems, Vol. 1, pp. 289-301 (IAEA, Vienna, 1968).

To check this technique for determining $\overline{\alpha}$, the ^{238}U capture-to-fission ratio was measured by the reactivity-reaction rate method and also by the radiochemical procedures of Armani which allow ^{238}U capture and fission rates to be measured in the same sample. For a depleted-uranium sample 0.035 in. thick, the radiochemical value for $\overline{\alpha}^{238}$ was 8.020 ± 0.225. A value of 7.855 ± 0.166 resulted from the reactivity-reaction rate method. Most of the error in these $\overline{\alpha}^{238}$ measurements results from the uncertainty (2-3%) in the ^{99}Mo yield in ^{238}U fission.

c. Planning and Evaluation of FFTF Critical Assembly Experiments (A. Travelli)

Last Reported: ANL-7553, p. 9-11 (Feb 1969).

(i) Calculated Worth of a Boron Carbide Blade Located Axially in ZPR-3 Assembly 51. The reactivity change due to insertion of a B_4C blade along the axis of ZPR-3 Assembly 51, as described in Progress Report for March 1968, ANL-7438, p. 16, was calculated in one-dimensional diffusion theory both by perturbation methods and by direct k calculations. The blade, 0.5 x 2 x 36 in. and containing 1,262.2 g of natural B_4C, was assumed to extend through the whole core and through part of the axial reflectors. The composition of the blade material was assumed to be 13.67 w/o ^{10}B, 63.31 w/o ^{11}B, and 23.02 w/o C.

The 29-group cross section set 29001 (see Progress Report for October 1967, ANL-7391, p. 38) was used in combination with the MACH-1 program in cylindrical geometry.* The cross sections of ^{11}B were approximated by carbon cross sections. The geometrical shape of the blade was simulated by a cylinder of equal cross-sectional area, and a rather dense mesh distribution was chosen for the region inside the cylinder and for the region immediately surrounding it (~3-mm mesh spacing). The core material was homogenized with the composition reported in ANL-7391. The transverse leakage was assumed to be constant over all regions and equal to the core transverse leakage, which was evaluated by means of axial calculations in plane geometry (B_z^2 = 7.17 x 10^{-4} cm^{-2}).

The reactivity change following replacement of a rod containing only homogenized empty-drawer materials with the B_4C blade was found (a) by means of perturbation calculations using the unperturbed core as the reference state, and (b) by means of direct k calculations. The results were converted to inhours by using the equivalence 1% $\Delta k/k$ ~ 1,036 Ih (see Progress Report for April 1968, ANL-7445, p. 15). Table I.B.1 shows the comparison of the final results of these calculations with the experimental results given in ANL-7438.

* Meneley, D. A., et al., ANL-7223 (June 1966).

TABLE I.B.1. B_4C Blade Worths, Ih

Perturbation Theory	Direct k Calculations	Experiment
-1,199	-994	-905

(ii) Calculated Worths of Edge Drawers in ZPR-3 Assembly 56B. Scoping calculations were run to anticipate the worths of edge drawers in ZPR-3 Assembly 56B.

The calculations were performed by means of the diffusion program MACH-1 in cylindrical geometry* and by using the 29-group cross section set 29004.2, which differs from set 29004 (see Progress Report for December 1968, ANL-7527, p. 9) only in the (n,2n) cross sections. The reactor sizes and compositions were assumed to correspond exactly to the values given in ANL-7527, and they differ slightly from the actual values used in the experiment.

The transverse buckling of the assembly was chosen to be the same for all groups and for all regions, and was found as the difference between the material buckling of the core region and the transverse buckling needed to achieve criticality in an axial calculation in plane geometry. The calculations yielded $B_z^2 = 6.25 \times 10^{-4}$ cm^{-2}, and the radial calculations run with this value converged to a critical core radius of 47.27 cm.

The reactivity change following replacement of a ring of reflector material with an equivalent homogeneous ring of A-drawer material and B-drawer material was calculated in perturbation theory. The compositions assumed for the drawers are given in Table I.B.2 and differ slightly from the compositions used in the actual experiment (see Table I.B.6 below).

TABLE I.B.2. Assumed Compositions in Core Drawers of ZPR-3 Assembly 56B (x 10^{24} atoms/cm^3)

Isotope	A-drawer	B-drawer	Isotope	A-drawer	B-drawer
O	0.0156687	0.0143435	^{238}U	0.0057968	0.0066442
Na	0.0112391	0.0066722	^{239}Pu	0.0008897	0.0017794
Fe	0.0093696	0.0159309	^{240}Pu	0.0001212	0.0002423
Cr	0.0026067	0.0026892	^{241}Pu	0.0000164	0.0000329
Ni	0.0013477	0.0013389	C	0.0022901	0.0000073
Mo	0.0002289	0.0004578	Mn	0.0002298	0.0002283
^{235}U	0.0000129	0.0000148			

The worth of the three materials under consideration (A-drawer material, B-drawer material, and reflector material) at any given radius R was obtained by calculating the real and adjoint fluxes of a reactor with a core radius equal to R, and by averaging the perturbation results of the two mesh intervals enclosing the core-reflector interface.

*Ibid., see previous page.

This modified perturbation procedure for evaluating the worths of edge drawers appears to be considerably more accurate than direct perturbation calculations based on the critical configuration, because the shifting of the core-reflector interface causes a large change in both the real and the adjoint fluxes.

The numerical results obtained for various radii in the modified perturbation method are shown in Tables I.B.3 and I.B.4, where they are compared with the experimental results (see Fig. I.B.4 below) and with the direct perturbation results based on the critical radius calculated by MACH-1.

TABLE I.B.3. Edge Worths of an A-drawer (Ih/fissile kg)

Radius (cm)	Direct Perturbation Calc	Modified Perturbation Calc	Experiment
45	38.29	41.85	43.97
46	35.12	38.91	41.31
47	33.28	36.22	38.64

TABLE I.B.4. Edge Worths of a B-drawer (Ih/fissile kg)

Radius (cm)	Direct Perturbation Calc	Modified Perturbation Calc	Experiment
45	51.04	52.13	51.17
46	47.10	48.73	48.51
47	44.01	45.60	45.84

3. ZPR-3 Operations and Analysis

a. Mockup Studies (W. G. Davey and R. L. McVean)

Last Reported: ANL-7553, pp. 12-13 (Feb 1969).

(i) FTR Critical Program. Experiments with Assembly 56B, which is Assembly I of the FTR Resumed Phase B Critical Experiments, continued. The radial worth traverses of B-10 and Pu-239 and the small-sample central worths of U-235, U-238, Pu-239, B-10, Ta, Fe, Cr, Ni, Na, and Li-6 were measured. Next the reactor was reloaded for the axial traverses. Axial reaction-rate traverses of Pu-239, U-238, and B-10 were measured, and the axial worth traverses begun. These data are now being reduced and analyzed.

(ii) Assembly 56B, As-built System. The core which is considered the reference for Assembly 56B is loading 56-17. The reactor inventory for loading 56-17 is presented in Table I.B.5. Figure I.B.2 depicts the core, axial reflector, and radial reflector zones in the reference core. The radii are those in an equivalent cylindrical geometry which has the area of the zone. The area of one matrix tube location is 4.75 sq. in.

As noted in Table I.B.2, the reference core had one control drawer withdrawn 8.62 in. when the reactor was at the reference power level (indicated 20 W) and the average of the thermocouple readings was 37.6°C. Corrections for these operating conditions are included in the critical-mass calculation for the unsmoothed heterogeneous cylinder.

TABLE I.B.5. Reactor Inventory for Reference Core of Assembly 56B

Drawer Type	Number	Fissile Mass Pu-239 + Pu-241 + U-235 (kg)
	Core	
A	216	110.069
B	203	205.738
Safety	16	15.645
Control[a]	2	1.955
	Radial Reflector	
Zone 1	200	0
Zone 2	122	0
Zone 3	122	0
	Total Fissile Mass	333.41

[a]Fissile mass includes one control drawer which was withdrawn 8.62 in. when the reactor was at the reference power level.

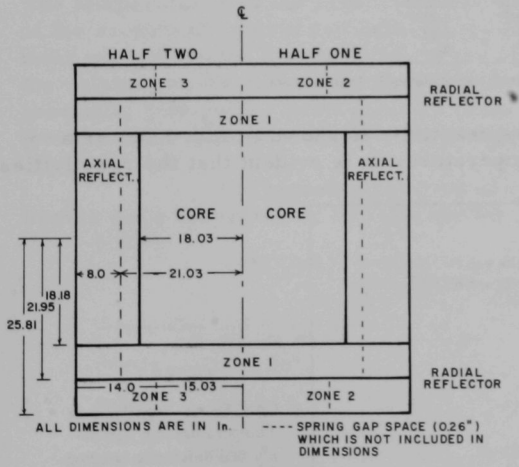

Fig. I.B.2. Equivalent Cylindrical Loading for Reference Core of Assembly 56B (Loading 56-17)

The as-built compositions have been calculated for Assembly 56B and are presented in Table I.B.6. The radial reflector zones correspond with those in Fig. I.B.2. The radial reflector is zoned because of the necessity to use different drawer lengths and platelet sizes, not because of any rearrangement of columns within the drawers.

(ii) Temperature Coefficient of Assembly 56B. The temperature coefficient of reactivity of Assembly 56B was determined by an analysis of data taken during the measurements of edge-drawer worths. Repeated measurements with the reference core loading provided values of the excess reactivity of the same loading at different temperatures. For each measurement the position

of the calibrated control rod required to maintain a standard subcritical power level and the readings of ten thermocouples placed between matrix tubes at various locations were reported. The control-rod worth was determined from a prior calibration. The core average temperature was defined as the average of the temperatures of the core halves, each of which were themselves defined as the averages of the thermocouple readings in that half. Although this is not a true core average, it gives a consistent sampling of the temperature distribution and provides a measure of the changes in core temperature. The excess reactivity of the core is the worth of the control-rod section withdrawn at the recorded position less the constant degree subcritical at the standard power level.

TABLE I.B.6. Compositions in ZPR-3 Assembly 56B
(x 10^{-2} atoms/b-cm)

	Core			Control and Safety Drawers	Reflector			
						Radial		
Nuclide	A Drawer	B Drawer[a]	Cell Average		Axial	Zone 1	Zone 2	Zone 3
Na	1.076	0.6609	0.8685	0.6546	1.346	0.6535	0.6628	0.6523
Fe	1.037	1.710	1.374	1.949	0.8825	0.7613	0.7621	0.7834
Cr	0.2579	0.2406	0.2493	0.3480	0.2188	0.1882	0.1890	0.1943
Ni	0.1129	0.1053	0.1091	0.1523	1.948	4.744	4.769	4.772
Mn	0.01077	0.01005	0.01041	0.01453	0.01810	0.02936	0.02869	0.02891
Si	0.01264	0.01179	0.01222	0.01706	0.01072	0.01127	0.01288	0.01341
Pu-238	0.00004	0.00008	0.00006	0.00007				
Pu-239	0.08857	0.1771	0.1328	0.1708				
Pu-240	0.01177	0.02354	0.01766	0.02268				
Pu-241	0.001672	0.003345	0.002509	0.003058				
Pu-242	0.000172	0.000345	0.0002585	0.000304				
U-235	0.001246	0.001457	0.001352	0.001419				
U-238	0.5762	0.6617	0.6190	0.6426				
Am	0.00008	0.0001639	0.0001229	0.000171				
Mo	0.02283	0.04566	0.03425	0.04403				
O	1.497	1.541	1.519	1.253				
C	0.2075	0	0.1038	0				

[a]B-type drawers (two fuel columns per drawer) are located in even-numbered ZPR-3 matrix columns.

The core excess reactivity is shown in Fig. I.B.3 as a function of the average core temperature. It is evident that the reactivities

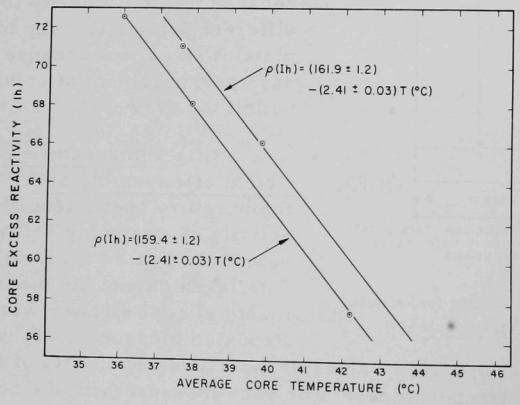

Fig. I.B.3

Core Excess Reactivity vs Temperature for Assembly 56B Reference Loading

fall into two sets. The first contains the first two reference core measurements; the second has the three later measurements. Between these sets, an experiment had been done and the core returned to the reference configuration. It is likely that the later reference core differed by approximately $2\frac{1}{2}$ Ih from the earlier one. This change would not be expected to change the temperature coefficient. Accordingly, a least-squares fit was made to the two sets of data with the constraint that the curves fit to the two data sets must have the same slope. The fitted lines are shown in Fig. I.B.3. It was assumed that all of the reactivities had equal uncertainties and no weighting factors were used. The root-mean-square deviation of the reactivities about the fitted lines was ±0.15 Ih. The temperature coefficient is the slope of the fitted lines, -(2.41 ± 0.03) Ih/°C, where the uncertainty was derived from the internal consistency of the reactivities, relative to the fitted lines. This coefficient is in the range typical of this type of ZPR-3 assembly. For example, the temperature coefficient for Assembly-51 Assembly I of the FTR Phase B Critical Experiment Program was 2.34 Ih/°C.

(iv) Core Edge Worths and Critical-mass Adjustment for Assembly 56B. The worths of core drawers relative to reflector material were measured at several core edge locations in Assembly 56B. Each worth was measured by determining the positions of the calibrated control rod necessary to maintain a standard subcritical power level before and after the exchange of a core drawer for a blanket drawer, or vice versa. The temperatures in the assembly were measured each time. The worth of the section of control rod between the two level subcritical power positions was corrected for the effect of the core temperature change to obtain the relative worth of the core drawer. The temperature coefficient of reactivity determined from analysis of the repeated measurements with the reference core was used for the temperature correction.

The measured worths are listed in Table I.B.7. These worths were converted to specific worths by dividing the mass of fissile

TABLE I.B.7. Summary of Worths of Core Drawers at Core-Reflector Interface
(Worths relative to radial reflector)

Drawer	Fissile Mass[a] (kg)	Worth[b] (Ih)	Specific Worth (Ih/kg)	Radius (cm)
2-X-17	0.5097	23.06 ± 0.25	45.24 ± 0.50	44.55
2-U-10	1.0136	57.91 ± 0.25	57.13 ± 0.25	43.25
2-X-18	1.0136	49.89 ± 0.25	49.22 ± 0.25	45.58
2-V-11	0.5097	24.40 ± 0.25	47.87 ± 0.50	43.22
2-U-23	0.5097	19.32 ± 0.25	37.90 ± 0.50	47.65
2-W-12	1.0136	51.75 ± 0.25	51.05 ± 0.25	44.59
2-V-22	1.0136	47.53 ± 0.35	46.89 ± 0.35	46.97

[a]Pu-239 + Pu-241 + U-235.

[b]The uncertainties listed are a measure of the reproducibility of the measurements. In addition, there is an uncertainty of approximately ±1% of the worth from the uncertainty in the control-rod calibration.

material in the drawer to adjust for there being two columns of fuel in drawers in even-numbered matrix locations and one column in drawers in odd-numbered locations. The uncertainty of ±0.25 Ih assigned to most of the measured worths was based on the normal reproducibility of the reference core loadings (±0.15 Ih) determined in the temperature-coefficient analysis. The measurements of the reference core loadings and the core-drawer manipulations between them were typical of all of the edge-drawer measurements, so this reproducibility should be representative of the uncertainty in each edge-drawer worth measurement (including the effect of temperature changes). Each drawer worth was the difference between two measurements, making the uncertainty ±0.22 Ih, which was rounded to ±0.25 Ih. The measurement in 2-V-22 involved the simultaneous removal of drawer 2-U-10 and the insertion of drawer 2-V-22. This increased the uncertainty for 2-V-22 to ±0.35 Ih. These uncertainties are a measure of the reproducibility of the measurements. They should be increased by approximately 1% of the measured worth to account for the uncertainty of the control-rod calibration.

The specific worths are shown in Fig. I.B.4 as a function of the distance from the core center to the center of the drawer. This figure reveals that the fissile mass normalization did not completely account for the differences between even- and odd-numbered drawers. It was assumed, however, that the slopes of the worth in radius curves were the same for both sets of drawers. A fit was made simultaneously to the two sets of specific worths with the restriction that both fitted curves have the same slope. In making the fit, the points were weighted by the inverse squares of their uncertainties. The fitted lines are shown in Fig. I.B.4. The even-numbered drawers (two columns of fuel plates) are worth more than the odd-numbered drawers by 7.2 Ih/kg. The root-mean-square deviation of the worth about the fitted lines is ±1.0 Ih/kg, which is

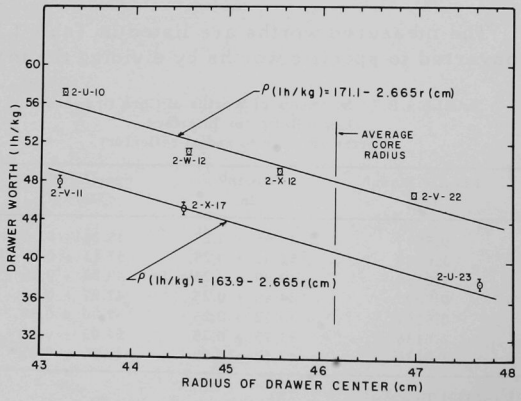

Fig. I.B.4. Worth of Core Edge Drawer in Assembly 56B

approximately three times that expected from the uncertainties of the individual worths. This larger deviation is the result of the actual drawer worth not following exactly the position dependence assumed by the fit, i.e., a dependence only on the radius of the drawer center, with no localized effects.

The average worth of the substitution of core for reflector material at the core radial boundary is the average of the two fitted equations:

$$\rho(\text{Ih/kg}) = 167.5 - 2.665r\,(\text{cm}) \quad 43\ \text{cm} < r < 48\ \text{cm}.$$

Evaluating this at the average core radius of 46.16 cm gives 44.5 Ih/kg for the average conversion factor from edge fissile mass to reactivity. (The average core radius is the radius of the circular cylinder having the same cross-sectional area as the core.)

The Assembly-56B critical mass is summarized in Table I.B.8. The average worth of core drawers at the core boundary was used to determine the fissile-mass equivalent of three adjustments to the reference-loading data: the full insertion of Control Rod No. 6 from its position for a level power, the raising of the core average temperature to 40°C, and correcting for the fact that, because of the high neutron source in the fuel, the assembly was subcritical at the reference power level. It should be pointed out that the 40°C core average temperature has only relative significance since this is an average of the thermocouple readings rather than a true average over the core. These adjustments conform to standard ZPR-3 practice. These corrections are equivalent to a fissile-mass removal of 1.47 kg and yield a critical mass of 331.24 kg. This value includes no corrections for smoothing of the core-reflector interface (which was of the order of -100 Ih, or just over -2 kg for the somewhat smaller Assemblies 48-50) for the reactivity effect of the interface gap at the assembly halves (40 ± 20 Ih for Assembly 48) or for the effect of the core's heterogeneity.

TABLE I.B.8. Critical Mass of Assembly 56B

	Reactivity (Ih) 1% $\Delta k/k$ = 1039.08 Ih	Pu-239 + Pu-241 + U-235 (kg)
Reference Loading (56-17)		333.41
Corrections to the Loaded Mass for:		
1. Control Rod No. 6 Partially Inserted	-74.74	-1.68
2. Core Average Temperature (raise from 37.6 to 40.0°C)	+5.78	+0.13
3. Reference Core Subcritical at Reference Power Level	+3.71	+0.08
Critical Mass of the Unsmoothed Heterogeneous Cylinder		331.94

(v) Radial Reaction-rate Traverses for Assembly 56B. Reaction-rate traverses in Assembly 56B were made with three different counters: two brass, gas-filled fission counters containing either Pu-239 or U-238, and a steel clad $^{10}BF_3$ counter (see Fig. II.B.8 of Progress Report for May 1968, ANL-7457, p. 23). The identical Pu-239 and U-238 counters were used.

The reaction-rate data are given in Figs. I.B.5, I.B.6, and I.B.7. The small variation in the repeated central measurements

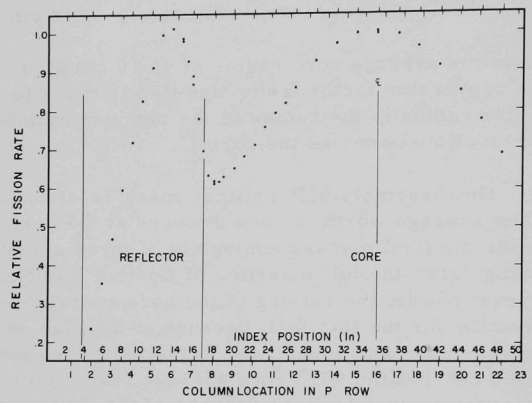

Fig. I.B.5. Pu-239 Radial Reaction Rates in Assembly 56B

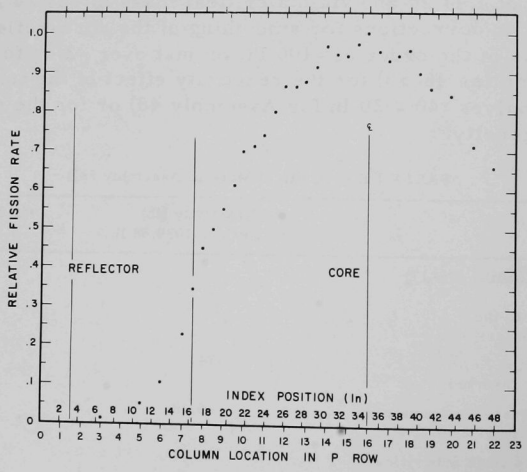

Fig. I.B.6. U-238 Radial Reaction Rates in Assembly 56B

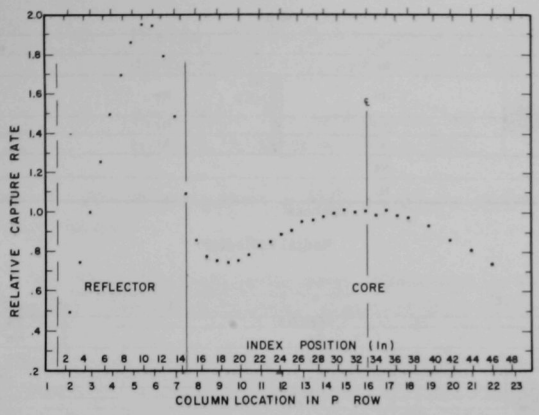

Fig. I.B.7. B-10 Radial Reaction Rates in Assembly 56B

indicate the precision of the data is that of count-rate statistics and not of counter-position reproducibility.

The data were taken while the reactor was held at a constant power level by an autorod located in the O-25 matrix position. Because of the autorod location, the traverses were terminated in the P-22 matrix position.

The two-drawer cell structure is evident in the U-238 and B-10 traverses as a periodic drawer-to-drawer reaction-rate variation superimposed on a radial shape. This variation is not evident in the Pu-239 traverse.

The drawer loadings through which the traverses were made are shown in Fig. I.B.8.

4. ZPPR Operations and Analysis (W. G. Davey and P. I. Amundson)

Last Reported: ANL-7553, pp. 13-15 (Feb 1969).

a. Doppler Effect

(i) Reactivity Doppler Equipment. All parts for the Doppler rod have been machined, and the subassemblies are being welded together. The silvered surface of the capsule has been inspected and is sufficiently reflective.

A system has been designed to measure the cooling air temperature downstream of the heated capsule. The necessary parts have been ordered.

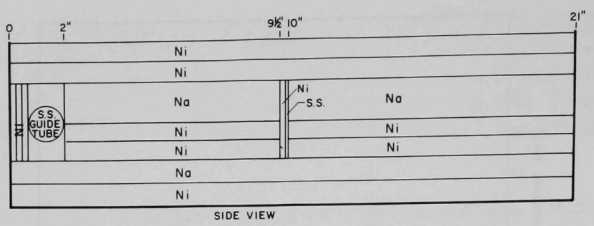

Radial Reflector

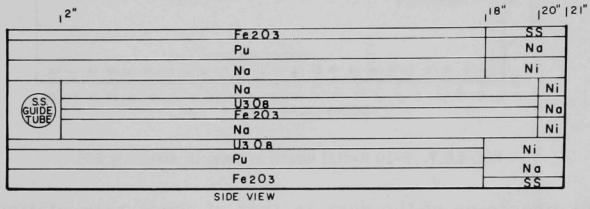

Type B Drawer

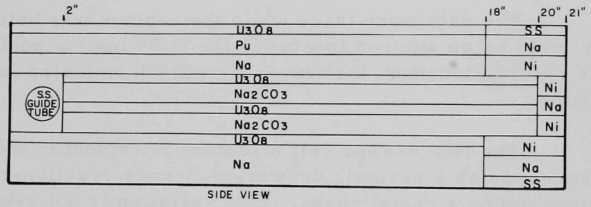

Type A Drawer

Fig. I.B.8. Radial-traverse Drawer Loadings for Assembly 56B

b. Reactor Equipment Development

(i) Equipment

(a) ZPPR Computer. The ZPPR On-line Computer System has been completely installed. Acceptance tests have been halted due to hardware malfunctions. The acceptance tests will resume when all hardware problems have been corrected. Construction of the initial remote I/O terminal is continuing. Each terminal will consist of three units:

1. Control Unit--Containing line drivers and receivers, a patch panel, and control-panel with associated logic.

2. Display Unit--Containing a six-decade display, display selector, and address logic.

3. AEC Bin--Containing counter register modules, timers, A/D converters, etc.

The display unit is 50% complete and the first control unit is under construction.

(b) Data Collection System. Delivery of the Data Logger portion of the Digital Collection System is anticipated by early April.

(c) Experimental Reactor Equipment. The procurement proceedings for Analog-to-Digital Converters for the Automated Gamma Spectrometer have been cancelled as a result of the manufacturer's inability to meet specifications. An order has been placed with a different vendor for three 100-MHz ACS's. The selected vendor has agreed to provide three (50-MHz) ADC's on a loan basis until the higher-frequency units are delivered. Interfacing of the SEL-810A computer with the PI-1207 magnetic tape unit is now complete and is operational. With the delivery of the three ADC's the Automated Gamma Spectrometer project will contain its full complement of equipment.

(d) Technique Development. The SPECB code (which produces spectrum-weighted delayed-neutron parameters) has been expanded to calculate effective betas and prompt-neutron lifetime, in addition to considering energy-dependent betas weighted over the spectrum of neutrons causing fission. The code is operational and will be given a final test run, with constant betas and data from Assembly 53, to attempt to calculate the same results as had been obtained from MACH-1 Bailiff.

The drift rates calculated by the CROC program (an inverse kinetics control-rod-calibration routine with a drift correction) appear to be one to two orders of magnitude greater than the slope of the δk versus time curve past the point where rod motion ceases. This would indicate that the drift rate is real, and not the result of statistical fluctuations in the data. ZPR-3 Assembly 51 data are being used in these tests. Further calculations are planned to confirm this indication.

C. Component Development--LMFBR

1. Reactor Mechanism and Instrumentation

a. FFTF Instrumentation (R. A. Jaross)

(i) In-core Flowmeter Development

Last Reported: ANL-7553, pp. 24-25 (Feb 1969).

(a) Flow-sensor Feasibility Studies. Several crude tests were performed to simulate a probe-type eddy-current flow sensor having two primary coils and one secondary coil. The uniform layer-wound coils were wound with great care; after much difficulty, a secondary coil of 2128 turns in 34 layers of Formvar-insulated copper wire (34 AWG) was completed. Each primary coil had 387 turns in 14 layers of 26-AWG wire. The electrical balance in the coil system was sufficient for the dry room-temperature tests.

Sodium flow around the assembly was simulated by mechanically moving a 6061T6 aluminum tube (of 1-in. ID, 1.5-in. OD, and 12 in. long); an oscilloscope measured the secondary voltage and a sine-wave generator and power amplifier drove the primaries connected in opposing series. With a relative motion of 2.09 ft/sec and approximately 300 mA rms of primary current at 70 Hz, a total signal of about 10 mV peak-to-peak was observed. Noise was negligible. The horizontal sweep of the scope was driven by a voltage derived from the primary current. The vertical axis displayed secondary voltage. For future models, it is planned to increase the two-section coil assembly to four or eight sections to increase sensitivity. Other secondary-coil designs are also being considered.

All parts required for the probe-type permanent-magnet flow sensor have been assembled. The flow sensor is being installed in the small NaK loop. The calculated sensitivity of the flow sensor is ~0.36 mV/gpm through the center of the flow sensor; the flowrate of the loop can be determined, and the sensitivity of the flow sensor will be demonstrated.

The flowrate through the flow sensor when it is located in the center of an FFTF coolant channel is being calculated in preparation for tests in a water loop.

(b) Materials Procurement. Seven prospective suppliers of ceramic-insulated nickel-coated silver magnet wire were invited to bid. Five, declined. Secon Metals Corp. bid partially, stating that it is not

equipped to perform the tests required; the company took exception to the entire specification ANL-HTI-FFTF 503-4-G. Physical Sciences Corp. bid on all items; its verification of conformance with the specifications is being awaited.

(c) Magnet Irradiation Tests. Assembly and shipment of the irradiation subassembly capsules have been delayed for metallographic resolution of questions about: (a) how the electrochemical etching process used for code numbering affects the capsules and (b) the effects of molten melt-wire materials on their stainless steel containers.

(ii) Signal Lead Connectors for Sodium Service
(A. P. Grunwald)

Last Reported: ANL-7553, pp. 25-26 (Feb 1969).

The FFTF prototype connector has been cycled up to 1000°F twice in an argon atmosphere and twice in sodium. After each heating cycle, the breech lock was opened and reclosed, and the performance of the main gasket was checked. All operations were performed without difficulty. The leakrate of the main gasket remained essentially unchanged; minor variations in leakrate were random.

The nipple leakrate was tested at 1000°F with consistently good performance. The leakrate of all nipples was less at elevated temperature than at room temperature. Making and breaking of nipple connections was made routinely without adverse effects on performance.

The straightening and tapering of pins has completely eliminated buckling of pins in the electrical connector. Since these modifications, the electrical connection has been made and broken perfectly. Resistance to ground remained within ~7% of the original value, with a small but probably significant trend toward increase. Pin-to-pin resistance has not changed measurably.

After the relatively massive seepage of sodium reported in ANL-7553, the sealing and working surfaces were cleaned and sliding surfaces relubricated. To maintain, as closely as possible, the original fit, reconditioning of the surfaces was limited to polishing, so it must be assumed that flatness and surface finish in some places were inferior to the as-built condition. Nevertheless, sodium seepage was very small (~2 cm^3, which is ~10% of the seepage observed in the first instance) despite the fact that the sodium temperature was sometimes 1000°F, as compared with a maximum temperature of ~550°F during the previous run. Thus we can speculate that, with the original surface conditions, no seepage would have occurred if the MoS_2 and sodium had not damaged the seal.

Although only very little sodium penetrated the seal the second time, its effect was relatively dramatic (see Fig. I.C.1). At the high temperatures, the sodium wet two distinct areas on the inside of the breech lock and crept up to the cylindrical guide sleeve above the breech lock. At that elevation, the bottom of the sleeve is engaged by the male part of the connector (not shown) so that there is a very narrow annulus between the sleeve and the male plug. In operation, the annulus is partly filled with MoS_2; apparently sodium filled most of this annulus by capillary action. The typical corrosive reaction observed previously whenever MoS_2 and sodium come into contact at elevated temperatures is clearly visible within the sleeve (the picture was taken after the connector was cleaned with steam). The crust formed as a result of the reaction is very hard. The connector could be disengaged fully only after the inner part was cooled with water while the outside was heated; inasmuch as the differential expansion permitted the connector to disengage freely, it is apparent that the corrosion did not cause the parts to fuse, but merely caused mechanical interlocking due to interference (the parts were free to move with respect to one another initially; only after the upper guide of the plug reached the corroded areas did interference occur; even then the parts freed up any time the plug was lowered again). After the crusts were removed carefully, the plug and sleeve again operated normally. There was no dimensional change of the sleeve. Thus, this phenomenon is not a recurrence of the creep of the weld zone, which coincides approximately with the corroded annulus of the sleeve.

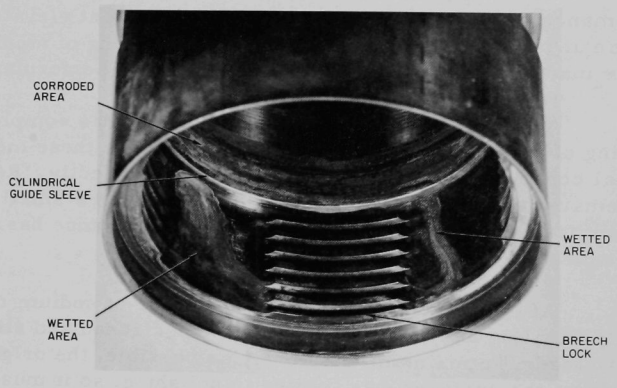

Fig. I.C.1. Breech Lock, Showing Areas Wet by Sodium and Corroded Area

After the assembly was reconditioned, the same gasket was reinstalled and the unit was assembled in the test apparatus. Initial leaktests with argon showed no significant change in leakrate.

The pin-to-pin resistance in the 36-pin connector (see Progress Report for January 1969, ANL-7548, p. 31) should have been reported as 9.9 megohms rather than 9.9 microhms.

(iii) Failed-fuel Location Method (E. S. Sowa)

Last Reported: ANL-7553, pp. 26-27 (Feb 1969).

The Fuel Failure Detection Loop (FFDL) was operated to determine its characteristics. After initial startup, the system was heated to 600°F and the electromagnetic pump was operated to achieve "wetting" of the pump tube. After one day of operation, wetting was achieved, and all subsequent operation was characterized by extremely good stability and response. Operation continued at 760, 850, 900, and 1000°F. At each temperature, the flowrate was determined for each setting of pump power; calibrations were checked against the flowmeter curve and the height of the stagnant-zone sodium in the riser pipe. A typical curve is shown in Fig. I.C.2, which also shows the contact point for each probe in the riser. The power required to achieve a given flowrate varied very little when the temperature was raised from 760 to 1000°F; approximately 6% less power was required for a given flowrate at 1000°F than at 760°F.

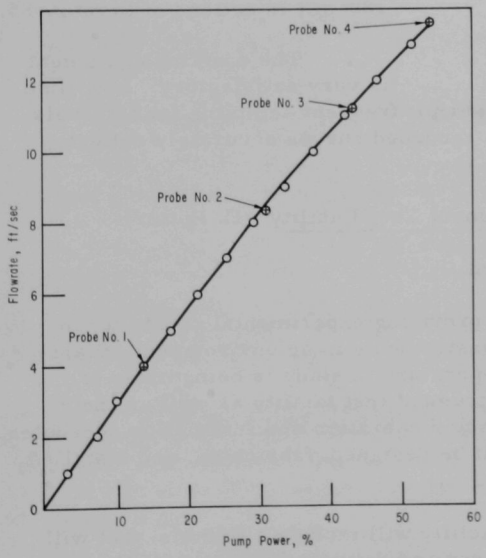

Fig. I.C.2. Pump Power vs Sodium Flowrate in the FFDL at 900°F

Cooling curves were also determined for the higher temperatures to measure the time required to freeze the loop between experiments. The cooling curve from 900°F (Fig. I.C.3) shows that freezing of the main loop system can be accomplished in 10 hr.

Arrangements have been made for loading the krypton-85 capsules; six are being filled for the initial experiments.

Temperatures were measured at the counting chambers when the gas-circulation pumps were operated with the loop at 1000°F. Little deviation from ambient was detected, which means that the G-M tubes will not require cooling when operating near the chamber.

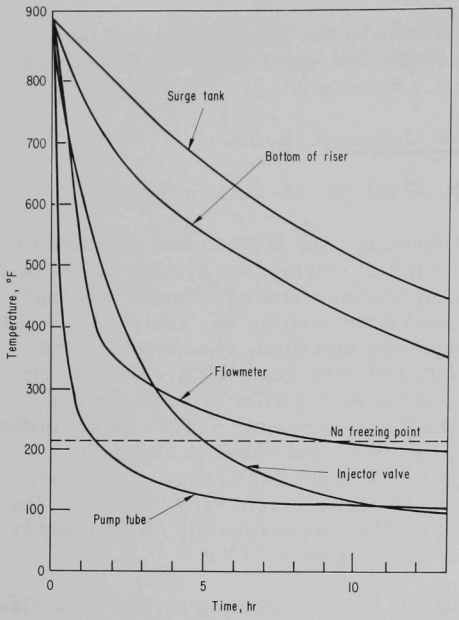

Fig. I.C.3. Cooling Curves for FFDL

Approximately 90% of the counting equipment has been received from Hewlett-Packard Co. Although one digital-to-analog circuit remains to be delivered, the one complete operational circuit was operated to determine its characteristics. A calibration with a thallium-204 source (emits 0.37-0.77-MeV betas with a half-life of 3.9 yr) showed that the geometry factor is linear over the volume of the detection chamber, with an average value of 0.65. The absorption factor for a 0.002-in.-thick aluminum foil was measured as 0.64; therefore, aluminum foil will be used to isolate the chamber. The measured overall factor of 0.41 shows the validity of the initial calculations calling for 100-μCi injections of krypton-85.

The counting equipment is very satisfactory. Low time constant and high-speed response permit frequent sampling for intervals as short as 0.1-sec duration. The recorded curves accurately reflect counting statistics.

b. EBR-II In-Core Instrument Test Facility (E. Hutter)

Not previously reported.

As a first step toward providing experimental capability in EBR-II for testing and evaluating instruments in an environment of fast-neutron radiation and variable temperature, a study is being made of various concepts of an in-core instrument test facility as well as their feasibility, cost, and impact on reactor operation and irradiation schedules. Based on this study, equipment will be designed, fabricated, and installed in EBR-II.

It is planned that the facility will include a thimble, that will occupy one of the existing control-rod and drive positions and will extend into the core region. A shielded handling machine, compatible with the existing systems for handling fuel and control rods, and other equipment for inserting and removing individual instruments will be required.

The thimble, of vertical nested-tube construction, will provide direct access into the reactor core. The bottom end of the innermost tube will be closed to exclude the primary-tank bulk sodium. The instrument sensors in the thimble will be either bare and exposed to a gas environment or individually encapsulated in sodium or other medium.

This task is arranged into the following subtasks:

(A) Preliminary Study of Various Concepts;

(B) Design, Development, and Fabrication of the Facility;

(C) Installation of the Facility in EBR-II.

(i) Preliminary Study of Various Concepts (O. S. Seim, T. Sullivan, and J. Pardini)

Several concepts have been sketched, alternatives and variations of these concepts are being developed, and certain analyses have been initiated. A meeting was held with potential users of the facility to aid in establishing the desired operational and design criteria for the facility.

2. Fuel Handling, Vessels, and Internals--Core Component Test Loop (CCTL) (R. A. Jaross)

Last Reported: ANL-7553, pp. 27-28 (Feb 1969).

The pressure differential across the FFTF subassembly under flow-test has remained constant at 45.9 psig.

From February 19 through March 19, the CCTL has been operating continuously for 666.4 hr at 1060°F and 400 gpm; the pump was off for 2.8 hr while a sodium sample was removed for analysis. The cumulative total operating time with the loop at any temperature and the pump on is 4395.0 hr, of which 3016.1 hr were at 1060°F and 400 gpm.

a. Sodium-purity Measurements. With the new operating mode of the plugging meter (see ANL-7553), the plugging temperature has been less than 250°F continuously. Two chemical analyses of sodium from a single sample tube showed an oxygen content of 5 and 12 ppm, and carbon content of 11 and 14 ppm.

Data from three thermocouples inside the CCTL cold trap indicate that the material around each thermocouple is not changing with time. With sodium flow constant, measurable relative changes of thermocouple readings would indicate a change in concentration of the sodium oxide. From

the lack of change, we conclude that the stainless steel mesh in the cold trap is relatively free of oxide deposit after the 4395 hr the sodium has circulated.

b. Acoustic and Vibration Measurements. During pump coastdown when the CCTL pump was stopped on March 3 so that a sodium sample tube could be removed and replaced, the acoustic monitor at the pump outlet indicated that the pump rotating member was rubbing slightly at very low speed (~10 rpm). When the pump was restarted after a new sample tube had been installed in the CCTL, the sound of the low-speed pump interference was recorded on tape. Study of the chart that continuously records the output of the acoustical monitor showed that there was no increase in the frequency or amplitude of the pump noise during the balance of the reporting period. Thus there is no indication of interference in the pump when it is operating in the range from 100 to 1000 rpm.

It is postulated that the interference was caused by slight closure of the rotating clearances; at very low speed, the negligible discharge pressure from the pump causes the hydraulic bearing to provide no centering force that would correct the closure.

D. Systems and Plant--LMFBR

1. 1000-MWe Plant

a. 1000-MWe Contract Management, Technical Review, and Evaluation (L. W. Fromm)

Last Reported: ANL-7553, pp. 78-79 (Feb 1969).

The Combusion Engineering, Inc., reports on Tasks II, III, and IV have received patent clearances and are being published for external distribution.

(i) Babcock & Wilcox Co. Subcontract. Volume 1, containing the overall conceptual system design description (CSDD) and capital-cost estimate, of the Task-II and -III report BAW-1328 was shipped to ANL. Volumes 2 and 3, containing CSDDs, have been reproduced and will be shipped this month. The Task-IV report, which describes the required research and development, is scheduled for release this month.

(ii) Westinghouse Electric Corp. Subcontract. The Task-III report was completed and is being printed. All sections of the Task-IV work have been drafted and are being reviewed by Westinghouse. The architect-engineer was asked for additional information for the CSDDs for the Task-II report, which is being completed.

(iii) General Electric Co. Subcontract. The Task-III report was received; the first draft of the integrated Task-IV report was completed and is being reviewed within GE.

(iv) Combustion Engineering, Inc., Subcontract. Work on the follow-on study has been completed. The Task-IV report, which describes the required research and development, has been received.

(v) Atomics International Subcontract. It is taking longer to review and edit the Task-III and -IV reports than had been anticipated. It is expected that the five volumes of the Task-III report will be ready for printing by the end of March and that the Task-IV report will be ready by mid-April.

E. EBR-II

1. Research and Development

a. Reactor Experimental Support--Reactor Analysis and Testing (R. R. Smith)

(i) Nuclear Analysis and Safety

Last Reported: ANL-7553, pp. 29-32 (Feb 1969).

(a) Feasibility Study for a Nuclear Prooftest Facility (J. K. Long)

A feasibility study for a nuclear prooftest facility to supplement EBR-II has been drafted. Such a facility would operate at low power as a critical facility. Instead of the plate structure of the ZPR's, however, the facility would use fueled pins, assembled into EBR-II subassemblies or near duplications of these subassemblies. According to various concepts, these subassemblies would be either filled with sodium, sealed or frozen, or immersed in a large reactor vessel of molten sodium.

The facility would provide flux-mapping and spectral-index information better to define EBR-II irradiations. Proposed loading changes for EBR-II could be studied in advance for their effects on reactivity and flux distortions. Clearances, displacements, and distortions of subassemblies could be modeled, and their reactivity effects reproduced. Blanket and reflector optimizations could be devised, and proposed future core loadings such as of oxide and Mark-II fuel could be studied.

It has been recommended that the present ZPR assemblies be investigated as alternative sources for the required EBR-II support

information. With the exception of the plate heterogeneity effects, many of the desired flux patterns and reactivity effects can be studied in these assemblies, provided time and materials are available.

(b) Prototype Reactivity Meter (J. R. Karvinen)

Calibration and preliminary testing of a prototype reactivity meter has provided encouraging results. Based on these tests, sensitivity to 0.1 Ih appears to be realizable. Parts to complete the fabrication are being awaited.

(c) Null Meter (J. R. Karvinen)

A null meter for evaluating the reactor performance with the standard control rods and with a stainless steel rod has been designed and tested. A procedure has been prepared to permit evaluation of the performance of the meter in the operating reactor.

b. Nuclear Analysis Methods Development

Last Reported: ANL-7553, pp. 32-37 (Feb 1969).

(i) Code for Computing Volume Fractions (L. B. Miller)

Several small codes have been written to facilitate the preparation of input for the one- and two-dimensional neutron-transport codes ANISN and DOT. One of these is particularly useful for computing volume fractions of regions of EBR-II fuel, blanket, and experimental subassemblies. Given the characteristic dimensions of each subregion containing a given material, the program computes the volume fraction of the material. The subregions may be in the form of an hexagonal prism, cylindrical prism, cylindrical shell, wire wrap, cone, frustrum, hemisphere, parallelipided triangular prism, or extended segment. Use of this code should reduce the probability of numerical errors in computing volume fractions for neutronics calculations of EBR-II.

(ii) Distributed-parameter Fuel-heat-transfer Model for Uranium-metal Core (D. Mohr)

The time constants relating power generation to fuel-pin heat flux were derived, using the following assumptions:

(1) Fuel and coolant properties are constant in space and time.

(2) Radial power distribution across the fuel pin is constant.

(3) No significant dynamic heat transfer occurs in the axial direction within the fuel pin.

(4) The cladding and bond sodium can be dumped into a combined region, separate from the fuel, for their heat-capacity effect.

(5) The conductivities of the cladding and film are combined to yield an overall heat-transfer coefficient.

(6) A certain fraction γ of the core heat is deposited directly in the coolant (zero lag).

The solution of the resulting modified Bessel equation (of zero order) yields a power-to-heat-flux transfer function of the following form:

$$\frac{\Delta Q_{(s)}}{\Delta P} = \frac{1 - \gamma}{1 + \tau_0 s}\left[\sum_{n=1}^{N} \frac{A_n}{1 + \tau_n s}\right] + \gamma,$$

where

$\Delta Q_{(s)}/\Delta P$ = Normalized transfer function;

γ = Fraction of prompt heat to coolant;

A_n = Individual gains;

τ_n = Individual time constants;

τ_0 = Cladding-bond time constant.

Values of A_n and τ_n have been evaluated at four different fuel conditions for the present EBR-II metal core. The results are as follows:

Term n	At Avg Temp with No Swelling*		At Avg Temp with Max Swelling		At High Temp with No Swelling**		At High Temp with Max Swelling	
	A_n	τ_n	A_n	τ_n	A_n	τ_n	A_n	τ_n
0	-	0.024	-	0.020	-	0.023	-	0.020
1	0.722	0.067	0.847	0.097	0.745	0.060	0.833	0.086
2	0.127	0.013	0.111	0.178	0.135	0.011	0.101	0.016
3	0.050	0.005	0.028	0.007	0.051	0.005	0.024	0.006
4	0.025	0.003	0.010	0.004	0.025	0.003	0.008	0.003
5	0.076	0.002	0.004	0.002	0.044	0.002	0.034	0.002

*Uranium, 1000°F; sodium bond, 850°F; cladding, 800°F.

**Uranium, 1200°F; bond, 950°F; cladding, 900°F.

These results show that the effects of both temperature and swelling--especially swelling--on the heat-flux response to power changes are important. The effect of the cladding-bond time constant τ_0 is also significant.

The value of the major fuel time constant, ranging from 0.060 to 0.097 sec, compares favorably with the lumped value of 0.104 sec reported in ANL-6484.*

If the prompt heat-transfer fraction γ is as large as 0.02 or 0.03, it is an important prompt negative (shutdown) effect because of the large expansion coefficient of sodium.

c. Fuel Performance Studies--Mark I Series (C. M. Walter)

(i) Driver Fuel Operation at High Temperatures and Burnups (J. P. Bacca)

Last Reported: ANL-7527, p. 48 (Dec 1968).

Three encapsulated Mark-IA elements (BF04, BF08, and BF11) from Subassembly XO52 were nondestructively examined. The elements had been irradiated to a calculated peak burnup of 2.9 a/o. Neutron radiographs of the capsules indicated no failure in the cladding of the enclosed elements; these observations were verified by the absence of fission-product gases in the gas plenums of the capsules. Preliminary data from precise diametral measurements of the three elements indicate peak diameter increases of the element jackets ranging from 0.9 to 1.2%. Post-irradiation examinations of these three elements are continuing.

Subassembly XO15, containing two encapsulated Mark-IA elements similar to the above, is being irradiated in EBR-II. Calculated burnup for these elements at the end of Run 33 will be approximately 3.8 a/o.

d. Mark II Driver Fuel Element Development (C. M. Walter)

(i) Element Irradiation Tests

(a) Irradiation of Encapsulated Mark-II Fuel Elements (J. P. Bacca)

Last Reported: ANL-7553, pp. 40-41 (Feb 1969).

The gas from the plenum region of Element 201 from Subassembly XO29 (2 a/o burnup) was sampled, and the pressure and

*Hummel, H. H., and Bryant, L. T., Stability Analysis of EBR-II, ANL-6484 (Jan 1962).

volume of the plenum was measured. The pressure in the element was 98 psi at an ambient cell temperature of 95°F. The gas-plenum volume that remained after irradiation was 1.55 cc, measured at approximately 95°F. Quantitative analyses of the plenum gas are in progress.

Elements 201 and 212 from the same subassembly have been sectioned, and determination of the axial burnup profile of these elements as well as metallography on selected samples are being carried out.

e. Equipment--Fuel Related (E. Hutter)

(i) New Control Rod Subassemblies (O. S. Seim, T. Sullivan, and J. Pardini)

Last Reported: ANL-7553, pp. 41-42 (Feb 1969).

(a) Higher-worth Control Rod. The first phase of flowtests of the prototype version of the higher-worth control rod has been completed. Water-flowtests in the test loop with the equivalent of 61 gpm of sodium flow produced the desired 38.8-psi pressure drop. These tests were conducted with the control rod at the 80% inserted position in the control-rod thimble, the position at which essentially 100% heat generation occurs during normal operation in the reactor.

The second phase of flowtests has been started to determine variation in flow with respect to other positions of insertion ranging from maximum to minimum. Initial phase-two tests indicate some deviations from the desired flow values, and minor modifications have been made of the configuration of the lower adapter of the rod to correct these deviations.

(ii) Oscillator Rod--Mark II (O. Seim, J. Pardini, and T. Sullivan)

Last Reported: ANL-7553, p. 42 (Feb 1969).

The Mark-IIB oscillator rod was stress relieved and balanced. The detailed drawings of the modified shaft of the new oscillator-rod drive were completed; fabrication will be started.

f. Instrumented Subassembly (E. Hutter and A. Smaardyk)

Last Reported: ANL-7553, pp. 46-47 (Feb 1969).

(i) Research and Development

(a) Controls and Interlocks (W. M. Thompson)

Last Reported: ANL-7527, p. 53 (Dec 1968).

The drive mechanism for the instrumented subassembly has been completely wired and tested. The wiring includes all the components, cables, and junction boxes associated with the control of the drive and

its interlocking with the fuel-handling system. All cables from the mechanism terminate in the main junction box, which will be located on the festoon cable pulley on the small rotating shield plug. Two other cables connected to this junction box will link the mechanism with the fuel-handling console during operation of the drive, but they will be disconnected during rotation of the plug. These two cables are now connected to the temporary control console. All circuits, including those not currently used for test operations, have been checked through to the console end of these cables. All the mechanism wiring diagrams have been revised to reflect the as-built conditions and to include wire colors.

The load-force sensing circuits were checked and set during a load-calibration test of the drive. The load-cell force reading was used as a basis for setting the circuit trip points. During vertical travel of the drive, the load force changes by about 70 lb because of the spring action of the bellows. Therefore, the alarm points on the load-cell amplifier were set about 25 lb above and below the range of load variation. The previously reported friction in the upper supporting-spring assembly (see Progress Report for February 1969, ANL-7553, p. 46) has been effectively eliminated; therefore, the trip points associated with the units that monitor the spring deflection were set. The linear potentiometer circuit was set to trip about 50 lb above and below the load variation caused by the bellows, and the limit switches about 100 lb above and below. These trip points may be reset at the time of installation to account for any changes due to buoyancy or other factors.

(b) Pressure-transducer Junctions (C. Divona)

An induction brazing technique has been used to make the four pressure-transducer junctions and one flux-monitor coupling located in the drywell annulus of the test-1 instrumented subassembly. The braze alloy used contains 82% gold and 18% nickel, and is commercially available as Nioro. This alloy was chosen because of its low melting point (960°C), ease of application in wire or sheet form, and good strength characteristics.

The brazing procedure consists of cleaning the stainless steel components by heating in pure hydrogen at 1050°C for 10 min, followed by cooling within the hydrogen atmosphere. The braze alloy is then positioned on the work, and the assembly is heated to the melting temperature of the braze while the hydrogen atmosphere is maintained. Hydrogen is also aspirated through the brazing annuli. Quality of the braze joint has been substantiated by metallographic techniques.

(c) Assembly of Test-1 Subassembly (C. Divona)

Last Reported: ANL-7553, p. 47 (Feb 1969).

Assembly of the test-1 instrumented subassembly was completed. The following operations were performed:

(1) Junctions of sheaths to flexible cables were made, and the three sodium-level probes were installed. Electrical tests indicated that all instruments were functioning properly.

(2) The outer extension tube, which forms the drywell annulus, was tungsten-inert-gas welded to the drywell bulkhead. The weld was inspected by dye penetrant and leak checked with helium; these tests indicated a sound, leaktight weld.

(3) The steel shot (for shielding) was installed in the drywell annulus in the area of the small rotating plug. A small amount of RTV-11 rubber compound was applied above the shot zone to hold the shot in place.

(4) The subassembly coupling was installed within the extension tube and sealed at the terminal-box elevation. A helium leaktest indicated leakage of less than 2×10^{-10} std cc of He/sec through the coupling seals.

(5) The terminal box was installed on the extension tube, and all flexible leads and stainless steel tubes were terminated within the box. The box was then sealed, leak checked, and filled to 15 psig with high-purity argon.

g. Process Chemistry (D. W. Cissel)

(i) Sodium Coolant Quality Monitoring and Control (W. H. Olson, C. C. Miles, E. R. Ebersole, and G. O. Haroldsen)

Last Reported: ANL-7548, pp. 48-50 (Jan 1969).

(a) Radionuclides in Sodium. The results of analysis for ^{137}Cs and ^{131}I in primary sodium are listed in Table I.E.1. The sample of 2/28/69 represents the level of these isotopes following a two-month shutdown of the reactor. Power Run 33A started on 2/25/69, with zero power operation extending through 2/27/69.

No analyses were made for radionuclides in secondary sodium.

TABLE I.E.1. ^{137}Cs and ^{131}I in Primary Sodium

Sample Date	^{137}Cs ($\mu Ci/g \times 10^2$)	^{131}I ($\mu Ci/g \times 10^5$)
2/28/69	1.4	3.0
3/5/69	1.3	5.9

(b) Trace Metals in Sodium. The results of analyses for trace metals in sodium performed from 9/12/68 to 1/7/69 are presented in Table I.E.2. Metal concentrations were determined by atomic-absorption spectrophotometry.

The reduction in copper concentrations in primary sodium during January and February is due to the reduction in the temperature of the bulk sodium from 700 to 350°F. Precipitation of copper was anticipated, based on solubility data presented by Atomics International (document AI-AEC-12671).

TABLE I.E.2. Trace Metals in Sodium (ppm)

Sample Date	Al	Bi	Cd	Co	Cr	Cu	Fe	Mn	Mo	Ni	Pb	Sn	Zn
						Primary Sodium							
9/12/68		1.1	<0.05	<0.1		0.36		<0.04			11.5		
9/17/68		1.5			0.12						11.0	20.6	
10/8/68		1.2	<0.05			0.4		<0.04			10.5		0.35
11/8/68		1.5	<0.05			0.5					11.1	19.3	
12/3/68	<0.6	1.8	<0.02	<0.08	0.05	0.25		<0.05	<0.3	0.1	11.4	18.3	
1/23/69						0.05							
2/6/69	~0.7	1.8	~0.02	<0.08		0.08		0.06			10.9	18.3	
2/14/69						0.10							
2/25/69						0.11							
2/28/69	<0.3	1.5	0.09	<0.05		0.09		0.06		0.26	11.5	20.0	0.05
						Secondary Sodium							
9/17/68		<0.5	<0.05	<0.1		<0.1		<0.04			<1.0		<0.05
10/27/68	<1.0	<0.5	<0.05	<0.2	<0.1	<0.2	<0.6	<0.1			0.7	<2.4	<0.1
12/3/68	1.0	≤0.1	≤0.02	<0.07	<0.04	≤0.03	0.25	<0.02		<0.08	0.8	≤1.0	
1/7/69	<0.6	<0.1	<0.02	<0.08	0.06	<0.08		<0.05	<0.3	<0.08	0.4	<2.6	

A sample of primary sodium collected in a tantalum cup on 12/27/68 was vacuum distilled in the laboratory, and the residue was sent to ORNL for analysis by spark-source mass spectrometry. The results of that analysis are listed in Table I.E.3 together with typical values obtained by atomic-absorption analysis in the Idaho analytical laboratory. Results of analysis of a sample of secondary sodium by spark-source mass spectrometry were reported in the November 1968 Progress Report, ANL-7518, p. 50.

TABLE I.E.3. Comparison of Results from Spark-source Mass-spectrometric Analysis and Atomic-absorption Analysis of Vacuum-distillation Residue from EBR-II Primary Sodium

Element	Spark-source Mass-spectrometry (ppm)	Atomic Absorption (ppm)	Element	Spark-source Mass-spectrometry (ppm)	Atomic Absorption (ppm)
Ag	0.02		Mn	a	<0.05
Al	0.03	<0.06	Mo	a	
As	a		Nb	0.02	
B	0.02		Ni	<0.1	<0.1
Ba	0.01		P	a	
Bi	2.0	1.8	Pb	7.0	11.0
Ca	0.3		Sb	a	
Cd	0.1[b]	<0.05	Si	a	
Co	0.02	<0.08	Sn	0.8[c]	10.0
Cr	a	<0.05	Ta	0.01	
Cu	0.05	0.25	U	<0.003	
Fe	0.06	<1.0	V	a	
Li	0.02	0.5	Zn	0.02[b]	0.05
Mg	0.20		Zr	0.25	

[a]Indicates that element was looked for but not found.
[b]Recovery tests indicate that cadmium and zinc may be lost during distillation (see the November 1968 Progress Report, ANL-7518, p. 49).
[c]Tin was lost during evaporation of aqua regia solution when preparing sample.

(c) Oxygen in Sodium. Oxygen concentrations in EBR-II sodium that were reported in the Progress Reports for December 1968, ANL-7527 and for January 1969, ANL-7548, are in error because the analytical blank in the mercury amalgamation method was not subtracted. A summary of corrected data obtained since October 1968 is presented in Table I.E.4. The oxygen concentrations determined from plugging runs are also listed for comparison.

The two samples of secondary sodium taken on 11/18/68 were used to compare results obtained with extrusion aliquoting to those obtained with total-consumption sampling (i.e., sectioned tubing which contained sodium). The corrected average values for the samples obtained with the latter method are approximately three times those obtained with the former. The values from a second set of samples of primary sodium taken on 11/25/68 for the same purpose show no statistical difference. Several more comparative sets of samples will be analyzed to see if segregation of oxide is a problem in extrusion aliquoting.

(d) Hydrogen in Sodium. The results of analyses for hydrogen in primary and secondary sodium are listed in Table I.E.5. Duplicate analyses were made of each sample.

TABLE I.E.4. Oxygen Content of Sodium

Sample Date	Aliquot Type	No. of Aliquots	Average Oxygen Content (ppm)	Oxygen Equivalent of Plugging Run[a] (ppm)
		Primary Sodium		
11/25/68	Extrusion	5	5.2 ± 1.7	~1.2
11/25/68	Sectioned tubing	4	5.6 ± 1.4	~1.2
12/12/68	Extrusion	3	3.5 ± 0.6	<0.5
1/3/69	Extrusion	6	4.0 ± 0.5	<0.5
2/18/69	Extrusion	4	4.1 ± 1.4	<0.5
		Secondary Sodium		
10/25/68	Extrusion	11	5.5 ± 3.2	~1.0
11/18/68	Sectioned tubing	3	11.4 ± 0.5	<0.5
11/18/68	Extrusion	3	3.7 ± 0.4	<0.5
2/19/69	Extrusion	3	7.5 ± 2.5	~0.7

[a] Oxygen solubility in sodium as given in Atomics International document AI-AEC-12685.

TABLE I.E.5. Hydrogen Content of Sodium

Date	Hydrogen (ppm)
Primary Sodium	
11/25/68	2.2
	<3.2
Secondary Sodium	
9/18/68	5.8
	2.3
10/24/68	2.3
	2.3
12/3/68	1.6
	1.6
1/7/69	1.5
	2.1

(e) Carbon in Sodium. A sample of primary sodium taken on 2/18/69 was analyzed for total carbon by the oxyacidic flux method. The average carbon content in three aliquots was 1.9 ± 0.2 ppm. A sample of secondary sodium taken on 2/19/69 was also analyzed for total carbon. The average carbon content in three aliquots was 2.2 ± 1.6 ppm.

Segregation of carbon in sodium has been investigated by comparison analyses of extrusion-aliquoted samples and total-consumption samples taken in small quartz vials. Table I.E.6 gives the results of these analyses. Apparently, significant segregation does not occur at these carbon concentrations. The higher uncertainty shown for the total-consumption samples reflects the difficulty in obtaining uncontaminated sodium samples by this method and the varying and high-carbon blank obtained for the quartz vials. This blank averaged 1.5 μg of carbon per vial even though each vial had been etched down to 40% of its original mass in 48% HF and then ignited for 16 hr in air at 1000°C.

TABLE I.E.6. Carbon Contents of Secondary Sodium Sampled by Two Methods[a]

Experiment No.	Extrusion Aliquots (ppm carbon) (2 runs per value)	Total Consumption (ppm carbon) (4 runs per value)
1	2.2 ± 0.1	4.2 ± 2.0
2	2.2 ± 0.3	2.2 ± 0.5
3	-	3.5 ± 1.6
4	1.9 ± 0.3	0.9 ± 0.5
Mean Value	2.1 ± 0.2	2.7 ± 1.3

[a]This work was completed in October 1968 but has not been reported previously.

Recovery tests on the carbides received from Consolidated Astronautics have been completed. Carbon recoveries were: zirconium carbide--100%; chromium carbide--<80%; boron carbide--<80%; and silicon carbide--<80%. Thermodynamic data indicate that the last three carbides should oxidize readily in the potassium dichromate flux. It was demonstrated by successive trapping runs on a given sample with flux that each carbon increment was smaller than its predecessor. However, more than 8 hr were required to achieve 80% oxidation by this process. The slowness of the oxidation is believed to be caused by the refractory nature of the carbides, which in the case of boron and chromium carbides were prepared at temperatures of >1600°C. Compounds of this type probably cannot form in sodium at reactor operating temperatures.

(f) Test of UNC Oxygen Meter. Two United Nuclear (UNC) oxygen meters are being tested in static sodium at 600°F. One is located in the high-γ-radiation field of the room containing the primary-sodium cold trap. The other is in a nonradioactive area. The outputs of the probes of both meters have remained stable following the first four days of initial drift. There has been no effect of γ radiation on the probe in the cold-trap room. To date, the γ field has exceeded 1000 R/hr for sixteen days. The maximum estimated field with saturated ^{24}Na at full reactor power is ~10,000 R/hr. [See item (h) below for information on calibration of these meters at ANL-Illinois before they were shipped to the EBR-II Site.]

(g) Hydrogen and Nitrogen in Cover Gas. Concentrations of hydrogen and nitrogen in the primary and secondary argon cover-gas systems are listed in Table I.E.7.

TABLE I.E.7. Hydrogen and Nitrogen in Primary and Secondary Argon Cover Gas (ppm)

	Primary			Secondary		
	High	Low	Average	High	Low	Average
			February			
H_2	65	0	0	590	0	20
N_2	7,200	0	2,100	19,000	200	8,700
			March			
H_2	250	0	20	60	0	25
N_2	8,900	2,000	6,700	11,400	3,600	8,500

(h) Calibration of UNC Oxygen Meters (W. E. Ruther, T. D. Claar, and S. Greenberg)

A pair of UNC oxygen cells scheduled to be installed on the EBR-II secondary sodium system were calibrated at 600°F. Oxygen was added quantitatively to the sodium analytical loop (see Progress Report for January 1968, ANL-7419, p. 25) as sodium hydroxide and removed quantitatively by uranium getter strips. The oxygen content of the sodium was determined by mass balance and checked with a distillation sampler. The cover gas was periodically purged to remove hydrogen derived from the reaction of sodium with sodium hydroxide. In addition, a zirconium trap (at 600°F) was inserted in the loop further to reduce the hydrogen content of the sodium. At this temperature, the zirconium picked up 38% of the hydrogen formed and essentially none of the oxygen added to the system.

The preliminary calibration equations for the UNC cells (based on the assumptions of no uranium loss and oxygen gettering only) are:

Cell TP 285: $\ell nC = 54.2 - 45.0\ V$;

Cell TP 286: $\ell nC = 56.4 - 46.9\ V$,

where C is the oxygen concentration in ppm and V is the true cell output in volts. The theoretical slope at 600°F is $-39.4\ V^{-1}$. At the present time, there is no explanation for the higher values for slope (-45 and $-46.9\ V^{-1}$) found in the ANL work. The UNC cells exhibited no sensitivity to hydrogen.

h. Experimental Irradiation and Testing (R. Neidner)

(i) Experimental Irradiations

Last Reported: ANL-7553, pp. 47-48 (Feb 1969).

Table I.E.8 shows the status of the experimental subassemblies in EBR-II as of March 15, 1969. New experimental subassemblies loaded into the grid for the start of Run 33 were XO21B, XO43, XO50, XO55, and XO57. Subassemblies which have been approved for irradiation since the start of Run 33, and which are to be charged for Run 33B are as follows:

Subassembly Number	Assigned Position	Capsule or Element Content and No. of Each ( )	Experimenter	Approximate Burnup Goal (fuels--a/o) (nonfuels--nvt x 10^{-22})
XO42A	7D5	FFTF Poison Material (7)	PNL	0.5
XO54	4E1	PNL-5, UO_2-25 w/o PuO_2 (37)	PNL	5
XO56	5C2	F9C, UO_2-25 w/o PuO_2 (37)	GE	5

Experimental Subassembly XO18 was removed from the grid for reconstitution; two of the seven Mark-B7 capsules were to be replaced with two new Mark-B7 thermocouple capsules from PNL (BT-3 and BT-4). However, during disassembly of Subassembly XO18, it was found that the hex can enclosing the seven capsules would not slip off. The subassembly was taken to the TAN hot shop, operated by INC, where the can is to be split longitudinally to free the capsules. Reconstitution plans for Subassembly XO18 will be reevaluated after the five capsules to be irradiated further are returned.

Also removed before the start of Run 33 was Subassembly XO52, containing three encapsulated Mark-IA fuel elements.

i. FCF Equipment Improvement (M. J. Feldman)

(i) Process Equipment (R. N. Grant, J. P. Bacca, and V. G. Eschen)

Last Reported: ANL-7548, p. 51 (Jan 1969).

The following pieces of equipment for remote examination or testing of experimental capsules are being fabricated:

(1) Capsule-leak Detector. The capsule will be heated in a chamber, the chamber will be evacuated, and gas removed from the chamber will be analyzed for fission products.

TABLE I.E.8. Status of EBR-II Experimental Irradiations as of March 15, 1969

Subassembly No. and (Position)	Date Charged	Capsule Content and No. of Capsules ( )	Experimenter	Accumulated Exposure (MWd)	Estimated Goal Exposure (MWd)	Approximate Accumulated Peak Burnup (fuels--a/o) (nonfuels--nvt x 10^{-22})
XG03 (7D1)	7/16/65	UO_2-20 w/o PuO_2 (2) Stainless Dummies (17)	GE	20,058	23,300	5.2
XG04 (7B1)	7/16/65	UO_2-20 w/o PuO_2 (2) Stainless Dummies (17)	GE	20,058	45,000	5.2
XA08 (4F2)	12/13/65	UC-20 w/o PuC (8) Structural (9) Structural (2)	ANL ANL GE	16,228	20,700	10.0 6.0 6.0
XO10 (7F3)	3/24/66	UO_2-20 w/o PuO_2 (4) Structural (11) Structural (4)	GE ANL PNL	16,989	20,400	6.3 3.4 3.4
XO12 (4B2)	8/10/66	UO_2-20 w/o PuO_2 (19)	NUMEC	12,828	21,400	7.8
XO15 (4A2)	11/15/66	UO_2-20 w/o PuO_2 (11) UO_2-20 w/o PuO_2 (2) UC-20 w/o PuC (4) U-Fs (Mark IA) (2)	NUMEC GE ANL ANL	11,173	11,500	6.7 6.2 6.8 3.5
XO19 (6D2)	1/13/67	UO_2-20 w/o PuO_2 (7) UC-20 w/o PuC (3) Structural (8) Graphite (1)	GE UNC PNL PNL	9,608	13,000	3.5 4.1 2.6 2.6
XO20 (6B5)	1/13/67	UO_2-PuO_2 (9) UC-20 w/o PuC (3) Structural (4) Structural (2) Graphite (1)	GE UNC PNL ANL PNL	10,021	13,000	3.6 4.2 2.7 2.7 2.7
XO21B (2D1)	2/23/69	Structural (7)	PNL	9,422	23,200	3.9
XO27 (4B3)	11/21/67	UO_2-25 w/o PuO_2 (18) Structural (1)	GE PNL	7,344	7,700	4.5 2.7
XO32 (6E5)	11/22/67	UO_2-25 w/o PuO_2 (19)	PNL	7,647	11,900	3.3
XO33 (5E2)	12/22/67	UC-20 w/o PuC (19)	UNC	6,491	10,900	3.4
XO34 (2F1)	4/13/68	Structural (7)	ORNL	6,873	14,800	2.8
XO35 (7B4)	4/13/68	Structural (7)	ORNL	6,456	44,800	1.4
XO36 (7E1)	7/25/68	UO_2-25 w/o PuO_2 (19)	GE	4,742	33,300	1.3
XO38 (7C5)	5/7/68	Structural (7)	INC	5,947	17,700	1.2
XO40 (5B2)	8/14/68	UO_2-20 w/o PuO_2 (19) UO_2-25 w/o PuO_2 (16)	ANL GE	4,032	7,000	2.0 2.1
XO41 (7A3)	7/24/68	Structural (7)	PNL	4,408	16,700	0.9
XO43 (4D2)	2/20/69	UO_2-25 w/o PuO_2 (37)	GE	458	5,500	0.2
XO44 (7A1)	9/28/68	Oxide Insulator (1)	LASL	3,083	8,100	0.6
XO50 (4C2)	2/23/69	UO_2-20 w/o PuO_2 (4) UO_2-28 w/o PuO_2 (4) UO_2-20 w/o PuO_2 (5) UC-18 w/o PuC (2) Structural (4)	GE GE ORNL W GE	458	7,500	0.2 + 7.7[a] = 7.9 0.2 0.2 0.2 0.2 + 4.7[a] = 4.9
XO51 (3A2)	12/16/68	UO_2-25 w/o PuO_2 (37)	PNL	1,003	16,400	2.0
XO53 (4E3)	11/27/68	Mark II (37)	ANL	1,855	3,800	1.1 + 2.3[a,b] = 3.4
XO55 (6A4)	2/23/69	UC-15 w/o PuC (19)	UNC	458	20,000	0.2
XO57 (2B1)	2/23/69	Structural (7)	PNL	458	15,000	0.2

[a]Previous exposure from another subassembly.
[b]Correction due to recalculation of irradiation-rate factor resulting from power change from 45 to 50 Mwt starting with Run 30.

(2) Bonder and Bond Tester. Capsules will be heated to 400-500°C to dislodge any gas bubbles in the bonding sodium; the completeness of sodium bond and the sodium level will be determined by eddy-current techniques.

(3) Stereomacroscope. A precision indexing stage will be used to place samples remotely under the objective lenses of the 1/2-25-power stereomacroscope.

(4) Dilatometer. A conventional dilatometer will be modified to measure phase transformation (changes in length) of irradiated samples remotely as a function of temperature.

j. Superheater and EM Pump Study and Test (R. A. Jaross and E. Hutter)

(i) Superheater Vibration Study (G. S. Rosenberg)

Last Reported: ANL-7548, pp. 51-52 (Jan 1969).

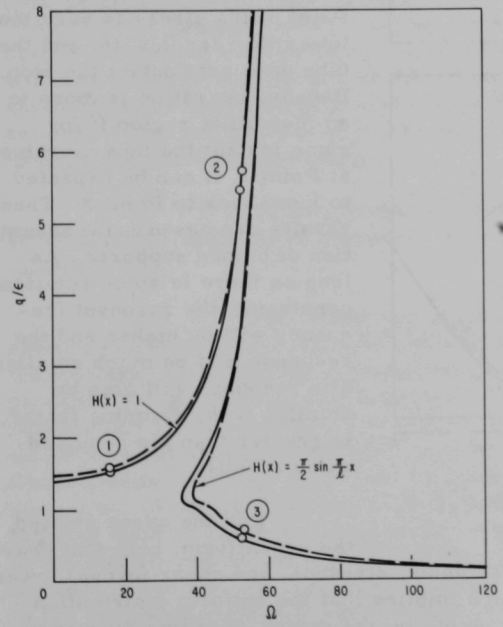

Fig. I.E.1. Amplitude Response of EBR-II Superheater Tubes

The tube-baffle impact effects in the EBR-II superheater are being studied with the aid of a code formulated to compute displacement, shearing force, and bending stress of a pinned-pinned beam with motion-constraint stops. Solutions have been obtained for two crossflow-velocity distributions: a uniform distribution and a half-sine wave; the amplitude-response curves are shown in Fig. I.E.1 for the two distributions.

For the EBR-II superheater, we compute Ω = 16.0 (N_s = 0.2; single-tube value) and Ω = 52.8 (N_s = 0.66; tube-bank value). The procedure is to enter the curves (obtained from a single-mode analysis) of Fig. I.E.1 with the calculated value of Ω and read off the corresponding amplitude value. Then this steady-state amplitude

is used in a multimode analysis to predict bending stress and shearing force. The resulting response curves for Ω = 52.8 (and Operating-point 2 of Fig. I.E.1) are given in Fig. I.E.2 at their extreme conditions.

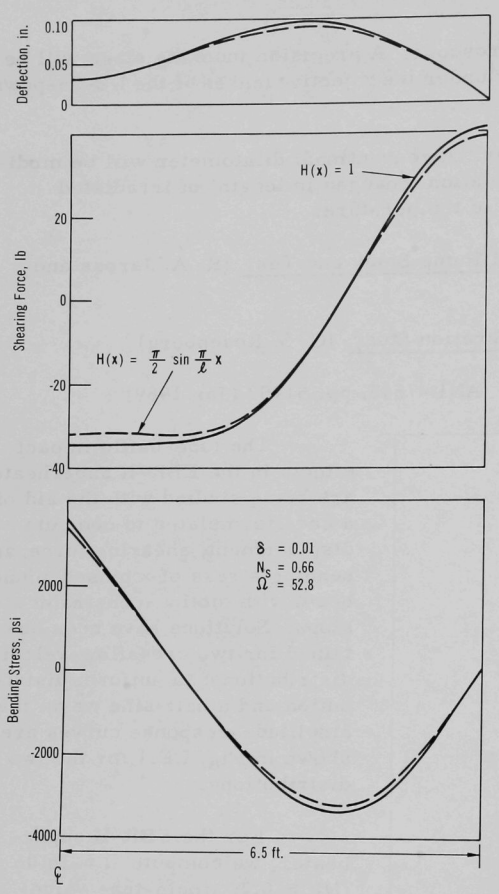

Fig. I.E.2. Dynamic Response of Tube in EBR-II Superheater

For Ω = 16.0 (N_s = 0.2), the maximum stress level was quite low, less than 1000 psi. For Ω = 52.8 (N_s = 0.66), the stresses are significantly higher (see Fig. I.E.2) because the tube is vibrating near a resonant condition (Operating-point 2 of Fig. I.E.1). However, even this situation is less severe than it may seem.

Due to the nonlinearity of the problem, at Ω = 52.8 the tube can vibrate at Operating Points 2 or 3. If it vibrates at Point 3, the stress is very low, lower than for Ω = 16, and the tube does not contact the stop. Because operation is close to an instability region if for some instant the tube vibrates at Point 2, it can be expected to jump back to Point 3. These results are based on the assumption of pinned supports. As long as there is some rotational constraint, the resonant frequency will be higher and the response will be much smaller. The response will also be smaller if the damping factor is greater than the assumed value of 0.01.

For the cases studied, the nonuniform, half-sine-wave distribution gave results (displacements, stresses, and shear forces) lower in magnitude (see Fig. I.E.2) which implies that the uniform distribution might be the conservative case. Actually, the vortex-shedding frequency would probably not be constant over the length of tube, nor would the vortices be in phase. These effects will be included in the study of crossflow-induced vibrations [see Sect. III.C.1.c.(ii)].

k. Feasibility Study of Fuel Failure Detection--Chemical and Mechanical Methods

(i) Trace Elements Analytical Techniques (C. E. Crouthamel)

Last Reported: ANL-7553, pp. 48-49 (Feb 1969).

The major objectives of this part of the fuel-failure detection program are to (1) select suitable sodium-soluble tags for individual subassemblies and (2) devise methods of identifying the tag in the event of fuel failure. The sodium-soluble tags are intended for use in EBR-II subassemblies containing driver fuel or encapsulated experimental fuel. Isotopic tagging has been selected as the most promising approach, and a system of tagging has been devised that involves the use of mixtures of gold and antimony.

In the proposed method, each fuel element in a subassembly would be tagged with the same mixture of ^{121}Sb and ^{197}Au; the weight ratios of ^{121}Sb and ^{197}Au would be varied to produce multiple tags. While in the core of EBR-II, these tag mixtures would be activated to ^{122}Sb (2.8 d) and ^{198}Au (2.7 d). Because of the varying weight ratios, each tag mixture would have a distinctive activity ratio. In the event of a fuel failure, the active isotopes would be discharged to the primary coolant. After appropriate sampling and separation procedures, the ^{122}Sb-^{198}Au activity ratio would be determined by gamma-ray spectrometry, and this ratio would be used to identify the faulty subassembly.

It is believed that the proposed tagging method will overcome several major difficulties connected with the use of sodium-soluble tags, as follows:

(1) One hundred milligrams of tag charged to the bond sodium of a driver fuel element would be below the part-per-billion concentration level when the tag is completely mixed with the primary coolant; detection at this level is a difficult analytical problem. (2) Only a limited number of chemical elements have a solubility such that 100 mg of them would be soluble in the bond sodium at the reactor operating temperature. Consequently, multiple tags must be devised from this limited number of elements. (3) No purification of EBR-II sodium, other than cold trapping, is being done at present. Thus, a tag, once released, will probably remain in the sodium and constitute a potential interference to the identification of the next failed fuel. A discussion of each of these difficulties in relation to the proposed method is given below.

(a) Detection. It has been calculated that the saturation activity of ^{198}Au produced from 1 mg of ^{197}Au in the core of EBR-II at full power will be about 6×10^8 dps (~98% of saturation is achieved in 15 days)

and that the activity produced in one day will be about 1.2×10^8 dps/mg of ^{197}Au. Release of 1 mg of ^{197}Au of the latter level of activity to the 3×10^8 g of sodium coolant will result in a sodium activity level of 0.4 dps/g of sodium. This level of activity should be more than adequate for detection of a 10-g sample after appropriate radiochemical separations have been performed. Calculations of this type for ^{121}Sb are not possible at the present time because its fast capture cross section has not been established.

(b) Number of Tags. A distinct advantage accrues from using the ^{121}Sb and ^{197}Au isotopes as tags because of the similarity in the half-lives of the daughter activities. During irradiation in the core of EBR-II, the ratio of ^{122}Sb to ^{198}Au activities produced will be nearly constant. For example, if one assumes that the saturation activity ratio will be 1.00, the activity ratio after one hour of irradiation will be 1.04, and, thereafter, will approach 1.00. The constancy of the activity ratio will permit numerous tags to be manufactured from these two isotopes. The exact number of tags that can be put into use will depend on the constancy of the ratio of the capture cross sections of ^{121}Sb and ^{197}Au as a function of neutron energy and on the precision of the radiochemical separations used to isolate the active isotopes. It is estimated that at least 10 tags and possibly as many as 100 will be available.

(c) Interference from Previous Tags or Impurities. Until LMFBR technology devises methods of purifying the primary coolant, any tagging method must consider the effects of previously released tags. Most of the potential methods would require purification of the coolant to remove previous tags. However, the proposed method is reasonably free from the effects of previous tags, as discussed below.

A fuel-element tag would reside in the core of the reactor 100% of the time, and as previously stated, would achieve a saturation activity level of about 6×10^8 dps/mg of ^{197}Au. Upon discharge of 1 mg of ^{197}Au to the primary coolant, the activity level of the tag in the sodium would be 2 dps/g of sodium. Any ^{197}Au already in the circulating sodium would spend only about 1/2000th of the time in the core, and the saturation level would be expected to be 3×10^5 dps/mg of ^{197}Au. A simple calculation shows that the circulating sodium must contain approximately 2 g of ^{197}Au before the activity level will be equal to that produced in 1 mg of ^{197}Au tag. Furthermore, a tag that has achieved the saturation activity level of 6×10^8 dps/mg of ^{197}Au in the core will decay rapidly to the lower saturation level of 3×10^5 dps/mg of ^{197}Au once it is released to the sodium.

Efforts will now be concentrated on obtaining the necessary information for further evaluation of the ^{121}Sb-^{197}Au tagging method, namely, data on stability, corrosion behavior, relative fast capture cross sections of ^{121}Sb and ^{197}Au, analytical methods, and methods of introducing the tags into fuel elements.

1. Materials-Coolant Compatibility (D. W. Cissel)

Last Reported: ANL-7548, p. 54 (Jan 1969).

(i) Surveillance Subassemblies (W. E. Ruther, T. D. Claar, and S. Greenberg)

(a) Bend Testing of SURV-I Specimens. The test specimens were fabricated from two pieces of 1/2-in.-thick Type 304 stainless steel plate welded together and then sliced transversely to the weld. The final size of the machined specimens was 3.75 x 0.425 x 0.125 in. Each specimen was supported on two pins separated by $2\frac{1}{2}$ in., and the bending force was applied perpendicularly to the 3.75- x 0.425-in. face of the specimen.

Eight specimens were tested. The force required to deform the specimens 1 in. ranged from 232 to 238 lb. Visual examination of the bent specimens showed no large cracks or other abnormalities. The slight crazing of the metal in bend areas was equivalent to that noted in a normal sheet of Type 304 stainless steel that had been bent under similar conditions.

(ii) Examination of Reactor Parts (W. E. Ruther, T. D. Claar, and S. Greenberg)

(a) Examination of Secondary-system Piping. A short section of 2-in. stainless steel pipe was removed from vent line Na 2-31-549 near the joint with the main secondary-sodium system of EBR-II. Metallographic study of a transverse section of the pipe revealed slight carbide precipitation along the grain boundaries at the inner surface (exposed to sodium) for a depth of 0.001-0.002 in. The inner surface also exhibited some evidence of dissolution of material, especially near areas where the grain boundaries met the surface. A rough inner surface resulted from the nonuniform material loss.

To determine if the precipitates made the grain boundaries susceptible to cracking, a section of the pipe was completely flattened and then re-examined. No evidence of grain-boundary tearing or cracking due to the deformation was noted. A microhardness traverse revealed no significant hardness gradients, either from inner to outer surface or from grain boundary to matrix. Chemical analyses are being made of the inner skin of the pipe (~0.003-in.-deep lathe cut) to confirm the presence of carbon.

(iii) Data Development (F. A. Cafasso)

Last Reported: ANL-7527, p. 66 (Dec 1968).

Type 304 stainless steel, in the form of coils of large [illegible] heated in liquid sodium at 650°C over long-term periods

to determine the distribution behavior of various constituents of stainless steel. The behavior of copper, a tramp metal sometimes present in amounts as high as 0.5%, is of particular interest. The materials are contained in tantalum capsules.

After one month, two of the capsules were opened for analysis, but the sodium from one was inadvertently contaminated during handling. Thus, analytical results are available for only one experiment, and these are as follows:

Metal	Initial Metal Content of Sodium (ppm)	Metal Content of Sodium after 30 days of Heating (ppm)
Copper	0.5	3.0
Iron	0.6	6.0
Chromium	0.1	0.6
Nickel	0.2	0.2
Manganese	0.5	0.5

The copper, iron, and chromium contents of the sodium were significantly increased by the exposure to the stainless steel at 650°C, whereas the nickel and manganese contents were not. Apparently, the leaching of elements from stainless steel by liquid sodium is selective.

Another capsule heated under the same conditions for two months has been opened for analysis. Two additional capsules being heated will be examined after three and six months at temperature.

m. Driver Fuel Transient Performance Studies--TREAT Experiments

Last Reported: ANL-7553, p. 53 (Feb 1969).

(i) Mark IA Fuel TREAT Experiments (A. B. Rothman)

A series of five transients were run on test element E-34 from Subassembly C-169 (see Progress Report for January 1969, ANL-7548, p. 55), leading to destruction on the last transient. High-speed photography from this transient showed that cladding failure was initiated near the bottom of the pin, most probably from expansion of trapped sodium. The failure was very rapid (of the order of milliseconds) and was accompanied by visible expulsion of sodium vapor but apparently no expulsion of fuel. The oscillograph records from the motion transducers in this test series were erratic and difficult to interpret. The nominal burnup of Element E-34 is 1.2 a/o.

n. Systems Engineering (B. C. Cerutti)

(i) Reactor and Primary System Improvements

Last Reported: ANL-7553, p. 54 (Feb 1969).

(a) Removal of Storage-basket Sense Rods (L. P. Cooper)

Three sense rods were originally provided for sensing the height of subassemblies in the storage basket when the basket is raised for fuel handling. These sense rods penetrated the shield plug above the basket. The rods did not perform satisfactorily because of alignment problems; therefore, they were clamped out of the way in 1964, and limit switches were installed on the superstructure to control the basket elevation.

In late 1968, removal of the sense rods was decided on to avert any interference from the rods if the clamps loosened. The rods were removed during the recent shutdown of EBR-II, and shield plugs were installed in the vacated openings.

Only a slight amount of oxide-caused binding was experienced when removing the sense rod over Row 3 (outer row) of the storage basket. However, a considerable amount of rotation and up-and-down movement was necessary when removing the sense rod over Row 1 (inner row) of the storage basket. At only 1 in. from complete removal, the bottom section of the sense rod separated from the upper section. This separation was caused by failure of a Type 420 stainless steel roll pin joining these sections. The bottom section was then secured in the hole by a wedge to eliminate any possibility of the piece returning to the primary tank. A T-handled rod was screwed into the top of this section after tapping with 9/16-in. threads. With lateral motion and a vertical force of approximately 275 lb, the piece was removed. Full-length shield plugs were inserted in the nozzles vacated by the two sense rods.

The sense rod over the middle row of the basket could not be entirely extracted because of oxide-caused binding and the limited amount of stress that could be placed on the roll pins joining the sections of the rod. The upper section of this sense rod was uncoupled and removed; the remainder of the rod was modified in place to form a shield plug.

A metallographic examination was made of the failed roll pin to determine the cause of failure. The fractured surfaces of the pin indicated that the pin was severely cracked prior to its failure. A microscopic examination of the failed piece showed very fine cracks at both the inner and outer surfaces. Some corrosion may have been present.

Hardness readings of 500 BHN indicated that the material was in the fully heat-treated condition. For this hardness, the Metals Handbook (1948 Edition, p. 555) indicates that the total elongation can be as low as 2%, the reduction of area as low as 4%, and the Izod impact strength as low as 10 ft-lb. It could not be ascertained definitely whether the cracks were ductile or brittle, although they appeared to be of the ductile type.

o. Oxide Driver (G. H. Golden)

Last Reported: ANL-7553, p. 57 (Feb 1969).

(i) Doppler Coefficient for a Proposed EBR-II Oxide Core (R. Sehgal)

Two oxide-driver cores have been proposed for the EBR-II. One of these, the 91-subassembly core, has been described in some detail (see Progress Reports for November 1968, ANL-7518, pp. 39-40; December 1968, ANL-7527, pp. 44-45; January 1969, ANL-7548, pp. 57-58). Briefly, this core consists of 91 subassemblies (including the control subassemblies) and is fueled by 20 w/o mixed PuO_2-UO_2. The plutonium contains $\simeq$20 w/o ^{240}Pu, and the enrichment of ^{235}U in uranium is $\simeq$54%. It is proposed to use a nickel-sodium reflector for the oxide-driver core in EBR-II.

With an oxide fuel, the mechanism of prompt shutdown reactivity of fuel expansion (available in a metal fuel) is rather uncertain, and the magnitude of the Doppler coefficient of reactivity for such a concentrated and small oxide core is rather small. It was therefore suggested to investigate the possibility of building in a sufficient Doppler shutdown reactivity coefficient by adding BeO to the 91-subassembly oxide core. For the preliminary calculations, the size of this softer-spectrum PuO_2-UO_2-BeO core was fixed at 127 subassemblies, and the potential target value of the Doppler coefficient of reactivity $[T(\partial k/\partial T)]$ to be attained was $\simeq$0.004. Under these conditions, the linear heat ratings of the fuel and the total fuel inventories (fissile plus fertile) are essentially the same for the 91- and 127-subassembly cores.

Two sets of broad-group cross sections for the 127-subassembly core were derived from runs with the MC^2 code* in homogeneous geometry, using the ENDF/B cross section data** and the resonance elements at temperatures of 700 and 1500°K, respectively. For reference, broad-group cross sections for the 91-subassembly core were also calculated with the MC^2 code, using ENDF/B data and the

* Toppel, B. J., Rago, A. L., and O'Shea, D. M., MC^2, A Code to Calculate Multigroup Cross Sections, ANL-7318 (1967).

** Honeck, H. C., ENDF/B; Specifications for an Evaluated Nuclear Data File for Reactor Applications, BNL-50066 (1966).

resonance elements at 700°K. Cross sections for the nickel-sodium reflector and the depleted-uranium blanket were similarly calculated, but at room temperature and zero buckling.

The SNARG-1D code* was used in calculating the critical composition for the 127-subassembly oxide core in an idealized homogeneous cylindrical geometry with an extrapolated height of ≃60 in. It was found that the critical enrichment of ^{235}U is ≃17.4.

With this critical core composition, more SNARG calculations were made by changing to the 1500°K cross sections for the various resonance isotopes. From the Δk obtained, the values of the Doppler coefficients were calculated, using the assumption that $T(\partial k/\partial T)$ was constant.** The results, listed in Table I.E.9, show that the total Doppler coefficient $T\partial k/\partial T$ is approximately equal to -0.005, that ^{238}U is the contributor of this negative coefficient, and that the positive and negative contributions of the other resonance elements cancel each other.

TABLE I.E.9. Doppler Coefficients for the 127-subassembly Oxide-driver Core for EBR-II; Temperature Change: 700 to 1500°K

Resonance Isotope	Doppler Coefficient $[T(\partial k/\partial T)]$
^{238}U	-0.004916
^{235}U	+0.000266
^{240}Pu	-0.000247
^{239}Pu	-0.000006
^{23}Na	-0.000007
Sum for All Resonance Isotopes	-0.00491

For comparison, the broad-group spectrum of the 91-subassembly core was also calculated with the SNARG-1D code. The median energies for flux, fission, and absorption for this core and the 127-subassembly core are compared in Table I.E.10. It is clear that a very substantial softening of the core spectrum occurs in going from the 91-subassembly core without BeO to the 127-subassembly core with BeO.

*Duffy, G. J., et al., SNARG-1D, A One-dimensional Discrete-ordinate, Transport-theory Program for the CDC-3600, ANL-7221 (1966).

**Froelich, R., and Ott, K., "Results of Doppler Coefficient Calculations for Fast Reactors and Comparison of Different Methods," Proceedings of the Conference on Safety, Fuels, and Core Design in Large Fast Power Reactors, Oct. 11-14, 1965, Part I, p. 440, ANL-7120 (1966).

TABLE I.E.10. Median Energies (keV) for Spectra of the 91-subassembly and the 127-subassembly Oxide-driver Cores

	91-S/A Core	127-S/A Core
Median Energy for Flux	395	155
Median Energy for Fission	340	23.1
Median Energy for Absorption	359	32.5

The preliminary nature of the calculations of the Doppler effect reported here must be stressed. Perhaps the most important shortcoming of the calculations is that the heterogeneity of the cell structure (and perhaps the core structure) of the oxide core was not taken into account. The effect of the heterogeneous self-shielding on the Doppler coefficient of the 127-subassembly core may be large because the spectrum is quite soft. Also, the ENDF/B cross sections may have errors in the range from 1 to 10 keV, from which the most contribution to the Doppler effect comes. Recent results (see ANL-7548, pp. 23-26) have shown large discrepancies between the calculated and measured Doppler coefficients for ^{238}U. Nevertheless, it may be possible to build in a Doppler coefficient $T(\partial k/\partial T)$ of $\simeq$-0.004 by adding BeO to the proposed 91-subassembly oxide-driver core. The result of that, of course, is the substantially softer spectrum obtained in the core, which may or may not be desirable. However, a possible practical approach may be a configuration whose properties are intermediate to those analyzed here.

(ii) Temperature Distribution and Doppler Effect of Mechanically Mixed Oxide Fuels (R. Lo)

To determine the temperature distribution and effective Doppler reactivity effect of a heterogeneous fuel of PuO_2 and UO_2, a transient heat-transfer computer code (THTB) is employed. In thermal modeling of one section of the fuel rod, the diameter of the PuO_2 particles is chosen to be 30 microns and that of the UO_2 particles 600 microns. The contact conductances are taken to be 4000 Btu/(hr)(ft^2)(°F), and the heat-transfer coefficient between the cladding and sodium is taken as 14,000 Btu/(hr)(ft^2)(°F). A trial calculation of steady-state and transient temperature distribution in the PuO_2 and UO_2 fragments is complete.

2. Operations

a. Reactor Plant (G. E. Deegan)

Last Reported: ANL-7553, p. 57 (Feb 1969).

Reactor operation during this reporting period consisted of 458 MWd in Run 33A, the first run after completion of the long shutdown

for maintenance and modifications. This raised the cumulative total of reactor operation to 23,223 MWd.

Fuel handling for Run 33A was completed routinely except for difficulty in releasing control rod No. 5 from its gripper when the platform was raised in handling sequence A. The control-rod subassembly was replaced with another from the basket because the same difficulties had been experienced previously with this rod. No difficulty was experienced with the replaced rod.

After startup on February 25, the reactor was shut down temporarily to adjust the position of the chambers for nuclear channels 7, 7A, 9, 10, and 11, and the special test channel for reactor kinetics monitoring. The reactor was then restarted, and a slow approach to 50 MW was made to check out new instrumentation and system modifications.

On March 3 the reactor was returned to 50 kW for scheduled physics tests. During these tests and subsequent 50-MW operation, six reactor scrams occurred. One was caused by a grounding in the FERD-loop electronics; the others were caused by an indicated high rate of change of primary-sodium flow. One of the latter was traced to a failure in the rate-of-change circuitry; the rest resulted from actual flow perturbations caused by malfunctions of primary-pump control.

The reactor was shut down for about 30 hr so that tests could be conducted in an attempt to simulate the conditions causing the flowrate scrams. During the testing, one of the thyratrons in the pump-control system failed, and a mismatch between the electrical neutral and the panel ground was detected. Both conditions could have contributed to the flow changes noted during this period.

As one corrective measure, the rate-of-change circuit was adjusted so that a 3%/sec rate now has to persist for 350 to 400 msec instead of 100 msec to cause a scram.

Throughout the run, gas samples from the primary tank were analyzed for ^{133}Xe and ^{135}Xe on a routine basis. These samples showed no abnormal activity levels during power operation or after scrams when the primary pumps were shut down.

The reactor was restarted on March 13 and was returned to 50 MW. On March 14 an alarm was received indicating a sodium leak past the first of two rupture disks in the north header of the secondary-sodium system. After confirmation of the signal, the reactor was shut down, and the secondary-sodium system was partially dumped. The leak probe was removed after the rupture disk assembly had cooled to approximately 120°F. Solidified sodium was observed around the probe. The secondary-sodium system was then completely drained and cooled to room temperature.

Postremoval examination of the first disk is in progress. Both disks in the assembly will be replaced. Another rupture-disk assembly, located in the south header of the secondary-sodium system, was inspected by removing the leak probe; no sodium was found.

b. Fuel Cycle Facility (M. J. Feldman)

Last Reported: ANL-7553, pp. 57-69 (Feb 1969).

(i) Fuel Production

(a) Hot Line (N. R. Grant)

Table I.E.11 summarizes production activities for February 15 through March 15, 1969, as well as for the year to date.

Phasing out of hot-line production activities is complete in the argon cell. The fuel elements remaining in the air cell are being processed for use in subassemblies.

(b) Cold-line Production and Assembly (D. L. Mitchell)

Table I.E.12 summarizes production activities for February 15 through March 15, 1969, as well as for the year to date.

Preparation of ingots of 95 w/o uranium-5 w/o fissium (64 w/o ^{235}U) for Mark-II fuel alloy has been started in the alloy-preparation furnace of the cold line. Five Mark-II subassemblies will be made in the cold line. Cold-line equipment has been modified for fabrication and inspection of Mark-II fuel elements.

(ii) Inspection of Vendor Fuel (D. L. Mitchell)

The acceptance rate for the ANL verification inspection of fuel produced by Aerojet-General Corporation has continued to be greater than 95% (see Table I.E.12).

(iii) Surveillance (M. J. Feldman, J. P. Bacca, and E. R. Ebersole)

(a) Chemical Analyses (E. R. Ebersole)

The number of fuel-product analyses of hot-line, cold-line, and vendor-fuel samples made during the reporting period, together with the average values and ranges, are tabulated in Table I.E.13.

TABLE I.E.11. Production Summary for FCF Hot Line

(Decanning, melt refining, and injection-casting steps have been discontinued)

	2/15/69 through 3/15/69	Total This Year
Subassemblies received		
Core, control, and safety	9	11
Other	2	4
Subassemblies dismantled for surveillance or examination	6	34
Subassemblies transferred		
To reactor	11	11
To L&O vault and interbuilding corridor for storage	0	0
Subassemblies transferred to ICPP for storage	0	1
Subassemblies returned from ICPP storage	0	2
Subassemblies fabricated	4	12
Processing		
Elements processed		
Accepted	566	1115
Rejected	127	291
Elements welded	884	1419
Elements rewelded	0	0
Elements leaktested		
Accepted	854	1353
Rejected	52	63
Elements bonded (including recycle)	1064	1905
Elements bondtested		
Accepted	551	1392
Rejected	36	144
Elements to surveillance	364	1138
Number from subassemblies	4	29
Fuel-alloy and Waste Shipments		
Cans to burial ground	3	9
Oxide and glass scrap to ICPP	0	2
Recoverable fuel alloy to ICPP		
Fuel elements	4 (69 kg of alloy)	10 (173 kg of alloy)
Subassemblies	1 (5.9 kg of alloy)	1
Nonspecification material	1 (18 kg of alloy)	4 (71 kg of alloy)

TABLE I.E.12. Production Summary for FCF Cold Line

	2/15/69 through 3/15/69	Total This Year
Alloy-preparation runs	0	1
New fuel	4	5
Remelts	4	6
Total		
Injection-casting runs	0	8
Pins processed		
Accepted	0	758
Rejected	0	22
Elements welded	867	1,909
Elements rewelded	0	0
Elements leaktested		
Accepted	669	1,509
Rejected	39	40
Elements bondtesting		
Accepted	572	1,374
Rejected	106	224
Subassemblies fabricated (cold-line fuel)	3	3
Elements received from vendor	5,074	14,837[a]
Inspected and accepted	3,446	11,736[a]
Inspected and rejected	186	946
Subassemblies fabricated (vendor fuel)	1	1
Total elements available for subassembly fabrication as of 3/15/69		
Cold-line fuel	1,402	
Vendor fuel	10,910	

[a]Total includes figures for 1968.

TABLE I.E.13. Analyses of Fuel-product Samples

Analyzed for	Number of Analyses	Average Value	Range
Total U	5	94.04 w/o	93.37-95.16
^{235}U (% of total U)	4	52.20 w/o	52.02-52.31
Mo	4	2.48 w/o	2.36-2.59
Ru	3	1.87 w/o	1.85-1.89
Rh	3	0.273 w/o	0.265-0.279
Pd	3	0.183 w/o	0.181-0.185
Zr	20	0.056 w/o	0.024-0.098
Nb	7	0.008 w/o	0.007-0.010
Si	8	370 ppm	200-590
Al	5	93 ppm	87-104
Cr	3	74 ppm	63-82
Fe	3	441 ppm	395-497
Ni	3	152 ppm	145-162
C	2	239 ppm	237-241
Total Analyses	73		

Analyses for surveillance of irradiated pins from the reactor during the reporting period are as follows:

Analyzed for	Number of Analyses	Average Value	Range
Rh	2	0.328 w/o	0.279-0.376
Zr	20	0.132 w/o	0.086-0.194
Nb	20	0.009 w/o	0.004-0.012
Si	19	344 ppm	97-605
Al	3	451 ppm	122-617
C	5	293 ppm	148-425
Tc	5	217 ppm	189-240
Burnup	18	1.35 a/o	0.83-2.00
Total Analyses	92		

(b) Postirradiation Analysis of EBR-II Fuel (J. P. Bacca)

(1) Cold-line Fuel Surveillance. Ten surveillance subassemblies (five core-type and five inner-blanket type), which comprise Phase II of the overall surveillance program, are being irradiated in the EBR-II core.

(2) Driver-fuel Silicon-surveillance Program. Postirradiation swelling determinations were made on elements from driver-fuel-surveillance Subassemblies B-3030, C-2163, C-2112, and C-2119. Fuel burnup for the subassemblies was approximately 1.2 a/o. The data obtained showed that U-5 w/o Fs driver fuel having silicon contents ranging to 920 ppm has swelling characteristics similar to those observed in the past for low-swelling fuel (silicon content of 200-500 ppm). From these latest data, it appears that the silicon specification for driver fuel can be widened from the currently used range of 280-520 ppm of silicon to one which specifies an upper limit of approximately 900 ppm of silicon.

Fuel composition and irradiation-swelling data for the key surveillance subassembly (C-2163) of the program are presented in Table I.E.14. The amount of irradiation swelling of each of the five casting batches of fuel represented in the subassembly, whose silicon contents range from 250 to 920 ppm, is almost the same. Furthermore, the amount of swelling ($4\frac{1}{2}$ to $6\frac{1}{2}$%) for all batches is very similar to that observed in the past for low-swelling fuel following comparable burnup (see ANL-7553, p. 72, Fig. I.E.10).

TABLE I.E.14. Fabrication and Irradiation Data for Silicon-surveillance Driver-fuel Subassembly C-2163

Injection-casting Batch No.	Silicon Content of Fuel (ppm)	Number of Elements	Element-burnup Range (a/o)	Total Volume Swelling of Fuel (ΔV/V, %)	
				Average	Range
4265	250	27	1.15-1.23	5.13	4.55-5.87
4266	370	25	1.18-1.20	5.11	4.42-5.72
4262	462	2	both 1.22	4.79	4.63-4.95
4263	835	3	1.18-1.22	5.75	5.60-5.94
4264	920	34	1.17-1.22	5.89	4.80-6.56

(3) Driver-fuel Extended-burnup Program. Four subassemblies containing low-swelling fuel (silicon > 200 ppm) are being irradiated to a target burnup of 1.5 a/o. Another subassembly (B-362), also containing low-swelling fuel, is being irradiated to a target burnup of 1.75 a/o. In addition, Subassembly C-2065, which contains both low- and high-swelling fuel, is being irradiated to a target burnup of 1.5 a/o.

(c) Materials Surveillance and Compatibility Studies
(J. P. Bacca, R. V. Strain, C. L. Meyers, and S. T. Zegler)

(1) Examination of Chrome Plating on Lower Adapters. Several sections cut from two irradiated lower adapters have been examined metallographically to determine the thickness of the chrome plate remaining after reactor service. One of the adapters was from the safety-rod thimble from Position 3D1, which had been exposed to primary sodium for 50,520 hr. The other adapter was from Subassembly C-2027, which had been exposed to primary sodium for 16,656 hr. Chrome plating was present in all areas examined.

No data were available on the thickness of the chrome plating on these adapters before irradiation, so no quantitative measure of any chromium loss could be made. The thickness of the plating was found to be slightly less than the minimum specified (0.0005 in.) on certain areas of both of the irradiated adapters. The thickness was 0.00037 in. near the flow holes and 0.00050 in. near the spherical radius on the lower adapter from Subassembly C-2027. The thickness was 0.00045 in. near the flow holes and 0.00055 in. near the bottom of the outside surface of the lower adapter from the safety-rod thimble.

The planned irradiation of two nickel surveillance subassemblies that contain several chrome-plated rings will make it possible

to obtain quantitative data on the loss of chromium. These subassemblies will be placed into the reactor soon.

(2) Thermal Expansion and Thermal-cycling Behavior of U-5 Fs Alloy Driver-fuel Pins. The purpose of this project was to determine if anisotropic thermal expansion may have contributed to the slightly larger-than-normal axial growth noted recently in pins from Batch No. 0456 as a result of irradiation.

Preliminary findings from dilatometric studies indicate that in the as-sodium-bonded condition, pins from the batch are completely transformed to the alpha-uranium structure and have a thermal-expansion behavior closely similar to that of an alloy having a randomly oriented microstructure. Thermal-cycling data are consistent with this; during 800 cycles between 100 and 520°C and also between 100 and 620°C, no thermal-cycling growth was observed to occur. Anistropic thermal expansion is thus largely, if not entirely, precluded as a cause of the axial growth noted during irradiation.

Presented in Table I.E.15 are dilation data and linear thermal-expansion coefficients determined in dilatometric studies.

TABLE I.E.15. Thermal-expansion Data for U-5 Fs Alloy Batch No. 0456[a]

Temperature (°C)	Dilation[b] (in./in. x 10^4)	Thermal-expansion Coefficient[c] [(in./in.)/°C x 10^6]
100	12.95	12.95
200	27.88	13.94
300	43.82	14.61
400	59.75	14.94
500	78.67	15.73

[a]Data were obtained on heating and cooling twice at a rate of 1°C/min between room temperature (25°C) and 500°C. No thermal-cycling growth was observed after either cycle.

[b]$\frac{L_t - L_0}{L_0}$, where L_t = length at temperature and L_0 = length at 0°C.

[c]Mean thermal-expansion coefficient between 0°C and indicated temperature on heating and cooling $\left(\frac{L_t - L_0}{L_0 \times \Delta T}\right)$.

(iv) Experiment Handling and Interim Examination
(V. G. Eschen and N. R. Grant)

Subassembly XO52, containing three encapsulated Mark-IA elements, was dismantled in the Fuel Cycle Facility (FCF).

Subassembly XO18, containing seven materials capsules, was received by the FCF. When its hex tube was being removed, the grid bars broke loose from the grid, allowing the capsules to remain in the tube. Rather than risking possible damage to the capsules by forcibly removing the hex tube, the subassembly was transferred to TAN, where the tube will be slit longitudinally. A hex-tube slitter is being fabricated for use in the air cell if this occurs in the future.

Subassembly XO42, containing seven materials capsules, was received and dismantled. Two of the capsules, containing boron carbide, were neutron radiographed, and these plus two others were shipped to the experimenter (PNL). The three other capsules together with four new capsules were reloaded into the reconstituted subassembly (XO42A) and returned to the reactor.

Subassembly XO50 was fabricated in the air cell and transferred to the reactor. It contains four irradiated oxide and four irradiated structural capsules from Subassembly XG05 and nine new oxide and two new carbide capsules.

The following experimental subassemblies were fabricated with new capsules and transferred to the reactor:

XO43 (F37) GE Group F9A mixed oxides

XO54 (F37) PNL Series 5 mixed oxides

XO55 (A19) UNC mixed carbides

XO56 (F37) GE Group F9C mixed oxides

XO57 (B7) PNL Structural

PUBLICATIONS

^{252}Cf Half-Life Determined by Neutron Counting
A. DeVolpi and K. G. Porges
Inorg. Nucl. Chem. Letters 5, 111-113 (1969)

The Bimodal Decay of Two Pulsed-Neutron-Coupled Cores of an Organic-Mediated and -Reflected System
U. Farinelli* and N. Pacilio
Nucl. Sci. Eng. 36, 39-46 (April 1969)

Efficient Programming in FORTRAN
C. E. Cohn
Software Age 2(5), 22-31 (June 1968); also FORTRAN-IV Programming for Engineers and Scientists, Ed. P. W. Murrill and C. L. Smith. Intern. Textbook Co., Scranton, Pa., 1968, Ch. 10

*Comitato Nazionale Energia Nucleare, Rome.

Resonance Moderation of Neutrons in Weakly Absorbing Mixtures
M. Segev
Nucl. Sci. Eng. 36, 59-66 (April 1969)

Application of Statistical Theory and Multilevel Formalism to Doppler Effect Analysis--II
R. N. Hwang
Nucl. Sci. Eng. 36, 82-96 (April 1969)

Application of Statistical Theory and Multilevel Formalism to Doppler Effect Analysis--I
R. N. Hwang
Nucl. Sci. Eng. 36, 67-81 (April 1969)

Error Estimated for Iterative Unfolding
R. Gold and E. F. Bennett
J. Comput. Phys. 3(2), 167-175 (October 1968)

Transfer and Analysis of Highly Radioactive Materials in a Shielded Electron Microprobe
R. Natesh, B. J. Koprowski, E. M. Butler, and D. A. Donahue
Proc. 16th Conf. on Remote Systems Technology, Am. Nucl. Soc., Idaho Falls, March 11-13, 1969, pp. 243-252

Compatibility of Vanadium Alloys with $(U,Pu)O_2$ and (U,Pu)C
T. W. Latimer
J. Metals 21, 107A (March 1969) Abstract

EBR-II Fuel Handling Equipment
J. R. Davis
Proc. 16th Conf. on Remote Systems Technology, Am. Nucl. Soc., Idaho Falls, March 11-13, 1969, pp. 161-173

Some Future Potentialities of Neutron Radiography
J. P. Barton, H. Berger, and D. C. Cutforth
Proc. 16th Conf. on Remote Systems Technology, Am. Nucl. Soc., Idaho Falls, March 11-13, 1969, pp. 276-288

EBR-II Intrasite Spent-Fuel Shipping Casks
R. F. Malecha, L. F. Coleman, P. Fineman, A. S. Kelecius, and M. A. Slawecki
Proc. 16th Conf. on Remote Systems Technology, Am. Nucl. Soc., Idaho Falls, March 11-13, 1969, pp. 205-211

Start-up of Shielded Fuel Evaluation Facility
J. O. Ludlow, L. F. Coleman, T. W. Eckels, J. E. A. Graaee, L. E. Ross, and M. A. Slawecki
Proc. 16th Conf. on Remote Systems Technology, Am. Nucl. Soc., Idaho Falls, March 11-13, 1969, pp. 56-61

Operating Experience with an Argon Atmosphere at the Fuel Cycle Facility
D. C. Hampson, W. L. Sales, and L. F. Coleman
Proc. 16th Conf. on Remote Systems Technology, Am. Nucl. Soc., Idaho Falls, March 11-13, 1969, pp. 91-111

II. OTHER FAST REACTORS--CIVILIAN--OTHER FAST BREEDER REACTORS

A. Fuel Development

1. Fuel Jacket Alloy Studies

a. Mechanical Properties of Fuel-jacket Alloys (F. L. Yaggee)

Last Reported: ANL-7553, pp. 73-74 (Feb 1969).

(i) Effect of Flowing Sodium on the Creep of Vanadium Alloys. The creeptests of two specimens of V-15 w/o Cr-5 w/o Ti alloy in flowing sodium at 650°C terminated in specimen failure after an exposure of 495 hr. Both specimens failed within 1 hr of each other. Specimens 2-V-15 and 3-V-15 were tested under uniaxial stresses of 50,000 and 47,060 psi, respectively, instead of the 42,600 psi previously reported for both specimens in ANL-7553. The surface-to-volume ratio (expressed as $in.^2/in.^3$) per unit length of specimen was ~110:1, and lineal sodium velocity past the specimen was calculated to be ~2.8 m/sec. The cold-trap temperature was maintained throughout the test at about 105°C.

The specimens exhibited a steady-state creeprate ($\dot{\epsilon}$) of 2×10^{-5}/hr, which persisted in both for more than one-half of the total exposure time. This creeprate was established in specimen 2-V-15 after about 6 hr and in specimen 3-V-15 after about 160 hr (specimen 3-V-15 was pre-exposed for 96 hr in flowing sodium at 650°C before the stress was applied). Both specimens exhibited a total fracture strain of slightly less than 1%, of which more than one-half was uniform strain.

Corrosion specimens exposed to the flowing sodium during the creeptests are being examined and evaluated, and a quantitative evaluation of the sodium purity (ppm oxygen) is being made.

Cycling of the output of the sodium flowmeter, which resulted in the apparent temperature fluctuations previously reported in ANL-7553, decreased to an insignificant level after about 400 hr. This cycling has been attributed to gas (argon) entrapped in the sodium.

b. Irradiation Studies of Fuel-jacket Alloys (R. Carlander)

Last Reported: ANL-7527, p. 81 (Dec 1968).

(i) Effects of Irradiation of Type 304 Stainless Steel. The effects of irradiation on the tensile properties of Type 304 stainless steel irradiated in EBR-II were examined. The specimens were taken from the

hexagonal guide tubes of EBR-II Subassembly XG05 and from an EBR-II safety rod; peak fluences of 5 x 10^{22} and 1 x 10^{23} n/cm^2, respectively, were calculated for the two structures.

The tensile tests were conducted at 450°C at a strain rate of 1%/min. The preliminary results presented in Figs. II.A.1-II.A.3 also include the results of previous tensile tests with specimens from the guide thimble of EBR-II control rod 12 irradiated to a calculated peak fluence of 5 x 10^{22} n/cm^2. The results of the previous experiments indicated that low irradiation temperatures, ~371°C, gave larger yield strengths and smaller uniform strains than the values obtained for higher irradiation temperatures (see Progress Report for July 1968, ANL-7478, Table I.E.6, p. 56). However, when the results from the tests of the three irradiated materials were compared in Fig. II.A.1, the mechanism that may govern the effects of irradiation temperature on the yield strength of Type 304 stainless steel could not be clearly ascertained. Similarly, Fig. II.A.2 shows that increases in the uniform strain of Type 304 stainless steel may not be a simple function of increased irradiation temperature.

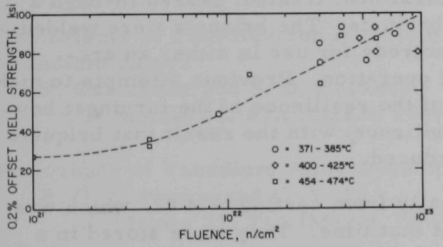

Fig. II.A.1. Effect of Fluence and Irradiation Temperature on the 0.2% Offset Yield Strength of Irradiated Type 304 Stainless Steel

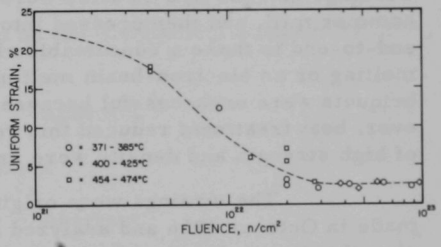

Fig. II.A.2. Effect of Fluence and Irradiation Temperature on the Percent Uniform Strain of Irradiated Type 304 Stainless Steel

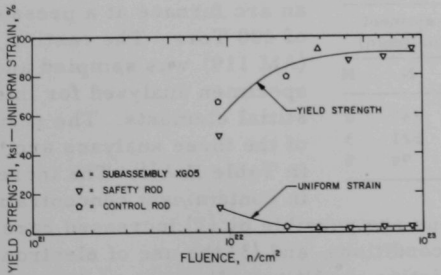

Fig. II.A.3

Effect of Fluence on the Tensile Properties of Type 304 Stainless Steel Irradiated at 371-385°C

The effect of fluence on the yield strength and the uniform strain of Type 304 stainless steel was not significant below fluences of approximately 5 x 10^{21} n/cm^2 (see Figs. II.A.1 and II.A.2). This might imply that a certain incubation period is necessary for a buildup of dislocation loops. These loops have been shown to be the main matrix strengthener in this range of irradiation temperatures* (371-480°C).

At higher fluences and low irradiation temperatures (371-385°C), the yield strength and the uniform strain of the irradiated stainless steel appeared to saturate at about 90,000 psi and at 1-2%, respectively (see Fig. II.A.3). A similar analysis for higher-temperature specimens (454-474°C) was not possible since there were no specimens available that had been irradiated to fluences >5 x 10^{22} n/cm^2.

c. Fabrication Development of Fuel-jacket Alloys
(N. J. Carson, Jr.)

Last Reported: ANL-7548, pp. 78-81 (Jan 1969).

A technique was developed to recycle vanadium-alloy scrap. Turnings of V-20 w/o Ti alloy were first heat treated, passed through a hammer mill, and then pressed into briquets. The briquets were welded end-to-end to make a consumable electrode for use in either an arc-melting or an electron-beam melting operation. Previous attempts to make briquets were unsuccessful because of the resilience of the turnings; however, heat treatment reduced this resilience, with the result that briquets of high strength and density were produced.

The turnings were originally from casting AM 82, which was made in October 1966 and analyzed at that time. They were stored in a closed but unsealed container for two years before being taken out for briqueting. The turnings were cleaned in acetone, heat treated for 1 hr at 900°C, and passed through a hammer mill. At this point a sample was removed for analysis and the remainder were briqueted. The briquets were melted in an arc furnace at a pressure of 400 Torr. The casting (AM 119) was sampled and the specimen analyzed for interstitial elements. The results of the three analyses are listed in Table II.A.1. The increase in contaminant concentration is small; even lower concentrations are possible by (1) increased care in machining, (2) improved storage conditions, and (3) the use of electron-beam melting. Even under the existing conditions, direct recycling of some vanadium alloy scrap appears to be feasible.

TABLE II.A.1. Impurity Concentration in Recycled Vanadium Alloy

Material Analyzed	Interstitial-element Concentration (ppm)			
	C	O	N	H
AM 82 (Original Casting)	198	720	147	4
Turnings	410	1200	221	3
AM 119 (Recycled Metal)	430	500	94	5

*Carlander, R., Harkness, S. D., and Yaggee, F. L., The Effect of Fast Neutron Irradiation on the Microstructure and Mechanical Properties of Type 304 Stainless Steel, to be published in J. Nucl. Mater.

PUBLICATIONS

Fabrication of Vanadium Alloy Tubing
N. J. Carson and F. J. Karasek
J. Metals 21, 108A (March 1969) Abstract

The Effects of Fast Neutron Irradiation on the Tensile Properties of Type 304 Stainless Steel
R. Carlander and S. D. Harkness
J. Metals 21, 44A (March 1969) Abstract

Precipitation Kinetics and Morphology at Grain Boundaries
P. G. Shewmon
J. Metals 21, 12A (March 1969) Abstract

Creep of Vanadium to $0.8T_m$
K. R. Wheeler, E. R. Gilbert,* F. L. Yaggee, and S. A. Duran**
J. Metals 21, 74A (March 1969) Abstract

The Effects of Fast Neutron Irradiation on the Mechanical Properties of Vanadium Alloys
R. Carlander and S. D. Harkness
J. Metals 21, 63A (March 1969) Abstract

Philosophy of Vanadium Alloy Development
P. G. Shewmon and C. Y. Li
J. Metals 21, 73A (March 1969) Abstract

*Battelle Northwest Laboratory.
**Washington State University.

III. GENERAL REACTOR TECHNOLOGY

A. Applied and Reactor Physics Development

1. Theoretical Reactor Physics--Research and Development

a. Reactor Computations and Code Development (B. J. Toppel)

Last Reported: ANL-7553, p. 76-80 (Feb 1969).

(i) Argonne Reactor Computation System. Testing of the one-dimensional perturbation-theory module and its associated standard path, PERT1D, continues. Problems were run to test the performance of the module with respect to: perturbations in the atom densities of isotopes in a material, perturbations in the volume fractions of materials in a composition, and perturbations in the assignment of compositions to regions. The description of the critical, reference reactor is given in ANL-7553.

The results of the computations for perturbations in the atom densities of isotopes in materials are given in Table III.A.1 along with the results of diffusion-theory calculations. In problems 4 and 5, the agreement between perturbation theory and diffusion theory is excellent. In problems 7 and 8 the great discrepancy is due to the limitations of perturbation theory. The addition of huge amounts of fissile material in region 4 (see ANL-7553, Table IV.A.1, p. 77) greatly alters the flux distributions, whereas perturbation theory is based on the assumption of only small perturbations.

TABLE III.A.1. Results of Isotope Perturbations

		Perturbed		$\Delta k/k^2$	
Problem	Material[a]	Isotope	Concentration (10^{24} atoms/cm^3)	PERT1D	PATH1D
4	M1	53	0.00015	0.0023298	0.0023962
5	M2	55	0.0010426	-0.0234203	-0.0234902
6	M8	37	0.0	-0.0047456	-0.0031934
		38	0.0		
		39	0.0		
7	M9	53	0.05	0.0050273	>2
8	M1	53	0.0015	-0.0208842	>2
	M2	55	0.0010426		
	M8	37	0.0		
		38	0.0		
		39	0.0		
	M9	53	0.05		

[a]See Progress Report for February 1969, ANL-7553, Table IV.A.2, p. 78.

The results of the computations for perturbations in the volume fractions of materials in a composition are given in Table III.A.2. Here the agreement between perturbation theory and diffusion theory is inconsistent. For two problems the agreement is good, but for two problems there is even disagreement as to the algebraic sign of the perturbation. It is difficult to explain these results in terms of the assumptions of perturbations. Therefore, the possibility of errors in PERT1D cannot be predicted.

TABLE III.A.2. Results of Composition Perturbations

Problem	Perturbed			$\Delta k/k^2$	
	Composition	Material[a]	Volume Fraction	PERT1D	PATH1D
9	C1	M1	0.5	-0.00027826	0.0018637
10	C2	M2	1.05	0.0249018	0.0218170
11	C3	M8	0.5	-0.0017729	0.0002159
12	C4	M2	1.0	0.0000913	0.0000614
		M9	1.25		
13	C1	M1	0.5	0.0229420	0.0241185
	C2	M2	1.05		
	C3	M8	0.5		
	C4	M2	1.0		
		M9	1.25		

[a]See Progress Report for February 1969, ANL-7553, Table IV.A.2, p. 78.

It is not permitted to perturb the placement of compositions in the reactor by changing the mesh spacing. Therefore perturbations of this kind must be made by changing the assignment of compositions to regions. For these problems the reactor was divided into more regions as shown by Table III.A.3. The results of these calculations are tabulated in Table III.A.4. As before, there is not always acceptable agreement between diffusion theory and the perturbation module, and it is difficult to ascribe the discrepancy to the limitations of perturbation theory.

TABLE III.A.3. Region-assignment Perturbations

Region	Outer Radius (cm)	Standard Composition
1	54.0	C1
2	56.8325	C1
3	59.3	C2
4	137.63	C2
5	181.8767	C3
6	218.0	C4
7	227.5967	C4

TABLE III.A.4. Results of Composition Perturbations

Problem	Region	Composition		$\Delta k/k^2$	
		Standard	Perturbed	PERT1D	PATH1D
14	2	C1	C2	0.0055936	0.0067420
15	3	C2	C1	-0.0068648	-0.0062211
16	2	C1	C2	-0.0012712	0.0004562
	3	C2	C1		
17	3	C2	C4	-0.0121118	-0.0054122
18	7	C4	C5[a]	-0.0007077	0.0000046

[a]C5 is ^{10}B with an atom density of 10×10^{24} atoms/cm^3.

More problems will be run to test PERT1D with respect to region-dependent buckling perturbations for rectangular coordinates and with respect to material perturbations resulting in perturbations in the chi matrix.

In the problems in which perturbation-theory calculations were compared with diffusion-theory calculations, we were unable to determine if the discrepancies arise from the assumptions of perturbation theory or from flaws in the perturbation module. Therefore these problems will be run on the fully operational perturbation-theory code, PERC. Discrepancies between the results of PERT1D and of PERC calculation can be ascribed to flaws in PERT1D.

(ii) The ARC System. The four modules that comprise the MC^2 capability in the ARC system on the IBM System/360 are available for production use and are being extensively tested for reliability. All of the ENDF/B Category 2 data for neutron cross sections are available, and all of the input options available with the MC^2 standard paths are being validated. At the present time, 60% of the testing is complete.

The various standard-path capabilities that exist in the ARC system with regard to MC^2 variants (see Table III.A.5) are also being tested on a production basis over the full range of input options.

TABLE III.A.5. Standard Paths Related to MC^2

	Standard-path Module	Capability
Multigroup Cross Sections	STP007	Complete MC^2 problem
Resonance Cross Sections	STP008	Calculate resolved and unresolved resonance cross sections only
Spectrum Average and Group Collapsing	STP009	Generate smooth cross sections and a fundamental-mode spectrum, and collapse to a broad-group set. Uses previously generated resonance cross sections.
Group Collapse	STP010	Generate broad-group set using previously generated data and spectrum
Multigroup Cross-section Sets	STP015	Invokes STP007 followed by repeated invocations to STP009. This uses one set of resonance data for several spectra and broad-group generations.

2. Nuclear Data--Research and Development

a. Cross Section Measurements (C. E. Crouthamel and N. D. Dudey)

Last Reported: ANL-7527, pp. 95-96 (Dec 1968).

(i) Integral Cross Section Measurements. The analyses of Ti, V, S, Fe, Ni, Co, Sc, Cu, and Au samples irradiated in the EBR-II Dosimetry Test experiment have been completed. Preliminary values of the spectrum-averaged reaction rates for most of the measured reactions are summarized

in Table III.A.6. These reaction rates are expressed as the number of atoms produced in the reaction per 10^9 atoms of target material (ppb) per megawatt-day and are reported for four different radial positions within the core of EBR-II. Further analysis of these data, in terms of spectrum-averaged cross sections or reactor flux levels, is awaiting completion of a transport-theory calculation of the spectral shape of the neutron distribution at each of the radial positions.

TABLE III.A.6. EBR-II Spectrum-averaged Reaction Rates

Reaction	Reaction Rate (ppb/MW-day) at Indicated Radial Position			
	5.9 cm	15.6 cm	27.0 cm	31.2 cm
$^{54}Fe(n,\gamma)^{55}Fe$	30.3	28.2	18.6	16.2
$^{62}Ni(n,\gamma)^{63}Ni$	27.8	27.3	22.5	19.4
$^{45}Sc(n,\gamma)^{46}Sc$	51.1	51.9	44.1	30.3
$^{58}Fe(n,\gamma)^{59}Fe$	14.1	13.6	11.0	9.1
$^{59}Co(n,\gamma)^{60}Co$	52.9	48.0	42.0	35.2
$^{63}Cu(n,\gamma)^{64}Cu$	-	64.0	59.7	-
$^{197}Au(n,\gamma)^{198}Au$	809	786	606	567
$^{54}Fe(n,p)^{54}Mn$	57.1	56.5	30.0	11.7
$^{58}Ni(n,p)^{58}Co$	84.3	76.0	45.2	15.7
$^{46}Ti(n,p)^{46}Sc$	7.4	7.0	3.9	1.4
$^{47}Ti(n,p)^{47}Sc$	16.0	14.7	8.7	3.2
$^{48}Ti(n,p)^{48}Sc$	0.19	0.17	0.10	0.03
$^{59}Co(n,p)^{59}Fe$	0.99	0.93	0.56	0.17
$^{63}Cu(n,p)^{63}Ni$	18.0	15.9	9.9	3.6
$^{32}S(n,p)^{32}P$	12.8	11.6	6.9	2.52
$^{54}Fe(n,\alpha)^{51}Cr$	0.62	0.61	0.34	0.11
$^{58}Ni(n,\alpha)^{55}Fe$	3.3	2.8	3.8	0.6
$^{50}V(n,\alpha)^{47}Sc$	0.78	0.32	0.23	0.11
$^{51}V(n,\alpha)^{48}Sc$	0.02	0.014	0.008	0.003
$^{63}Cu(n,\alpha)^{60}Co$	0.37	0.31	0.20	0.07

Determinations of alpha (capture-to-fission cross-section ratios) for 65 samples of ^{233}U, ^{235}U, ^{238}U, ^{239}Pu, ^{240}Pu, and ^{242}Pu are continuing. With the exception of the final mass-spectrometric results, the analyses of the ^{233}U samples have been completed. An electroplating

apparatus (see Progress Report for January 1969, ANL-7548, p. 84), now being assembled, is expected to provide an improved method of sample preparation for alpha spectrometric measurements of the reaction products.

Samples of Ti, V, S, Fe, Ni, Co, Sc, Cu, Cr, and Au have been prepared and encapsulated for an irradiation in ZPR-3.

(ii) Low-mass Fast-neutron Fission Yield. The equipment for the identification of low-mass particles has been completed and calibrated. The system was tested in a series of irradiations with the Tandem Accelerator, in which C, Au, ^{62}Ni, and ^{60}Co targets were bombarded with protons and alpha particles. The particle resolution of the system was tested by irradiating ^{62}Ni with protons and ^{60}Co with alpha particles; the low-mass products ^{1}H, ^{2}H, ^{3}H, and ^{4}He were clearly separated. The energy range and calibration were checked by scattering alpha particles by gold targets, and the detection efficiency was confirmed by measuring the known cross section of the ^{12}C(p,p') reaction. These experiments demonstrated that the required dynamic range of the particle identification system was achieved; specifically, the system will simultaneously identify all particles of masses 1 to 6 having energies between 5 and 40 MeV.

Irradiations of ^{235}U and ^{239}Pu will be carried out in the Physics Division's Dynamitron. However, since a delay is anticipated because the Dynamitron is not yet completed, an experiment is being designed to measure the low-mass particles produced in the ^{232}Th(α,f) reaction. This reaction, when compared with the ^{235}U(n,f) reaction, should provide valuable information about the mechanism of third-particle fission. Both reactions produce the same compound nucleus, ^{236}U*, and the excitation energies of the fissioning compound nuclei in the two reactions can be made identical by controlling the energies of the incident particles. The only difference will be the higher angular momentum imparted in the ^{232}Th(α,f) reaction. It is expected that the tritium yield per fission will be approximately the same for the two reactions; therefore, the ^{232}Th(α,f) measurement should provide good estimates of tritium production in LMFBRs using ^{235}U fuel.

3. Burnup Analysis and Fission Yields for Fast Reactors (R. P. Larsen)

a. Determination of the Absolute Fast Fission Yields of Burnup Monitors and Nonfission Nuclear Transformations in a Fast Reactor

Last Reported: ANL-7548, p. 83 (Jan 1969).

An experiment is being designed to measure the effective capture-to-fission ratio (alpha) for three isotopes: ^{239}Pu, ^{233}U, and ^{235}U. This will be accomplished by an irradiation in a critical facility having a neutron spectrum that emphasizes the 10-keV region, in which the greatest

uncertainty in the alpha exists. The basic concept is to perform an irradiation of sufficient length (~5 days) to produce (1) a change in the ^{240}Pu, ^{234}U, and ^{236}U contents that can be measured mass spectrometrically and (2) an amount of a fission product isotope (^{140}Ba) that can be adequately measured by gamma spectrometry. The number of captures will be determined from the change in ^{240}Pu, ^{234}U, or ^{236}U content, and the number of fissions from the ^{140}Ba content and a factor that relates the ^{140}Ba content to the number of fissions.

Preparations are being made for a short irradiation (~2 hr) which will provide data for establishing the factor that relates ^{140}Ba counts to the number of fissions (see Progress Report for November 1968, ANL-7518, p. 81). The materials to be irradiated include (1) fission foils (~15-mg disks of each fissionable isotope identical to the disks that will be used in the long irradiation) and (2) fission track counters. The fission track counters consist of mica disks alternately stacked with platinum disks on which are mounted nanogram amounts of the fissionable isotope being investigated. The fission foils will be assayed for ^{140}Ba and the fissionable isotope; the number of fission tracks on the mica disks will be counted under a microscope. The ^{140}Ba-to-fission factor will be calculated from the ^{140}Ba counts, the number of fission tracks, and the weights of the fissionable isotope in the fission foils and fission counters.

In the preparation of fission track counters, the nanogram amounts of fissionable isotopes must be deposited very uniformly on the platinum plates, and the amount of fissionable isotope on each plate must be determined accurately. Uniform deposition will be achieved by extracting the fissionable isotope into hexone, pipetting small drops of the hexone onto the platinum plate, and evaporating to dryness (see ANL-7518, p. 82). The amount of ^{239}Pu, ^{233}U, or ^{235}U on each plate will be determined by alpha counting.

The specific activity of ^{239}Pu ($t_{1/2} = 2.4 \times 10^4$ yr) is high enough that nanogram amounts can be assayed with the requisite accuracy by alpha counting. However, the specific activities of ^{233}U and ^{235}U ($t_{1/2} = 1.6 \times 10^5$ and 7×10^8 yr, respectively) are lower, and the alpha assays of nanogram amounts are not of comparable accuracy. The specific activities of the ^{233}U and ^{235}U solutions were, therefore, increased by the addition of radiochemically pure ^{232}U ($t_{1/2} = 72$ yr). (The small amounts of ^{232}U on the plates of the fission track counters will not have a significant effect on the determination of the number of fissions of ^{233}U or ^{235}U.)

Radiochemically pure ^{232}U was prepared by an ion-exchange separation of the ^{232}U from the numerous short-lived daughters with which it is associated. The impure ^{232}U solution was made 6N in HCl and passed through a small Dowex-1 column. The ^{232}U was absorbed on the column and subsequently eluted with 0.1N HCl. Of the active daughters originally

present, only ^{212}Pb (11 hr) accompanied the ^{232}U. The ^{212}Pb was allowed to decay by allowing the solution to stand for 3 days. At the end of this period, the ion-exchange procedure was repeated to separate the ^{232}U from the small amount (~1%) of ^{228}Th that had grown in during the ^{212}Pb decay period.

b. Supplemental Determination of Absolute Fission Yields of Burnup Monitors for Fast Reactor Fuels

Last Reported: ANL-7527, pp. 97-98 (Dec 1968).

The techniques that have been developed for the measurement of alpha for ^{239}Pu, ^{233}U, and ^{235}U (see Sect. a, above) are being evaluated as a means for determining the absolute fast-fission yields of burnup monitors. In the method under consideration (see ANL-7527) two irradiations in EBR-II will be required: one of about 2-hr duration at a power level of 50 kW and the other of sufficient duration (90-120 days) at full power to produce samples having a burnup of 1 to 2%. In the 2-hr irradiation, fission track counters and fission foils will be used to provide data for establishing a factor relating the count rate of a particular fission product, e.g., ^{144}Ce ($t_{1/2}$ = 285 days), to the number of fissions that occurred. Included in the full-power irradiation will be gram amounts of the fissionable isotopes, which will be subsequently analyzed for ^{144}Ce and the fission product burnup monitors of interest. The number of fissions that occurred in each material will be calculated from the ^{144}Ce analysis and the previously established ^{144}Ce-to-fission factor. It is expected that the number of fissions and, hence the fission yields, can be determined with an accuracy of ±1%, which is comparable to the accuracy expected from the irradiations now being performed in EBR-II (see Progress Report for January 1969, ANL-7548, p. 83).

The major advantage of the new approach is that the need for lengthy irradiations (4 to 5 yr) of the type now being carried out in EBR-II will be obviated. Thus, fast-fission yields can be readily measured at a given position in a particular reactor. The method would also make it practical to determine fission yields as a function of the neutron energy spectrum of the reactor of interest, if such data were required.

An evaluation of this technique will be made by determining the yield of ^{137}Cs from the thermal fission of ^{235}U. This method of evaluation was chosen because (1) the ^{137}Cs yield from the thermal fission of ^{235}U has been more accurately established than any other fission yield, (2) reliable methods for determining ^{137}Cs are well established, and (3) an excellent ^{137}Cs standard is available.

4. Reactor Code Center (M. Butler)

Last Reported: ANL-7553, p. 80 (Feb 1969).

Five program packages have been added to the Code Center library: -- [illegible] ENDL, the experimental neutron-data library and its associated

service routines, developed for the IBM 7094 by R. Howerton and associates at Livermore; No. 358, TWOTRAN, a two-dimensional multigroup transport solution for xy geometry programmed for the UNIVAC 1108, by K. D. Lathrop, LASL; Nos. 360 and 361, the TOR and GLEN programs for calculating the thermal-neutron-scattering cross sections for crystalline materials (TOR) and from these the thermal-neutron diffusion length and group-averaged cross sections (GLEN) for transport programs. These two programs were written for the CDC-6600 by W. W. Clendenin, LASL; an IBM 360 version of the two-dimensional multigroup diffusion code CRAM received from the Australian Atomic Energy Commission.

B. Reactor Fuels and Materials Development

1. Fuels and Cladding

a. Research and Development

(i) Behavior of Reactor Materials

(a) Fuel Element Behavior Modeling--Effect of Local Thermal Stresses on Pore Deformation and Migration (R. W. Weeks and C. Y. Li)

Not reported previously.

A preliminary study of the influence of local thermal stresses on pore deformation and migration in ceramic fuel elements has been completed. The distribution of local thermal stresses* was incorporated into an analysis of pore migration by the evaporation-condensation mechanism** in ceramic fuels.

The relative effect of the distribution of local thermal stresses was found to be quite small for the typical conditions of oxide fuel elements. In addition, the influence on pore deformation and migration was in the same direction as predicted by the evaporation-condensation mechanism, i.e., the pore tends to elongate along the temperature gradient.

Although the local-stress effect is small for the conditions of interest for oxide fuel elements, this effect may well be of significance in studies of voids subjected to thermal gradients in other systems.

---

*Florence, A. L., and Goodier, J. N., J. Appl. Mech. 26, 293 (1959).

**Nichols, F. A., J. Nucl. Mater. 27, 137 (1968).

(ii) Thermodynamics of Fuel Materials

(a) Vapor Species Partial Pressures in the Ternary U-Pu-C System (P. E. Blackburn and J. E. Battles)

Last Reported: ANL-7527, p. 100 (Dec 1968).

Mass-spectrometric studies of the volatilization behavior of the U-Pu-C system are being conducted to determine (1) the composition of the vapor phase in equilibrium with the condensed phase(s), (2) the partial pressures of the vapor species as a function of temperature, and (3) the thermodynamic properties of the vapor species and condensed phases.

The binary Pu-C system is being investigated first to establish the relationships between the vapor and condensed phases. These relationships will be helpful in the study of the ternary system.

According to the Pu-C phase diagram,* which is based mainly on the original work of Mulford et al.,** there are, at selected temperatures, five thermodynamically invariant two-phase fields consisting of solids only: Pu_3C_2 + PuC,† PuC + Pu_2C_3, Pu_2C_3 + C, Pu_2C_3 + PuC_2, and PuC_2 + C. The condensed system Pu_3C_2 + PuC exists only at low temperatures (<575°C). The condensed systems PuC + Pu_2C_3 and Pu_2C_3 + C are stable from room temperature to approximately 1654 and 1750°C, respectively. The condensed systems Pu_2C_3 + PuC_2 and PuC_2 + C are stable only at temperatures above 1750°C. However, more recent data referenced by Rand†† indicate that the eutectoid decomposition of PuC_2 occurs at 1660 ± 15°C, rather than at 1750°C. In fact, the precise homogeneity ranges and temperature dependency of all the phases, except those of PuC around 600°C, have not been firmly established. For this study and in accordance with the present tentative phase diagram, we have assumed that the phase boundaries for Pu_2C_3(s) and PuC_2(s) are very narrow and independent of temperature.

Mass-spectrometric analysis of the vapor phase in equilibrium with the condensed systems Pu_2C_3 + C, Pu_2C_3 + PuC_2, and PuC_2 + C in the temperature ranges 1365 to 1659°C, 1659 to 2026°C, and 1659 to 2075°C, respectively, showed that Pu(g) was the predominant vapor species. No evidence was found for PuC(g) or PuC_2(g) over the condensed

---

* Livey, D. T., and Fischotte, P., Atomic Energy Review 4, Special Issue No. 1, 53 (1966).

** Mulford, R. N. R., Ellinger, F. H., Hendrix, G. S., and Albrecht, C. D., Plutonium 1960, Cleaver-Hume Press, London (1961), p. 301.

† It should be noted that the designation PuC represents a compound with a fairly wide range of composition, but less than the stoichiometric value.

†† Rand, M. H., A Thermochemical Assessment of the Plutonium-Carbon System, presented at a panel meeting, September 1968, IAEA, Vienna.

systems Pu_2C_3 + C and Pu_2C_3 + PuC_2, which indicated that their abundance in the vapor phase was less than 0.1% at the higher temperatures. $PuC_2(g)$ was detected in the vapor phase over condensed PuC_2 + C (<0.1% at about 2000°C). Olsen and Mulford* reported about 0.1% of $PuC_2(g)$ in the vapor phase over condensed Pu_2C_3 + C at 1717°C. From our mass-spectrometric data, X-ray diffraction and chemical analyses of sample residues, and the phase diagram, we assume that vaporization of Pu(g) is the result of the reactions

$$1/2\ Pu_2C_3(s) = Pu(g) + 3/2\ C(s), \tag{1}$$

$$2Pu_2C_3(s) = Pu(g) + 3PuC_2(s), \tag{2}$$

and

$$PuC_2(s) = Pu(g) + 2C(s), \tag{3}$$

although, as noted above, the exact composition of each of the condensed phases is unknown.

Tungsten effusion cells were used in both the temperature-dependency and the rate-of-effusion measurements. Some reaction between the tungsten cell and sample was observed at temperatures near 2075°C, which caused a reduction from 2.2 to 1.9 in the atom ratio of carbon to plutonium. No reaction was observed at temperatures up to 2025°C.

The enthalpies of reaction calculated from the slope of the log IT versus 1/T data (see Progress Report for April 1968, ANL-7445, p. 124-127) for reactions (1), (2), and (3) are, respectively, 98.1 ± 1.1 (four series of measurements), 118.7 ± 2.3 (five series of measurements), and 88.3 ± 0.6 (three series of measurements) kcal/mol Pu(g).

Vapor pressures of 5.11×10^{-6} atm at 1854°C for reaction (2) and 3.62×10^{-6} atm at 1897°C for reaction (3) were determined from measurements of the rate of mass effusion (weight-loss method). When these values for the vapor pressures and the slopes derived from the temperature-dependence data are used to evaluate the intercepts, the following equations for the vapor pressures as a function of temperature are derived for reactions (1), (2), and (3), respectively:

$$\log P(atm) = \frac{-21{,}440 \pm 240}{T} + 4.560 \pm 0.120\ (1365\text{-}1659°C), \tag{4}$$

*Olsen, W. M., and Mulford, R. N. R., "Thermodynamics of Plutonium Carbides," Thermodynamics of Nuclear Materials, IAEA, Vienna (1967), p. 467.

$$\log P(atm) = \frac{-25,950 \pm 500}{T} + 6.910 \pm 0.190 \quad (1659\text{-}2026°C), \qquad (5)$$

and

$$\log P(atm) = \frac{-19,300 \pm 120}{T} + 3.450 \pm 0.060 \quad (1659\text{-}2075°C). \qquad (6)$$

The errors indicated for the intercepts of Eqs. (4), (5), and (6) are the standard deviations in the slopes combined with an estimated standard deviation of 7% in the measurement of mass-effusion rates.

The eutectoid temperature, i.e., the temperature at which $Pu_2C_3(s)$, $PuC_2(s)$, and C(s) are in equilibrium, was determined to be 1659°C. This temperature was obtained from the intersections of the log IT versus 1/T data for the binary systems PuC_2 + C and Pu_2C_3 + C (2 experiments: 1679 and 1610°C, C/Pu ~2.5) and for the binary systems Pu_2C_3 + C and Pu_2C_3 + PuC_2 (1696°C, C/Pu ~1.8), and from the additional temperature (1651°C) calculated by equating the vapor pressures given in Eqs. (5) and (6) for the binary systems Pu_2C_3 + PuC_2 and PuC_2 + C. The eutectoid temperature of 1659°C, obtained from the average of the four values given above, supports the recent value of 1660 ± 15°C reported by Rand. The vapor pressure reported in Eq. (4) for the Pu_2C_3 + C system was obtained by equating the vapor pressure for this system with that for the PuC_2 + C system at 1659°C. This method was selected since the rate of effusion in the Pu_2C_3 + C system is not sufficient for accurate measurement by the weight-loss method using our present equipment.

2. Radiation Damage on Structural Materials--Research and Development--In-Reactor Creep Studies

a. Void Formation and Growth (S. D. Harkness)

Last Reported: ANL-7553, pp. 86-88 (Feb 1969).

(i) Results of Immersion Density on Safety-rod Guide Thimble. Immersion densities have been measured for three flats of a safety-rod guide thimble irradiated in EBR-II position 3-D-1 to a peak fluence (total neutrons/cm^2) of 10^{23} n/cm^2. The largest observed density change was 4.1%, for a fluence of 9.1×10^{22} n/cm^2 and a calculated irradiation temperature of 413°C. A number of axial measurements of the two flats were made, and peak swelling occurred at a position that compromised the neutron exposure with rising irradiation temperature.

Prior to the density measurements, all samples were electropolished to eliminate surface contamination. Table III.B.1 presents the density results as a function of axial position along each flat. Figure III.B.1 presents a comparison of the data with the predicted swelling profiles that

were generated by a computer routine based on a nucleation and growth model* of void formation. The model predicted the correct position of maximum swelling and gave good quantitative agreement with the density results. No adjustable parameters were used in the computer routine other than those established during earlier work with a control-rod thimble irradiated in position 5-C-12 in EBR-II (see Progress Report for October 1968, ANL-7513, pp. 107-110).

TABLE III.B.1. Results of Immersion Density of a Safety-rod Guide Thimble

Distance from Midplane (in.)	Flat	Estimated Irradiation Temp[a] (°C)	Estimated Total Fluence x 10^{-22} (n/cm^2)	Density[b] (g/cm^3)	Density[c] Change (%)
Control		-	-	7.8950	-
30.5	D	446	0.5	7.91	0
7.3	D	418	5.6	7.75	1.9
3.9	D	407	9.1	7.60	3.7
0.7	D	396	10.0	7.69	2.6
2.5	D	385	9.1	7.84	0.6
8.5	D	371	2.7	7.85	0.5
14.8	D	371	1.4	7.87	0.4
2.0	F	410	9.1	7.64	3.2
24.5	A	460	0.5	7.85	0.5
13.5	A	480	1.6	7.82	0.9
7.3	A	426	5.6	7.70	2.5
3.9	A	413	9.1	7.57	4.1
0.7	A	401	10.0	7.79	1.3
14.8	A	371	1.4	7.44	0.4

[a]Derived from the calculations of R. Cushman, ANL-EBR-II, Idaho.
[b]±0.02%.
[c]±0.3%.

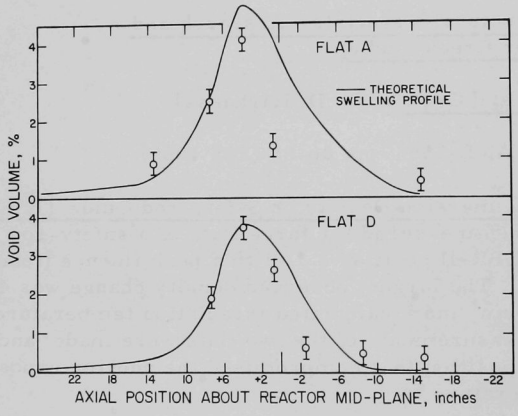

Fig. III.B.1

Comparison of Experimental and Predicted Swelling Profiles for Two Flats of a Safety-rod Guide Thimble Irradiated to a Peak Fluence of 10^{23} n/cm^2

*Harkness, S. D., and Li, C. Y., A Model for Void Formation in Metals Irradiated in a Fast Neutron Environment, to be presented at the IAEA Symposium on Radiation Damage in Reactor Materials, Vienna, Austria, June 2-6, 1969.

b. Effects of Irradiation on the Thermal Diffusivity and Thermal Conductivity of Reactor Materials (R. A. di Novi)

Last Reported: ANL-7478, pp. 98-99 (July 1968).

The postirradiation thermal diffusivities and thermal conductivities of six Type 304 stainless steel specimens obtained from Flat F of Subassembly XG05 have been measured. This material was irradiated to a peak fluence of 5×10^{22} n/cm^2 at an estimated irradiation-temperature range from 410 to 430°C. A final analysis of these measurements is not yet complete, but the results indicate that, within the experimental accuracy of the method (5%), no change occurred in the thermal properties of Type 304 stainless steel irradiated to this level. These results are consistent with irradiation-induced change in density of this flat, 0.8-1%.

3. Techniques of Fabrication and Testing--Research and Development

a. Nondestructive Testing--Research and Development

(i) Development of Nondestructive Testing Techniques (C. J. Renken)

Last Reported: ANL-7548, pp. 95-98 (Jan 1969).

(a) Development of an Electrodynamic Ultrasonic Transducer. Although the contactless electrodynamic transducer for the generation and detection of ultrasound in metals has potential application for use in thermally and radioactively hot environments, the large size of the magnet now required to supply the magnetic fields prohibits the use of this technique for in-reactor work. However, since nondestructive in-reactor tests and surveillance are to be performed with reactor components that are to a large extent ferromagnetic, recent development efforts have concentrated on a magnetostrictive transducer.

The difference between the magnetostrictive transducer under development and existing transducers of this type is that the tested material (stainless steel components of a reactor) forms part of the transducer. Initial tests were made with stainless steel and nickel rods, 30.0 cm long and 1.5 cm in diameter. A bank-wound, double-layer pancake coil of approximately 1.5-cm diameter was mounted on the rods and insulated with tape, 0.007 cm thick. The detector, a PZT-4 piezoelectric transducer, was positioned on the other end of the rod. The ultrasonic signals that were generated in the stainless steel rod when a pulse of current passed through this coil are shown in Fig. III.B.2.

The reverse of this effect (the magnetoelastic effect) can be used through induction in the coil to detect the ultrasound. However, this effect is small in stainless steel, and attempts to detect ultrasound with

the coil have been unsuccessful. Coils of other designs and preamplifiers for the receiving coil have been constructed, and they are presently under evaluation.

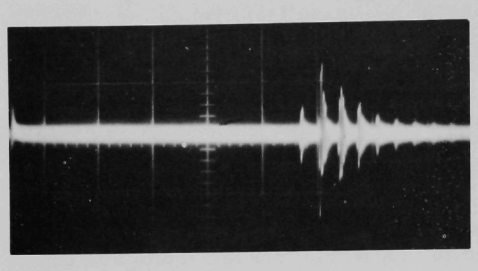

Fig. III.B.2
Ultrasonic Pulses Generated by the Magnetostrictive Transducer on a Type 304 Stainless Steel Rod. The initial pulse is on the left of the figure, and the detected reflections from the end of the rod are on the right (scale--0.05 V/cm, 10 μsec/cm).

(b) Feasibility Study of Ultrasonic Inspection of Sodium Bond in Capsules. The study of the feasibility of applying ultrasonics to the detection of nonwet areas (outer-jacket ID) in EBR-II Mark-II capsules continues.

A dc recorder board was purchased and installed in the Magnaflux PS-902 ultrasonic instrument. This addition to the ultrasonic system allows the production of pen recordings.

Several dummy capsules were inspected in the high-temperature facility (110°C) at a frequency of 5 MHz. The focused transducer probe was positioned normal to the capsule. Four longitudinal scans (90° apart) of each capsule were recorded, and a 2-cm pen deflection was achieved when the scan passed from the plenum to the sodium. Large pen fluctuations were noted in most of the sodium-filled areas, which indicates that the ultrasonic system is detecting nonwet areas in the capsules.

Dummy capsules with outer jacket-wall thicknesses of 0.254 mm are being fabricated for correlation purposes. These capsules will be inspected by ultrasonics, eddy currents, and X-radiography prior to destructive examination.

(c) Development of a High-temperature Piezoelectric Transducer. A gold-nickel alloy was used successfully to braze a Z-cut lithium niobate crystal, about 1 mm thick, to a container diaphragm and a backing plate, both of which were constructed of Type 304 stainless steel. Prior to the brazing operation, the crystal surfaces had been coated with a Au-Pt-Pd metal paste and fired in an oxygen furnace. This partially assembled transducer probe was able to detect and generate ultrasonic signals in a water tank. Assembly of the probe has been completed, and further proof-tests have been conducted. The maximum operating temperature of this type of probe will be determined in a sodium tank.

C. Engineering Development

1. Research and Development

a. Instrumentation and Control

(i) Boiling Detector (T. T. Anderson, B. B. Spillane, R. H. Selner, and S. L. Halverson)

Last Reported: ANL-7553, p. 96 (Feb 1969).

(a) Acoustic Method

(1) High-temperature Detector Development. An experimental high-temperature acoustic sensor has been tested in water to determine its frequency response to pressures in the range from 20 to 100 kHz. Signals were detectable in the range from 50 to 90 kHz; a pronounced resonance occurred at 75 kHz. Sensor sensitivity at the peak of the resonance was -117 db (relative to a reference level of 1 $V/dyne/cm^2$) with 10 ft of connecting cable to the preamplifier. Additional tests are planned to determine bond integrity and transducer sensitivity in liquid sodium. When a supply of premium-grade lithium niobate is received, it will be used to fabricate additional sensors.

(2) Irradiation Tests of Piezoelectric Materials. Preliminary design of heated specimen holders is underway. Specifications are being prepared for an immittance bridge for piezoelectric measurements.

Problems associated with experimental evaluation of lithium niobate as a piezoelectric transducer material in a liquid-metal (>650°C) high-gamma ($>10^8$ R) environment are being defined by study of previous related work. The experimental program can follow either of two approaches: (1) a phenomenological approach to specific crystal cuts and transducer designs or (2) evaluation of twelve crystallographic constants from measurements on rotated-crystal cuts. These methods are being examined for applicability to the program objectives. Measurements of immittance can yield some of the applicable constants. The Smith-chart format for immittance measurement is being investigated.

(3) Sound Measurements in EBR-II. Acoustic tests have been completed on the Core Components Test Loop (CCTL) to corroborate results obtained from tests on the EBR-II. The signals from the two accelerometers mounted on the CCTL pump flange and from the accelerometer mounted at the sodium-sampling line were recorded on tape. Acoustic spectra (0-10 and 0-100 kHz) retained the same basic shape, changing only in amplitude with reduced flowrate.

A significant test result was the appearance of discrete acoustic pulses of approximately 10-kHz content near 60% flowrate. Each burst had a duration of 10-30 msec, corresponding to a liquid-volume reverberation. Apparently, the continuous acoustic emission at higher flowrates is the superposition of many individual acoustic bursts. Thermal-expansion noise, observed by turning off line heaters, was of larger amplitude and lower repetition rate. To test the possibility of gas-entrainment causing these noises, a small amount (< 100 cm^3 at 1 atm) of argon was injected through a new sample line; the only observed effect of the entrained gas was to reduce overall noise level whenever loop flowrate was perturbed by presence of a gas pocket.

(4) Heater Tests for Sodium-boiling Detection. To develop the technology of sodium-boiling detection, it is desirable to simulate boiling of sodium in tests with a blocked-flow dummy subassembly. To simulate boiling from fuel pins, a 0.5-in.-OD, 12-in.-long heater is being used to boil sodium in a narrow annulus. The heater was installed in an EBR-II-type hexagonal-can assembly, with an evacuated canister between the annulus and the can to provide thermal insulation. Thermocouples installed at the bottom, midplane, and top of the heater indicated that thermal convection was higher than anticipated; the top-to-bottom temperature difference varied eightfold with heater power according to the relationship $\Delta T = 290 P^{0.61}$, where T is in °F and P is in kW; the exponent can be obtained theoretically in terms of natural-circulation turbulent flow of the sodium for changing specific heat and density. The acoustic sensors were accelerometers mounted on a 0.5-in. waveguide and on the containment flange. Nonboiling tests were successful at heater powers to 2.5 kW and a sodium temperature of 450°F. When system temperature was gradually raised to 800°F for the boiling tests, the heater lead opened before power could be applied. Although boiling was not achieved in the heater test, the thermal time constants and flow-performance data will be used to specify reliable heaters for future tests.

b. Heat Transfer and Fluid Flow

(i) Fog Flow Heat Transfer and Fluid Flow (R. P. Stein)

Last Reported: ANL-7513, pp. 114-116 (Oct 1968).

In droplet "diffusion" studies in the Fog Flow Test Facility, hot-wire anemometer measurements are being made downstream from a source of liquid droplets in turbulent pipe flow (see Progress Report for December 1967, ANL-7403, p. 115).

Consider the radical distribution of droplet mass-flux measured at a distance d downstream from a source of droplets as shown in Fig. III.C.1. Assume that the local mass flux is proportional to the local

concentration. Let this "source" distribution be f(r). If the droplet flow downstream of z = 0 can be described by a turbulent "diffusion" model with constant diffusivity, then the concentration distribution at z = z can be written as*

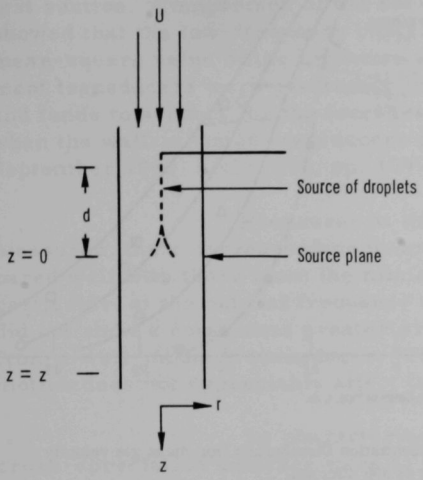

Fig. III.C.1. Flow Geometry

$$\phi(r,z) = \frac{N(r,z)}{N(0,z)} = \frac{\int_0^\infty f(r')r'\,dr'\, I_0\left(\frac{rr'}{2\frac{\epsilon}{U+u_t}z}\right)\exp\left[-\frac{r^2+r'^2}{4\frac{\epsilon}{U+u_t}z}\right]}{\int_0^\infty f(r')r'\,dr'\exp\left[-\frac{r'^2}{4\frac{\epsilon}{U+u_t}z}\right]},$$

where ϵ is the "particle diffusivity," U the mean gas velocity, and u_t the droplet terminal velocity.

Measurements of f(r) and $\phi(r,z)$ are being made. Data are being reduced by assuming a value of $\epsilon/(U+u_t)$, using the experimentally determined f(r) to compute $\phi(r,z)$, comparing the calculated and experimentally measured $\phi(r,z)$, and determining the value of $\epsilon/(U+u_t)$ that best fits the computed and measured $\phi(r,z)$. This method is being used for each axial location at which measurements are made. It is desired to learn whether a single value of $\epsilon/(U+u_t)$, independent of z, can be used to predict the quantity $\phi(r,z)$ downstream from the "source" plane z = 0.

Typical results of measurements are shown in Fig. III.C.2, together with the calculated $\phi(r,z)$. The resulting values of $\epsilon/(U+u_t)$ obtained for each curve are shown in Table III.C.1.

TABLE III.C.1.
Diffusivity Data[a]

$\epsilon/(U+u_t)$ (ft)	z (ft)
0.000030	4.0
0.000038	8.0
0.000025	20.0

[a]For U = 25 ft/sec, u_t = 13 ft/sec, Reynold's No. = 125,000, and drop size = 350 μ.

A model has been proposed to describe the statistical behavior of particles in turbulent flow (see Progress Report for March 1968, ANL-7438, pp. 105-106). For large u_z, the "particle diffusivity" was found to be

$$\frac{\epsilon}{U+u_t} = \frac{\overline{v^2}}{u_t^2}L,$$

where L is a turbulent integral scale. With a typical experimental result for $\epsilon/(U+u_t)$, the integral scale can be deduced for the conditions

*Carslaw, H. S., and Jaeger, J. C., Conduction of Heat in Solids, Oxford University Press, p. 260 (1959).

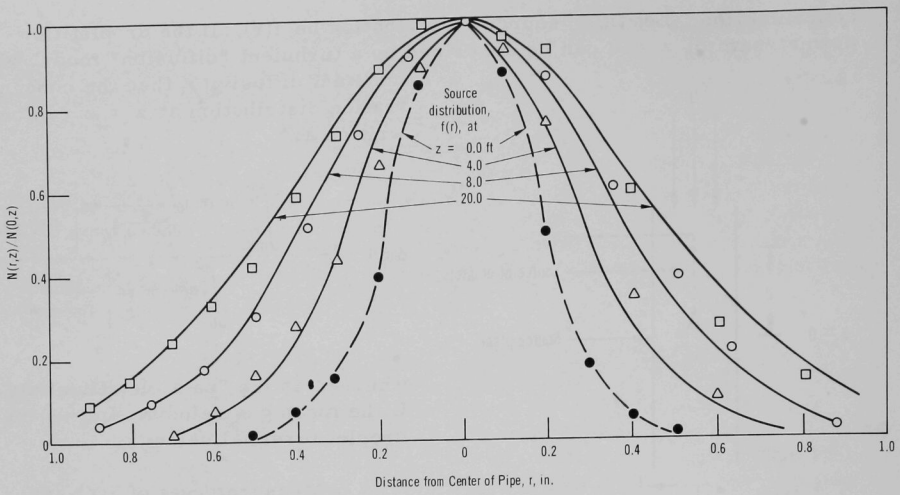

Fig. III.C.2. Experimental and Computed Concentration Distributions (for mean gas velocity U = 25 ft/sec and drop diameter of 350 microns).

presented in Table III.C.I. For this case, L = 0.02 ft. If one assumes that the integral scale is roughly half the duct radius,* for this system L = 0.16 ft. Calculations of L, based on Laufer's energy-spectrum measurements,** are being made to obtain a more definitive estimate of this integral scale. At present, however, it appears that the experimentally determined integral scale agrees, within an order of magnitude, with the rough estimate made above.

Experiments are continuing to cover a range of drop sizes and air-flow conditions.

c. Engineering Mechanics

(i) Structural Dynamics Studies--Parallel-flow-induced Vibrations (M. W. Wambsganss, Jr.)

Last Reported: ANL-7548, pp. 101-103 (Jan 1969).

(a) Structural Dynamics Test Loop. Design of the large loop and specification of components continues. Construction start will be delayed because of deferment of purchasing until July.

(b) Flowtest Single Cylinders. Flowtests were performed with a stainless steel rod instrumented with flush-mounted miniature pressure transducers. The data were processed on a spectrum analyzer; cross-correlation of the pressure-time signals was attempted.

*Hinze, J. O., Turbulence, McGraw-Hill Publishing Co., p. 535 (1959).

**Laufer, J., The Structure of Turbulence in Fully Developed Pipe Flow, NACA Report 1174 (1954).

Tests were run with and without displacement transducers, which acted as turbulence generators, mounted on the wall of the test section. Comparison of the corresponding spectral-density curves showed that the low-frequency contribution (attributed to turbulence) to the mean-square value of the pressure was slightly greater when the displacement transducers were protruding into the flow field. This was expected and tends to account for the increased test-element displacement measured when the wall-mounted transducers are in place (see Progress Report for September 1968, ANL-7500, pp. 109-110).

Pressures at the wall of the test section also were measured; their corresponding mean-square-value spectral densities compared well with those from the miniature rod-mounted transducers. In particular, at the natural frequency of the rod, the rod-mounted transducers did not show a component greater or significantly different from that obtained from a wall-mounted transducer. This supports the assumption that rod motion does not appreciably affect the surface pressure field.

To characterize the convecting random pressure field, cross-correlation analyses were to determine convection velocities, eddy decay-life, and correlation lengths. However, interpretation is difficult because of the pump-caused low-frequency acoustic noise in the test section. Specifically, for cross-correlations between closely spaced transducers, the long wavelengths of the pressure pulsations at the pump vane-passing frequency, running-speed frequency, and harmonic of the running speed tend to mask the desired correlation results associated with turbulence. The new pump and test loop should alleviate these difficulties.

(c) Damping Analysis. Experiments were performed to obtain a quantitative understanding of how water flow velocity influences the effective damping characteristics of a cylindrical rod. Modal magnification factors were measured using an internally mounted eddy-current proximity transducer. Preliminary results show that the effective damping increased significantly with mean axial flow velocity. Further tests with a tube instrumented with a miniature accelerometer will allow larger input amplitudes and variations.

(ii) Structural Dynamics Studies--Crossflow-induced Vibrations (M. W. Wambsganss, Jr. and S. S. Chen)

Last Reported: ANL-7548, pp. 103-105 (Jan 1969).

The motion of cylindrical rods and banks of rods as influenced by a crossflowing fluid is being studied to develop new methods for analyzing, testing, and evaluating the reliability and structural life of heat exchangers. Because reactor heat exchangers have relatively complex geometries, boundary conditions, and flow patterns, the initial investigation is of a fundamental nature.

The impact at a stop developed by an instantaneous arrest of a moving tube has been analyzed. The characteristics of the impact of the tube with the stop are being investigated further. The flexural stress σ and impact I are

$$\sigma(\xi,\tau) = C_\sigma(\xi,\tau)\left(\frac{EM}{I}\right)^{1/2} ru;$$

$$I(\tau) = C_I(\tau)(EIM)^{1/2}\left(\frac{u}{\ell}\right).$$

The coefficients C_σ at midpoint of the tube and C_I are shown in Figs. III.C.3 and III.C.4. Note that there are double peaks for impact if the relative stiffness, K_s/K_b, is large. If the two bodies are perfectly rigid at the contact area, the first peak occurs at $\tau = 0$ and is infinite because an infinite force of zero duration is required to bring the tube to rest locally. On the other hand, if the relative stiffness is small, the first peak disappears. The second peaks of C_I also depend on the relative stiffness and occur when τ is equal to a quarter of the period of fundamental mode of the two-span continuous tube. The bending stress (see Fig. III.C.4) possesses only one peak, except when the stop is perfectly rigid; even in that case the first peak is much smaller. The differences in the time-histories of the impact and bending stress are because some time, which depends on wave velocity, is required to obtain maximum response for the bending stress. However, if the stop is quite strong, it can develop large impact instantaneously and the force developed by the impact is localized in the contact area.

D. Chemistry and Chemical Separations

1. Aqueous and Volatility Processes--Research and Development--Fluoride Volatility Process

a. Purification Procedures and Fission Product Chemistry (M. J. Steindler)

Last Reported: ANL-7548, p. 107 (Jan 1969).

(i) Decontamination of PuF_6. In the step of the fluid-bed fluoride volatility process in which nuclear fuel is reacted with fluorine, a mixture of the hexafluorides of uranium and plutonium which contains the volatile fluorides of ruthenium, niobium, molybdenum, technetium, and antimony is produced and transported away from the fuel residue. A series of seven bench-scale experiments (see Table III.D.1) has been performed to study the separation of volatile ruthenium fluoride from a gas stream also containing plutonium hexafluoride and fluorine. The ruthenium fluoride was prepared by fluorinating, in a stream of fluorine, each of three materials: ruthenium metal powder alone, a ruthenium-PuF_4 mixture, or a

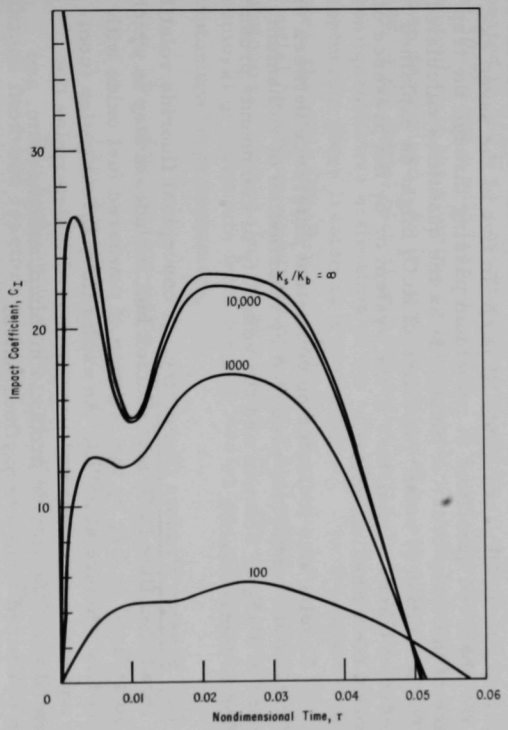

Fig. III.C.3. History of Impact Developed by the Instantaneous Arrest of a Moving Tube

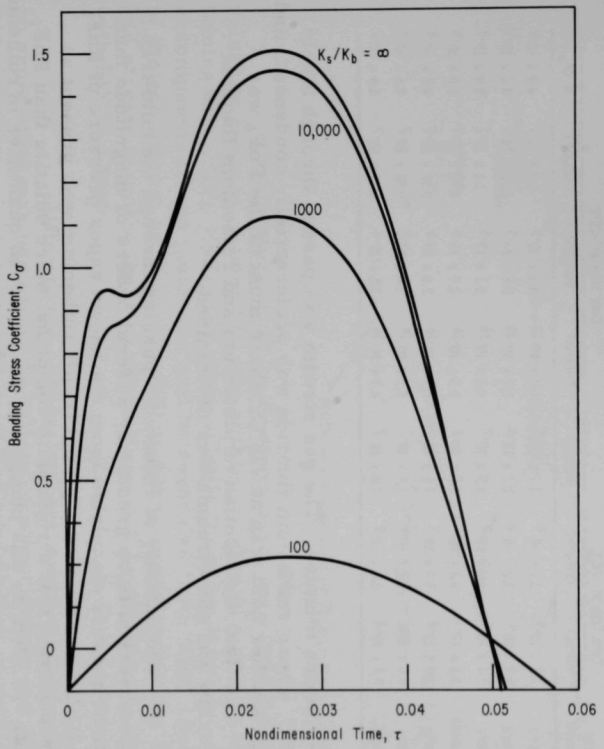

Fig. III.C.4. History of Bending Stress at Midspan Developed by the Instantaneous Arrest of a Moving Tube

TABLE III.D.1. Observed and Theoretical Quantities of Ruthenium Compounds in Exit Gases from Cold Traps

Expt.	Material Fluorinated	Moles in Exit Gas from Cold Trap at -10°C		Moles in Exit Gas from Cold Trap at -78°C				
		Ru(obs)	RuF_5(th)	Ru(obs)	RuF_5(th)	RuF_6(th)	RuO_4(th)	$RuOF_4$(th)
1	Ru-PuF_4	1.3×10^{-5}	3.7×10^{-9}	1.7×10^{-6}	6.8×10^{-16}	3.1×10^{-5}	1.1×10^{-7}	4.9×10^{-9}
2	Ru-PuF_4	1.9×10^{-5}	3.2×10^{-9}	2.7×10^{-6}	6.3×10^{-16}	2.8×10^{-5}	0.98×10^{-7}	4.6×10^{-9}
6	Ru Only	2.4×10^{-6}	3.7×10^{-9}	1.5×10^{-7}	6.8×10^{-16}	3.1×10^{-5}	1.1×10^{-7}	4.9×10^{-9}
8	Ru-Alumina	3.8×10^{-7}	3.2×10^{-9}	2.0×10^{-7}	6.3×10^{-16}	2.8×10^{-5}	0.98×10^{-7}	4.6×10^{-9}
10	Ru-PuF_4	2.0×10^{-6}	3.2×10^{-9}	4.8×10^{-7}	6.3×10^{-16}	2.8×10^{-5}	0.98×10^{-7}	4.6×10^{-9}
11	Ru Only	9.4×10^{-7}	3.2×10^{-9}	2.9×10^{-7}	6.3×10^{-16}	2.8×10^{-5}	0.98×10^{-7}	4.6×10^{-9}
12	Ru-PuF_4	5.8×10^{-7}	3.2×10^{-9}	1.6×10^{-7}	6.3×10^{-16}	2.8×10^{-5}	0.98×10^{-7}	4.6×10^{-9}

ruthenium-alumina mixture. The gas stream was passed through a cold trap at -10°C, where ruthenium fluoride was preferentially condensed, and then through another cold trap at -78°C, where most of the PuF_6 was condensed. The final distribution of plutonium and ruthenium fluoride in the cold traps and gas streams was determined.

The quantity of ruthenium passing through the cold trap at -10°C was observed to be greater by several orders of magnitude than the theoretical quantity claculated from the known vapor pressure of RuF_5 (see Table III.D.1) on the assumption that all ruthenium was present as RuF_5. This indicated that a ruthenium compound more volatile than RuF_5 was present. To identify this compound, the observed quantities of ruthenium in the exit gas from the cold trap at -78°C were compared with the theoretical quantities (calculated from vapor pressures) if ruthenium were present as RuF_5, RuF_6, RuO_4, or $RuOF_4$ (see Table III.D.1). In five of the seven experiments, the observed quantities of ruthenium passing through the trap at -78°C were of the same order of magnitude as the quantities calculated for RuO_4. The formation of small quantities of RuO_4 might be explained by the presence of traces of moisture in the system or by the presence of an oxide film on the ruthenium metal.

Results also indicated no consistent difference between the volatility of ruthenium compounds produced by fluorination of ruthenium in the presence of PuF_4 or alumina and the volatility of compounds produced by fluorination in their absence.

(ii) Fission Product Chemistry. A conceptual fluoride volatility process for irradiated UO_2-PuO_2 fast reactor fuel includes a step in which uranium is volatilized as UF_6 by the reaction of powdered fuel oxide with an oxygen-fluorine mixture at 350°C. An exploratory investigation (comprising flow and static experiments) was performed to determine the products formed when the fission products niobium, molybdenum, and ruthenium in powdered form are oxyfluorinated.

Preliminary results obtained in the oxyfluorinations (1 part fluorine to 10 parts oxygen) at 315 and 355°C indicate that the following intermediates and products are formed:

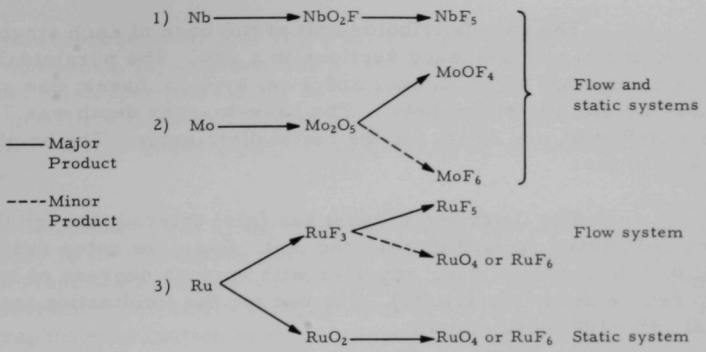

(iii) Neptunium Fluoride Chemistry. In a fluid-bed fluoride volatility process, a possible step will be passage of a gas stream containing PuF_6, UF_6, NpF_6, and other volatile fluorides through a thermal decomposer, where plutonium will be separated from other constituents of the gas stream as PuF_4. Plutonium hexafluoride remaining in the exit gas stream from the thermal decomposer will be removed by reaction with LiF in a trap.

Although the process stream would contain many elements, an experiment was performed to determine only the behavior of neptunium and plutonium. A gaseous mixture of NpF_6 and PuF_6 was prepared and pumped through a series of process units: a bed of granulated alumina heated to 350°C in a thermal decomposition vessel, a bed of LiF pellets at 300°C, and a cold trap at -197°C. The amounts of neptunium and plutonium in the alumina, in the LiF pellets, and in the cold trap were then determined. An incomplete material balance has accounted for 49% of the initial plutonium. Nevertheless, data obtained thus far allow semiquantitative estimation of the efficiency of plutonium separation from neptunium (here treated as a contaminant). For the thermal-decomposition step, the ratio $(Np/Pu)_{initial}/(Np/Pu)_{final}$ was 1.6×10^2. The ratio, (initial plutonium)/(plutonium in cold trap), which indicated overall plutonium removal, had a value of 5×10^5. These values show adequate removal of plutonium from the gas stream and adequate separation of plutonium from neptunium.

b. Engineering-scale Development of FBR Fuels (N. M. Levitz)

Last Reported: ANL-7527, pp. 119-120 (Dec 1968).

(i) Continuous-feed, Two-stage Fluid-bed Reactor. Slab-shaped fluid-bed reactors of 4-in. thickness are being considered for the continuous fluorination of powdered fast reactor material. To obtain design information for such reactors, preliminary fluidization tests were performed in a two-stage, transparent Lucite column having a 2-ft by 4-in. cross section.

The gas-distributor unit at the base of each stage consisted of six inverted pyramid-shaped sections in a row. The pyramidal sections had 1/2-in. openings at the apexes and 4-in. by 4-in. bases; one gas distributor was Lucite, the other metal. The base-to-apex depth was 7 in. for the Lucite distributor, and $3\frac{1}{2}$ in. for the metal distributor. The height of each stage was 30 in.

The fluidizing reagent gas (air) entered through the lower orifices and passed upward through the unit. Gas-flow rates ranging from zero to 0.75 ft/sec were used, together with various degrees of humidification (to reduce static electricity). The bed for the fluidization tests was nominal -48 +100 mesh alumina.

In the first studies, only the lower stage of the unit was operated. A 10-in. bed (static depth) was employed. Fluidization with all six gas inlets functioning was achieved temporarily by adjusting gas flow to the orifices and thereby controlling pressure drop. The second stage was then added to the unit, and the unit was fitted with an ejector-type conveyor for conveying material from the lower stage to the upper stage. Two-stage operation was begun with the upper stage empty; alumina was continuously introduced into the upper stage, allowing study of 0- to 10-in. expanded beds above the upper gas distributor. Complete fluidization in the top stage with all six gas inlets functioning simultaneously was achieved for periods up to 30 min. More frequently, only four of the six inlet sections functioned, thus indicating that some modifications in design or in the operation of the column are needed. Nonfunctioning of some of the inlet sections was attributed to internal static charges (although the metal gas distributor was grounded) and to the low pressure drop of the gas distributor (~1 in. H_2O at 0.4 ft/sec). Since relatively large openings are needed to allow solids to pass downward from the upper stage, it may be desirable to insert a pulsing or jet-type device in each opening to "prime" that section when it becomes static.

2. Closed Cycle Processes--Research and Development--Compact Pyrochemical Processes

a. Laboratory Process Development (I. Johnson)

Last Reported: ANL-7548, pp. 107-108 (Jan 1969).

The phase relations of the Cu-Mg-U system are being investigated to provide additional information on the factors influencing the separation of plutonium and uranium in the reduction step of the current pyrochemical flowsheet. In one set of experiments, equilibrium alloys were prepared whose compositions lay within the triangular section of the phase diagram defined by UCu_5, Cu_2Mg, and copper. In this region of the phase diagram, UCu_5 is the uranium-rich phase that is formed upon cooling. Preliminary

electron microprobe studies of these alloys indicated the following: (1) UCu_5 is a line compound, (2) uranium has a slight solubility in both copper and Cu_2Mg, and (3) copper and Cu_2Mg have an appreciable mutual solid solubility. The intermetallics UCu_5 and Cu_2Mg form a binary system which can deviate slightly from a true quasi-binary system owing to the solid solubility of Cu_2Mg.

In another set of experiments alloys were prepared whose compositions lay in the remaining portion of the Cu-Mg-U phase diagram, namely, a trapezoidal region whose corners are uranium, UCu_5, Cu_2Mg, and magnesium; these alloys encompass the region of process interest. Metallographic examination of these alloys showed that in each case elemental uranium had separated from the alloy and formed a layer at the bottom of the alloy. In no case was UCu_5 noted. These observations indicate that elemental uranium, rather than a uranium intermetallic, is the uranium-rich phase in equilibrium with these alloys. Very little, if any, plutonium is expected to coprecipitate with elemental uranium during the reduction, and, therefore, good separations of plutonium and uranium should be possible.

b. Experimental Flowsheet Investigation (R. D. Pierce)

Last Reported: ANL-7553, p. 102 (Feb 1969).

Work has continued on the installation of equipment in the Plutonium Salt Transport Facility. The helium-purification systems and piping from the systems to the gloveboxes were leaktested, and all observed leaks were repaired. All of the electrical work for the purification systems was completed, and piping for the liquid nitrogen supply to the systems is nearly complete.

Shop work on the agitator drives for the processing vessels in box 3 (see Progress Report for September 1968, ANL-7500, p. 115) was completed, and one of the drive units was installed in the box and tested successfully.

The bag-in port for introducing transfer lines to box 3 was completed and welded into place in one of the window openings in the ceiling of the box. A gasketed cover was subsequently installed over the port and leaktested. A small port for removing samples from glovebox 4 was also fabricated and installed.

Shop work on the mechanisms for lowering and raising the transfer lines in box 3 is nearly complete, and work is underway on the Mo-30 wt % W transfer lines. The transfer lines and their lifting mechanisms are the last major process equipment items that are to be fabricated for glovebox 3.

c. Liquid Metal-Molten Salt Contactors (R. D. Pierce)

Last Reported: ANL-7553, pp. 102-103 (Feb 1969).

A multistage mixer-settler is being developed for use with liquid metal-molten salt systems in the Plutonium Salt Transport Facility. Tests were conducted with water in a model having a plastic mixing chamber and a stainless steel mixer-pump (see ANL-7553) which will be used in a single-stage, high-temperature mixer-settler that is being fabricated. Figure III.D.1 is a sketch of the lower portion of the mixer-pump inside the mixing chamber. This design was developed after a series of tests in which mixing power was measured with various arrangements of mixer blades and baffles.

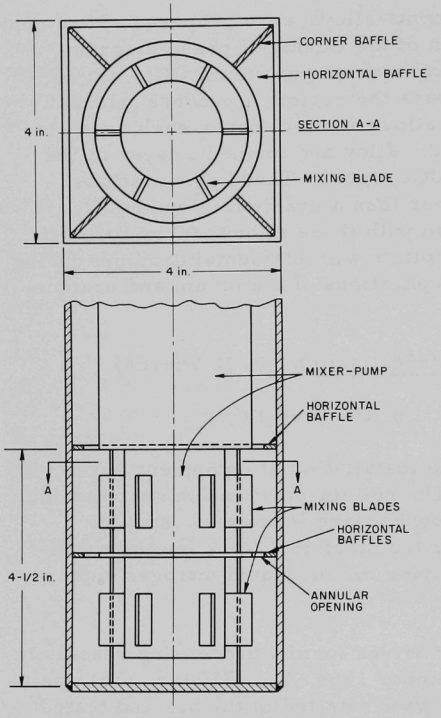

Fig. III.D.1. Mixing Chamber and Pump Test Assembly

One of the major developments that resulted from these tests is the placement of a horizontal baffle and sleeve (sleeve not shown in Fig. III.D.1) at the top of the mixing region to eliminate gas entrainment in the mixing chamber. (Gas entrainment decreases the effective mixing power at any mixing speed and depresses the normal rise in mixing-power input that accompanies increasing mixing speed.) The baffle is located approximately $4\frac{1}{2}$ in. above the bottom of the mixing chamber in line with the bottom of the upper section of the pump. The sleeve is positioned directly above this baffle. Because variation in the total amount of material that is held above the baffle will not affect the performance of an individual stage, it will not be necessary to provide precise level-control devices in each stage of the multistage system. Another horizontal baffle, which is located between two sets of agitator blades, divides the mixing chamber into two mixing zones with an annular connection. This division reduces the amount of unmixed material that might otherwise bypass the mixing region.

Four 1-in.-wide vertical baffles placed in the corners of the mixing chamber resulted in a threefold increase in mixing-power input per liter. The number of mixing blades used in the tests varied from 9 to 17. It was found that 12 blades having a radial width of 1/2 in. produced about twice the mixing power of 17 blades with a radial width of 3/8 in., and that when the number of blades was increased from 9 to 17, the effect on mixing power was relatively minor. The final design incorporates 12 blades, 6 above and 6 below the horizontal baffle. Mixing-power input for water with this design was about 5×10^{-2} hp/liter. It is anticipated that the power input to a metal-salt system in a mixer-settler of the same design would be about 0.15 hp/liter.

When a very high (~99%) stage efficiency is desired, it is imperative that the phases being contacted in the mixing chamber have adequate residence times. The multistage mixer-settler will operate under continuous-flow conditions with a mean residence time of about one minute. Since the actual rates of reaction in the metal-salt systems of interest have not been established, efforts are being made to develop a design that minimizes the quantity of solution leaving the mixture after a short residence time.

Tests are being conducted with water in the plastic model to determine the shape of the residence-time distribution curve for the current mixer-pump and mixing-chamber design. The data obtained in these tests will be used to calculate residence-time distribution curves for experiments that will be performed with liquid metals and molten salts in the high-temperature model that is being fabricated. This residence-time information will be used with performance data from the high-temperature tests to determine reaction rates for the metal-salt systems at high temperature.

3. General Chemistry and Chemical Engineering--Research and Development

a. Studies on the Formation and Stabilization of Carbon-bearing Dispersions in Sodium (F. A. Cafasso)

Last Reported: ANL-7527, p. 123 (Dec 1968).

Attempts are being made to prepare stable, well-characterized dispersions of carbon-bearing materials in liquid sodium. The purpose is to determine whether particulates play a role in the transport of carbon through sodium, e.g., in the carburization of austenitic steels.

Recent effort has been directed toward evaluating methods for preparing dispersions of carbon in sodium. Two methods believed to be useful for in situ generation of finely divided carbon were tried: surface graphitization of ferritic steels at 600°C (1018 carbon steel and an iron-0.1% carbon alloy), and cracking of tetralin at 500°C. Both were found to be ineffectual for dispersing carbon in sodium. Encouraging results, however, were obtained with ultrasonic dispersion.

Carbolac 1,* a 90-Å carbon black, was heated in sodium at 510°C under ultrasonic stimulation. Unfiltered samples of the sodium were taken after various periods of settling. The samples were analyzed for total carbon or were hydrolyzed and the resultant off-gases were analyzed to determine the carbon species, other than elemental carbon, that had existed in the sodium. The total carbon analyses showed that about 0.1% carbon remained dispersed in the sodium after ~100 hr of settling. The off-gases from the hydrolyzed samples contained C_2-hydrocarbons. In separate experiments, it was found that treatment of Carbolac 1 with aqueous acids or bases did not yield gaseous C_2-hydrocarbons. Therefore, the C_2-hydrocarbons in the sodium samples most likely resulted from the reaction of the Carbolac with liquid sodium.** That elemental carbon reacts with liquid sodium to form C_2-hydrocarbons is noteworthy, since previous work† had indicated that the C_2-hydrocarbon disodium acetylide (Na_2C_2) might be responsible for transport of carbon in sodium systems.

Factors that might influence the reaction of elemental carbon with sodium will be examined. For example, the Carbolac 1 used in the above experiments is rich in surface oxygen, which could have catalyzed a carbon-sodium reaction; hence, the effect of oxygen is under study.

b. Determination of the Solubility of Helium in Sodium
(F. A. Cafasso)

Last Reported: ANL-7553, p. 103 (Feb 1969).

The solubility of helium in liquid sodium is being determined as a function of temperature (350-550°C) and pressure (3-10 atm). To date, measurements have been made at three temperatures, 500, 450, and 400°C, yielding the average solubilities 26, 14, and 8 ppb/atm, respectively. All experiments were carried out at 6-7 atm helium pressure, with at least three measurements at each temperature. The heat of solution calculated from these data is ~12 kcal/mol. Further solubility experiments are in progress.

c. Phase Diagram Study of the Ternary System U-Pu-O
(P. E. Blackburn and A. E. Martin)

Last Reported: ANL-7518, pp. 113-115 (Nov 1968).

The dominant feature of the U-Pu-O ternary phase diagram†† is the existence of a fluorite solid-solution phase that extends across the

*Cabot Corporation, Boston, Massachusetts.

**The C_2-hydrocarbon content of the sodium before adding the Carbolac 1 was below detectable limits.

†Luner, C., Feder, H. M., and Cafasso, F. A., Carbon Transport in Sodium Systems, presented at AEC-ANL Int. Symp. on Sodium Technology and Large Fast Reactor Design, Argonne, Illinois (Nov. 7-9, 1968).

††Markin, T. L., and Street, R. S., J. Inorg. Nucl. Chem. 29, 2265-2280 (1967).

diagram between the UO_2 and the PuO_2 compositions. The hypostoichiometric boundary of the fluorite phase in the U-UO_2 system was established by equilibrating urania crucibles with liquid uranium at various temperatures, and analyzing either the crucibles or the oxide growths that formed between the crucibles and the liquid uranium.* An attempt is being made to establish the hypostoichiometric boundary of the fluorite phase in the U-Pu-O system by a similar technique, namely, by equilibrating mixed-oxide crucibles with liquid uranium-plutonium alloys at various temperatures and subsequently analyzing the crucibles. Obviously, the method would be useful only in a composition region and over a temperature range in the system where such two-phase equilibrations are possible. The initial experiments are being conducted with mixed-oxide crucibles having a plutonium-to-uranium ratio of 0.25.

The first two experiments were carried out at equilibrium temperatures of 1862 and 1976°C. The oxygen-to-metal (O/M) analyses of the product crucibles were 1.735 and 1.683, respectively. A metallographic examination of the product crucibles showed that a metallic phase, presumably a uranium-plutonium alloy, had precipitated out at the grain boundaries of the oxide phase. Additional tests are being made to determine whether the crucible analyses represent points on the hypostoichiometric boundary plane of the fluorite phase at the temperatures of the experiments.

The temperature of the monotectic between plutonium and Pu_2O_3 in the Pu-PuO_2 binary system was previously shown (see ANL-7518) to be between 1778 and 1863°C. In those experiments, liquid plutonium was heated in a Pu_2O_3 crucible for short periods at successively higher temperatures; above the monotectic temperature, the plutonia reacted with Pu_2O_3 crucible. Additional tests of the same type have now located the temperature between 1836 and 1854°C. From these experiments, the monotectic temperature is considered to be 1845 ± 15°C.

d. Vapor Species Partial Pressures in the Ternary U-Pu-O System (P. E. Blackburn and J. E. Battles)

Last Reported: ANL-7513, pp. 127-130 (Oct 1968).

Mass-spectrometric studies of the volatilization behavior of the uranium-plutonium-oxygen system continue to determine (1) the composition of the vapor phase in equilibrium with the condensed phase(s), (2) the partial pressures of the vapor species as a function of temperature, and (3) the thermodynamic properties of the vapor species. The first phase of this study has been devoted to the plutonium-oxygen system, since mass-spectrometric data for this system are not available.

*Edwards, R. K., and Martin, A. E., Thermodynamics, Vol. 2, p. 423, Proc. Symp. Vienna, 1965, IAEA, Vienna (1966).

Mass-spectrometric data on the vaporization of material (atom ratio for oxygen to plutonium of 1.52-1.56) assumed to be diphasic $Pu_2O_3(s)$ + $PuO_{1.61}(s)$ have been reported previously (see ANL-7513). The vapor phase over this material contained the gaseous plutonium species Pu(g), PuO(g), and $PuO_2(g)$. This information, coupled with X-ray diffraction and chemical analysis, implies that vaporization proceeds according to the reactions

$$7.33\ Pu_2O_3(s) = 13.66\ PuO_{1.61}(s) + Pu(g); \quad (1)$$

$$2.77\ Pu_2O_3(s) = 4.54\ PuO_{1.61}(s) + PuO(g); \quad (2)$$

$$4.54\ PuO_{1.61}(s) = 1.77\ Pu_2O_3(s) + PuO_2(g). \quad (3)$$

It should be kept in mind, however, that these reactions are based on the assumption that the phase-boundary compositions are Pu_2O_3 and $PuO_{1.61}$, and that they are independent of temperature as indicated in the tentative plutonium-oxygen phase diagram.*

The data previously obtained for Reaction (3) were limited, and additional experiments were needed to establish the enthalpy of reaction and the amount of $PuO_2(g)$ in the vapor phase, values which are important in the determination of thermodynamic properties. For these additional experiments, the appropriate amounts of $PuH_3(s)$ and $PuO_2(s)$ to give an atom ratio for oxygen to plutonium of 1.50-1.52 were mechanically mixed and heated as previously described (see Progress Report for July 1968, ANL-7478, p. 121). However, the composition of the sample material is uncertain, since chemical analysis of duplicate samples yielded values of 1.49 and 1.55 for the atom ratio.

Because of the small concentration of $PuO_2(g)$ in the vapor phase, the temperature dependencies of the three vapor species were determined at higher temperatures (2028-2239°K) than had been previously (1657-2148°K). The enthalpies of reaction obtained from the slopes of the data for Reactions (1) and (2) were about 15-20 kcal less per mole than the values obtained in the earlier measurements (see ANL-7513, p. 129). In a subsequent experiment over the temperature range from 1800 to 2239°K, the data exhibited a significant change in slopes for Reactions (1) and (2) at about 2050°K. The enthalpies of reaction obtained from the slopes at temperatures above ~2050°K corresponded to those of the 2028-2239°K experiment, whereas the values at temperatures below ~2050°K corresponded to the values obtained in the measurements reported earlier. Since Reaction (3) could only be measured accurately above about 2025°K, a change in slope was not observed for this reaction; both experiments yielded enthalpies of reaction only slightly higher than the

*The Plutonium-Oxygen and Uranium-Plutonium-Oxygen Systems: A Thermochemical Assessment, Technical Reports Series No. 79, p. 18, IAEA, Vienna (1967).

values reported in ANL-7513. Because of the unexplained two-slope behavior observed in the two more recent experiments, additional experiments are being conducted.

The study of the volatilization behavior of the ternary U-Pu-O system will be initiated shortly. The UO_2-20% PuO_2 material for this study has been received and materials with 5, 10, and 40% PuO_2 are on order.

e. Preparation of Nuclear Materials (P. A. Nelson)

Last Reported: ANL-7527, pp. 124-125 (Dec 1968).

A 25-kW, inductively heated plasma torch (see ANL-7527) has been installed for studying the continuous preparation of UC from uranium oxides.

A series of preliminary experiments was completed to study the effect of several operating parameters on the amount of heat transferred to a solid in the plasma. Crushed alumina particles were used as a stand-in for uranium oxide in these experiments. The fraction of alumina particles that were fused was used as the measure of heat transferred to the solid. The use of about 4% H_2 in the argon stream to the torch greatly increased the fraction of particles that fused. An increase in the solid feed rate from 10 to 23 g alumina/min had no apparent effect on the fraction fused, thereby indicating that feed rates higher than 23 g/min are practical.

The operating conditions that were established in the experiments with alumina will be used in the preliminary experiments that are being set up for the preparation of UC from UO_2-carbon agglomerates.

PUBLICATIONS

Analytical and Experimental Studies of Double-Pipe Counter-Flow Liquid Metal Heat Exchangers
R. W. Brown
ANL-7479 (August 1968)

Swelling of Fast Neutron Irradiated Austenitic Stainless Steels
S. D. Harkness and D. G. Letzring
J. Metals 21, 44A (March 1969) Abstract

A Model for Void Formation in Irradiated Metals
S. D. Harkness and C. Y. Li
J. Metals 21, 44A (March 1969) Abstract

Densification Processes of Actinide IVA-VIA Compounds
O. L. Kruger and J. B. Moser
Proc. Brit. Ceram. Soc., pp. 125-143 (March 1969)

Cathodic Etcher
J. O. Ludlow, L. F. Coleman, V. M. Drabek, L. E. Ross, and M. A. Slawecki
Proc. 16th Conf. on Remote Systems Technology, Am. Nucl. Soc., Idaho Falls, March 11-13, 1969, p. 309 Note

Evaporation of Hypostoichiometric Plutonium Dioxide from 2070° to 2380°K
D. R. Messier
J. Am. Ceram. Soc. 51, 710-713 (December 1968)

Thermal Diffusivity of Actinide Compounds
J. B. Moser and O. L. Kruger
Proc. 7th Conf. on Thermal Conductivity, Gaithersburg, Maryland, November 13-16, 1967. NBS Special Publ. 302, U.S. Govt. Prtg. Office, Washington, D.C., 1968, pp. 461-467

Kinetics of the Reduction of UO_2 by Mg or Ca Dissolved in Molten Chlorides
R. A. Sharma and Irving Johnson
J. Metals 21, 32A (March 1969) Abstract

Reduction of Uranium Dioxide in Molten Salt-Metal Systems
D. A. Wenz, R. D. Wolson, and Irving Johnson
ANL-7463 (November 1968)

On the Completeness of a Set of Stress Functions Appropriate to the Solution of Elasticity Problems in General Cylindrical Coordinates
C. K. Youngdahl
Intern. J. Eng. Sci. 7, 61-79 (January 1969)

IV. NUCLEAR SAFETY

A. Reactor Kinetics

1. Reactor Control and Stability

a. Reactor Stability Design Criteria for Spatially Dependent Systems (C. Hsu)

Last Reported: ANL-7500, pp. 34-36 (Sept 1968).

(i) Nonlinear Model. A method of improving the stability region of nonlinear reactor systems has been developed. The method directly extends the semigroup method by introducing transformation with unknown parameters, which then are determined by maximizing the stability region of the system. The approach has been applied to a point-model reactor system;* it improved the region of stability significantly.

2. Coolant Dynamics

a. Critical Flow (H. K. Fauske and M. A. Grolmes)

Last Reported: ANL-7548, pp. 117-119 (Jan 1969).

(i) Voiding Models. In the analysis of reactor conditions such as power excursions, pump failure, or subassembly blockage that lead to coolant-channel voiding, the ultimate voiding rate depends on two major considerations: superheat before vapor formation and the flow regime in the two-phase region.

Expulsion phenomena are being studied by tests in which the fluid is brought to a superheated state by rapid depressurization. To simulate liquid-metal expulsion consideration must be given to the liquid-vapor density ratio and the fact that a liquid-metal coolant is likely to have a more uniform radial temperature profile than a nonmetallic fluid. Freon-11 was selected because, at suitably low pressures, its liquid-vapor density ratio is comparable to that of sodium at 1 to 2 atm. Upon sudden depressurization, the Freon-11 is superheated uniformly with no radial temperature gradients.

The apparatus (see ANL-7548) consists of a glass test channel fastened to a large reservoir that has a diaphragm across its opening. After a vacuum is established in the reservoir, the diaphragm is ruptured mechanically to depressurize the fluid in the test channel. The

*Devought, J., and Smets, H. B., Determination of Stability Domains in Point Reactor Dynamics, Nucl. Sci. Eng. 28, 226-236 (1967).

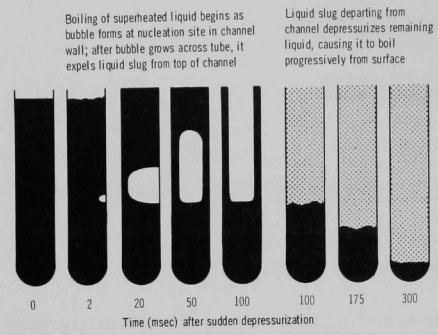

Fig. IV.A.1. Boiling and Expulsion Patterns Observed after Atmosphere above Channel Containing Freon-11 Is Suddenly Depressurized, Causing Freon To Be Superheated Instantaneously

subsequent expulsion is recorded on high-speed motion-picture film so that characteristic flow patterns can be studied in detail. A typical event is summarized in Fig. IV.A.1. First, a single bubble forms at a nucleation site on the channel wall, grows rapidly across the channel, and expels the upper liquid column as a slug. A liquid film remains on the channel wall as the vapor expands and expels the liquid slug, lending support to voiding models that assume this mode. The remaining lower column of liquid is expelled by a different mechanism: a dispersed two-phase mixture is rapidly expelled from a rather well-defined liquid-vapor interface. This interface propagates into the remaining liquid column as shown in the later stages in Fig. IV.A.1. Later, depressurization of the channel following a slug-type expulsion in a postulated accident might result from rapid condensation of vapor in the subcooled liquid of the upper plenum.

Additional test sections have been fabricated. These include three single-channel sections of various diameters and an annular and seven-pin section.

A simple expulsion model that satisfies all conservation conditions has been developed to predict the expulsion and re-entry behavior of sodium coolant upon overheating of a reactor channel. Parametric studies have been made of how the expulsion behavior is affected by the wall-film thickness, the liquid superheat at inception of boiling, the point of bubble initiation, and the magnitude and shape of the wall heat flux; re-entry problems associated with blanket and plenum cooling were also studied. The vapor is assumed at all times to be in equilibrium with the surrounding liquid interfaces. The heat-conduction equation is solved in the end liquid regions and also in the liquid film adhering to the wall in the vapor zone. This allows expulsion and re-entry to be calculated both in the presence and absence of wall film.

Figures IV.A.2 and IV.A.3 indicate the strong effect of the presence of wall film. With a dry wall, the voiding rate is much slower and the pressure quickly drops, approaching the external pressure. Furthermore, energy storage in the wall film is significant for thicknesses greater than 0.005 cm, which is an order of magnitude less than those reported by Grass et al.* The reduction in film thickness is negligible during expulsion,

*Grass, G., et al., Das Sieden von flussigen Alkali-metallen, Z. Atomkernenergie 12, 101-110 (1967).

so that film dryout is not likely to occur during the initial expulsion phase if the wall is well wetted. Moreover, re-entry of a liquid slug will not occur until the wall film has been largely evaporated. Finally, the superheat at which boiling is initiated governs the early voiding behavior; for reasonable values of the wall heat flux (reactor conditions), the evaporation rate from the wall film dominates the expulsion rate during the later stages.

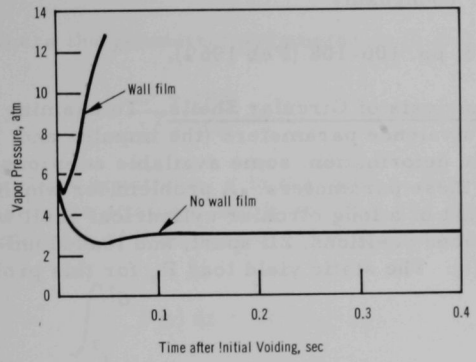

Fig. IV.A.2
Calculated Pressure in Vapor Region after Initial Voiding with Superheat of 105°C

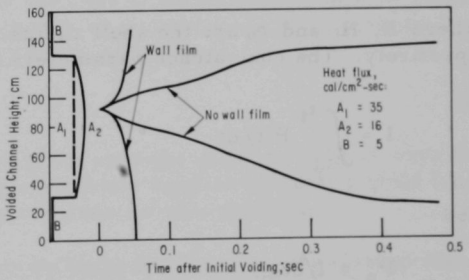

Fig. IV.A.3
Calculated Position of Vapor-Liquid Interfaces as Function of Time after Initiation of Voiding from Superheat at 105°C

b. Coolant Dynamics (R. M. Singer and R. E. Holtz)

Last Reported: ANL-7548, p. 119 (Jan 1969).

(i) Sodium Superheat Experiments. The sodium-superheat data are being examined further to gain insight on the ratio of the cosines of the advancing and receding contact angle of sodium in surface cavities.

(ii) Coolant-expulsion Experiments. After several additional runs of the sodium-expulsion experiments, the strain-gauge-type pressure transducer failed because of excessive temperature exposure, so cooling coils have been placed around the tubing that leads to the replacement transducer. Experiments are continuing.

(iii) Transient Experiments. Assembly of the loop is proceeding. All difficulties with the calorimetric flow-measurement device have been resolved, and it has been calibrated in a sodium system. Several valves to be used in the system did not pass the helium leakcheck, so new O-rings have been ordered.

3. Core Structural Safety (C. K. Youngdahl)

Last Reported: ANL-7553, pp. 106-108 (Feb 1969).

a. Dynamic Plasticity Analysis of Circular Shells. To examine the generality of the proposed equivalence parameters (the impulse and effective load) for dynamic plastic deformation, some available solutions will be reformulated in terms of these parameters. A problem for which a closed-form solution* exists is that of a long circular cylindrical shell with reinforcing rings at regularly spaced positions, 2L apart, and loaded uniformly by a dynamic pressure P(t). The static yield load P_s for this problem is given by

$$P_s = \left(1 + \frac{RH}{L^2}\right) \frac{\sigma_0 H}{R}, \tag{1}$$

where R, H, and σ_0 are the shell radius, thickness, and yield stress, respectively. The equivalence parameters are defined by

$$I = \int_{t_y}^{t_f} P(t)\, dt$$

and

$$P_e = I/2t_m, \tag{2}$$

where I is the impulse (per unit shell area), P_e is the effective load, and t_m is the mean time of the pulse defined by

$$t_m = \frac{1}{I} \int_{t_y}^{t_f} tP(t)\, dt. \tag{3}$$

In the above, t_y and t_f are the times when plastic deformation begins and ends. If the results in the reference are recast in terms of the equivalence parameters, the final radial deformation u_f at the midpoint between reinforcing rings is

*Hodge, P. G., Jr., The Influence of Blast Characteristics on the Final Deformation of Circular Cylindrical Shells, J. Appl. Mech. 23, 617-624 (1956).

$$u_f = \frac{3I^2}{4\rho P_s}\left(1 - \frac{P_s}{P_e}\right), \qquad 1 \le \frac{P_M}{P_s} \le \mu;$$

$$u_f = \frac{3I^2}{4\rho P_s}\left[1 - \frac{P_s}{P_e} - \frac{1}{3}\left(\frac{I_b}{I}\right)^2\left(\frac{1}{\mu} - \frac{P_s}{P_{eb}}\right)\right], \qquad \mu < \frac{P_M}{P_s}, \tag{4}$$

where the geometric parameter μ is defined by

$$\mu = \frac{L^2 + 3RH}{L^2 + RH}. \tag{5}$$

In these equations, ρ is the surface density of the shell, P_M is the maximum pressure attained, and I_b and P_{eb} are analogous to I and P_e with t_f in the integrals of Eqs. (2) and (3) replaced by t_b, which is found from the relation

$$\int_{t_y}^{t_b} P(t)\, dt = \mu P_s(t_b - t_y). \tag{6}$$

The second of Eqs. (4) pertains to the case in which a hinge band is produced by the load; t_b is the time at which this hinge band reduces to a hinge circle. The time t_f at which deformation ends is found from

$$I = P_s(t_f - t_y). \tag{7}$$

Thus the conjecture that the average value of the load over the duration of the deformation is approximately equal to the static yield load (see ANL-7553) is found to be exactly true for this problem.

For loadings such that no hinge band occurs, the first of Eqs. (4) shows that the final plastic deformation of the shell depends only on the proposed equivalence parameters. If a hinge band is produced, other quantities are involved also. However, Fig. IV.A.4 shows that the final deformation still very nearly depends only on the equivalence parameters, i.e., the curves of u_f/I^2 versus P_e are very close together. For comparison, the same results are plotted in Fig. IV.A.5 as a function of peak load P_M.

4. Fuel Meltdown Studies with TREAT

a. Development of Experimental Methods (C. E. Dickerman)

Last Reported: ANL-7553, pp. 109-112 (Feb 1969).

The prototype Mark-II integral sodium loop has been prooftested, and the power and instrumentation circuits thoroughly checked out. The test section for the first TREAT transient experiment using this advanced integral

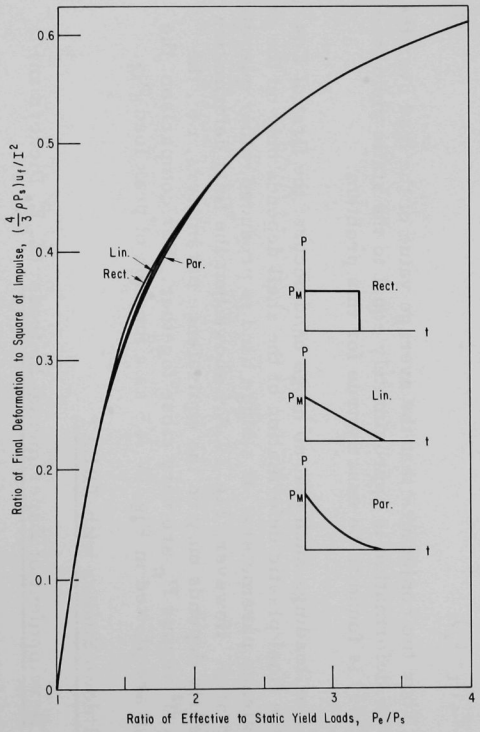

Fig. IV.A.4. Ratio of the Final Deformation to the Square of the Impulse as a Function of the Effective Pressure for Pulses Decaying Rectangularly, Linearly, and Parabolically (for $\mu = 1.5$)

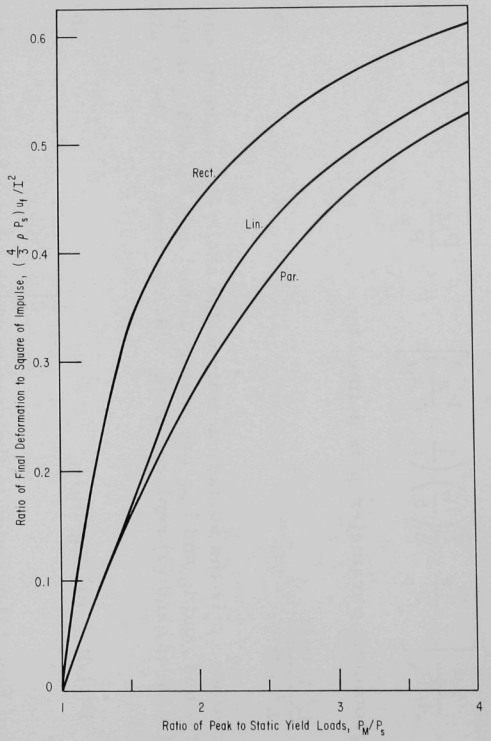

Fig. IV.A.5. Ratio of the Final Deformation to the Square of the Impulse as a Function of the Maximum Pressure for Pulses Decaying Rectangularly, Linearly, and Parabolically (for $\mu = 1.5$)

loop is being prepared for insertion into the facility. This experiment will contain a single oxide-fuel pin, clad with a 0.290-in.-dia stainless steel can, surrounded by a hexagonal array of six dummy fuel pins consisting of 0.290-in.-dia cladding tubes filled with argon gas. The 7-element cluster is held apart by 0.056-in.-dia separator wires spirally wound upon each pin, and fits snugly into a specially sized fuel holder.

Two control consoles (one for the TREAT facility in Idaho, and the other to remain at Argonne, Illinois) have been completed, and the final corrected wiring schematics for the controls, loop, and accessories are being checked. All circuits perform satisfactorily and as expected.

The compact silicone/water heat-exchanger, pump, and reservoir package for the Dow-200 polysiloxane liquid-coolant circulatory system, intended for use at TREAT, has been completed and checked out in operation with the prototype loop. The silicone fluid is used to cool the Annular Linear Induction Pump (ALIP) and to solidify the sodium in the two freeze valves during operation of the loop at elevated pretransient temperatures. The previously completed, more extensive silicone fluid supply-exchanger package, which utilizes a Freon-12 evaporative chiller in addition to the silicone-water heat exchanger, will be kept at Argonne for use with the integral loop during outfitting, testing and experimental preparations.

(i) Quality Control for the Mark-II Integral Sodium Loops. Considerable work has been done in compiling and recording the quality-assurance specifications and procedures used in the design, construction and test of the Mark-II integral sodium TREAT loops. This effort should permit future integral loops to be constructed according to the same rigid specifications, with the details of Quality Control preserved in an easily followed formal record consistent with the new Argonne Quality Assurance procedures.

Quality control is recorded for the 6 loops under construction or completed in the form of a Quality Control Index. Appended to these indices are the specifics of material-chemistry records, heat-treatment records, locations of radiographic and ultrasonic records, and written accounts of design and construction details.

5. Materials Behavior and Energy Transfer

a. High Temperature Physical Properties (M. G. Chasanov)

Last Reported: ANL-7527, p. 132 (Dec 1968).

(i) Heat Capacity of Liquid UO_2. Measurements of the heat content of UO_2 sealed in tungsten capsules are continuing. Data obtained for liquid UO_2 are as follows:

Temp (°K)	$H^{\circ}_{T} - H^{\circ}_{298}$ (cal/mol)
3173	91,699
3329	96,277
3404	99,292

Previous data* for liquid UO_2 enthalpies extended only to 3258°K. Thus, our results have already extended the range of data by about 150°K. Additional experiments are in progress that will extend the measurements of UO_2 enthalpies to even higher temperatures.

b. Pressure Generation due to Violent Meltdown (R. O. Ivins)

(i) Calculational Studies

Not previously reported.

A reactor accident, such as an excursion or a failure of the cooling system, could result in the fragmentation and dispersion of molten core materials as fine particles into the liquid coolant. Such dispersion of small hot particles into the coolant would lead to high rates of heat transfer per unit weight of particles and, for an optimum coolant-particle weight ratio, would result in very sudden heating of the coolant. For example, the rapid heating of water under constraint (not necessarily resulting in the production of steam by boiling) would induce expansion of the system and produce large dynamic pressure pulses, a phenomenon loosely known as a "steam explosion." Similar behavior is expected for other reactor coolant systems, such as liquid sodium.

This calculational study concerns the pressures developed due to the rapid addition of heat to a localized volume of coolant, which may have considerable vapor-void volume, surrounded by a larger volume of unheated liquid coolant. It is assumed that heat is added uniformly at a constant rate to a given volume of liquid coolant, which initially might have a uniform vapor-void fraction. It also is assumed that the liquid volume being heated is at a uniform pressure.

The surrounding unheated liquid coolant acts as a tamper. It is compressible and offers an acoustic constraint to expansion of the heated coolant. If the coolant can expand in one direction only, say out the ends of the reactor core, linear or one-dimensional constraint occurs. If the coolant can expand in all three directions, spherical constraint occurs.

*Hein, R. A., and Flagella, P. N., Enthalpy Measurements of UO_2 and Tungsten to 3260°K, GEMP-578 (1968).

The following nomenclature is used:

a	= surface area of heated coolant per unit weight of the heated coolant,	ft^2/lb
c	= velocity of sound in unheated coolant,	ft/sec
g	= gravitational conversion factor,	$\frac{ft}{sec^2}\ \frac{lb\text{-mass}}{lb\text{-force}}$
ΔH	= enthalpy added per unit mass of heated coolant,	Btu/lb
δH	= increment of ΔH for iteration,	Btu/lb
ΔP	= gauge pressure	$lb/in.^2$
q	= heat transfer or heat-addition rate per unit mass of heated coolant,	Btu/sec-lb
R	= radius of coolant volume being heated,	ft
t	= time,	sec
U	= acoustic coolant flow velocity,	ft/sec
V	= average specific volume of heated coolant,	ft^3/lb
x	= initial void fraction by volume in heated coolant,	
ρ	= density of unheated coolant,	lb/ft^3

For linear constraint, the equation for the acoustic velocity at the interface of the heated and cold coolant is

$$U = 144\, g\, \Delta P/\rho c,$$

and for spherical constraint the relationship becomes*

$$U = \frac{144\, g}{\rho}\left[\frac{\Delta P}{c} + \frac{1}{R}\int_0^t \Delta P\, dt\right].$$

To solve the case of linear constraint,

$$aU = \frac{144\, ga\, \Delta P}{\rho c} = \frac{dV}{dt} = q\frac{dV}{dH};$$

for iteration,

$$\Delta P_{n+1}/k = V_{n+1} - V_n,$$

*Adapted from equations given by H. Lamb, Hydrodynamics, 6th Ed., Dover Publications, New York (1945), pp. 489-491.

where

$$k = \rho cq/144\ ga\ (\delta H).$$

To solve the case of spherical constraint,

$$aU = \frac{144\ ga}{\rho}\left[\frac{\Delta P}{c} + \frac{1}{R}\int_0^t \Delta P\ dt\right] = \frac{dV}{dt} = q\frac{dV}{dH};$$

for iteration,

$$\Delta P_{n+1} = \frac{V_{n+1} - V_n - \frac{1}{z}\sum_0^n \Delta P_n}{\frac{1}{k} + \frac{1}{z}},$$

where the constant z is defined as:

$$\frac{(3)(144\ g)}{(1-x)^2\ c^2}\ k^2.$$

To solve the equations, values of V for the coolant as functions of P and ΔH must be available. As an example, the equations were solved for the case of a water coolant by using data from steam tables.

These solutions are plotted for water coolant in Figs. IV.A.6 for linear constraint and IV.A.7 for spherical constraint, in which the pressure ΔP and specific volume V are plotted against total heat added, ΔH, for various values of the parameter k (which includes the heat-addition rate q and the initial void fraction x).

These equations and graphs present solutions to simplified situations, but they are useful for estimating the magnitude of pressures developed from heat-transfer rates (dispersed particle size and temperature) and total heat transferred (coolant-fuel ratio). The model assumes a large volume of surrounding unheated coolant and does not include reflected shock waves. Waves reflected from free surfaces would reduce the pressure and waves reflected from solid surfaces would increase the pressure. The time for reflected shock waves to be evident in affecting the pressure would be 2 L/c seconds, where L is the distance to the reflecting surface in feet.

The case of sodium coolant is being studies in a similar manner.

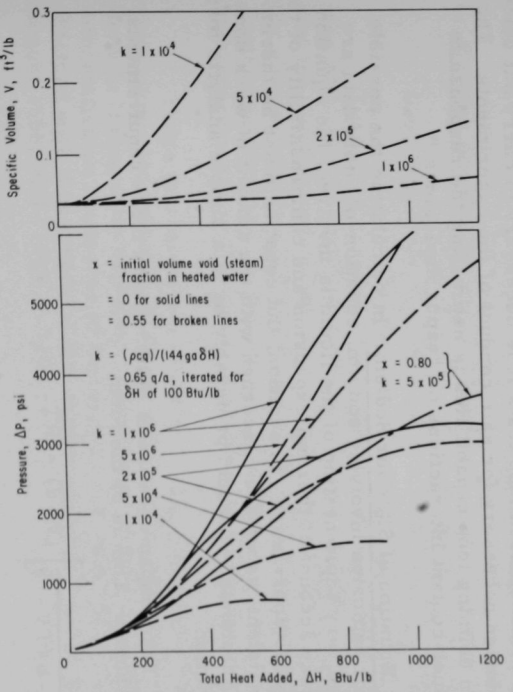

Fig. IV.A.6. Pressures Developed by Addition of Heat to Water under Linearly Acoustically Constrained Steam-Water Expansion

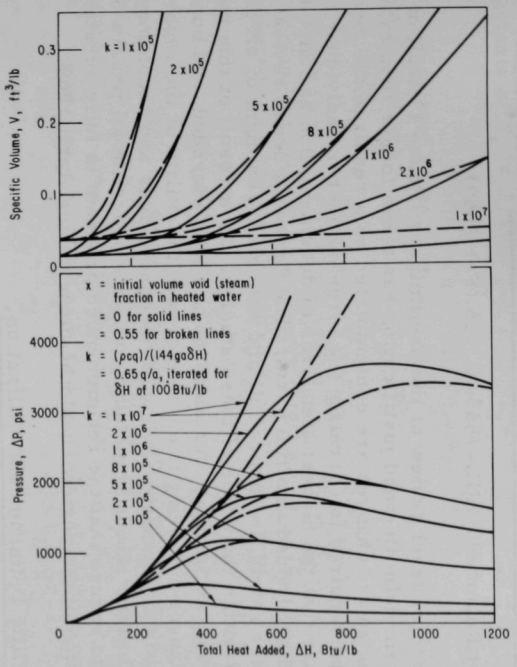

Fig. IV.A.7. Pressures Developed by Addition of Heat to Water under Spherically Acoustically Constrained Steam-Water Expansion

6. Fast Reactor Safety Test Facility Study

a. Programmatic Definition and Justification (C. N. Kelber)

Last Reported: ANL-7553, p. 116 (Feb 1969).

The third level review of the preliminary (Phase 1) draft of the report on program definition and justification has taken longer than expected. Although no substantive changes are contemplated as a result of the reviews, a month has been required to correlate the large number of individual reviews. To assure that the highest standards of documentation are met this review has been subdivided into two parts. The first is a broad review by experts in reactor safety, to ensure full and accurate treatment of all phases of the problems within the scope of these studies. As a result of this part of the review the work on ultimate containment has been extended, and numerous editorial changes are being made to increase the utility of the report. The second part is an intensive review of the conclusions and recommendations by a small group (about 5) including persons expert in all phases of LMFBR safety to ensure that the recommended program is fully substantiated. This portion of the review should be made during April 1969.

b. Facility Definition and Utilization

(i) Loop Capabilities. To define the facility capabilities needed for carrying out recommended loop tests it is necessary to carry out calculations of loop design necessary for safe conduct of the experiments. The chief problem in defining loop capabilities is estimating the response to violent molten fuel-coolant interactions or "vapor explosions."

(ii) Equation of State for Sodium. In calculating the possible effects of a vapor explosion involving sodium, equation-of-state data are needed. Because very rapid heating of the liquid is involved, the equation of state has to take account of thermal expansion and compressibility of the liquid as well as of vaporization. In addition, the equation must be thermodynamically consistent, as we are concerned with the amount of work done by the expanding fluid, and it should preferably be in a simple analytic form for easy computation.

The Himpan equation of state* meets these requirements, adequately it is hoped. This is of the form

$$P + \left[\frac{a}{(V - b)(TV - c)}\right](V - d) = RT.$$

*Himpan, J., Monatshefte für Chemie 86, 259-268 (1955).

If P is in atmospheres, V in cm^3/g-mole, and T in °K, then a = 1.902×10^{11}, b = 25.1391, c = -6.187×10^5, and d = 31.2391 give agreement with the highest-temperature liquid-density measurements* and estimated critical constants of T_c = 2733°K and P_c = 408.2 atm.

Work is proceeding at present to put this equation, together with consistent vapor pressure and heat capacity relationships, into a form suitable for computation.

These computations will eventually be compared with standards developed in conjunction with TREAT Mark-II loop design and Fuel Element Failure Propagation loop design to estimate the validity of the projected capabilities required for larger loops.

c. Neutronic Needs

First surveys of neutronic needs were carried out using transport theory with the CDC-3600 computer. It is desirable at this point to change over to the ARC system on the IBM-360/50-75 to take advantage of ARC capabilities for large surveys. An unexpected reactivity difference has been found for the reference problem, however, and the changeover has been delayed pending its resolution. Some minor programming errors have been corrected.

B. TREAT Operations

1. Reactor Operations (J. F. Boland)

Last Reported: ANL-7553, p. 117 (Feb 1969).

Testing of the EBR-II fuel element with a previous burnup of 1.2% (see ANL-7553) continued. A sodium deposit on the capsule wall indicated that the cladding had failed during the fifth transient, but examination of the element with a telescope did not disclose any holes in the cladding. Further information on the results of this test will not be available until the high-speed motion-picture film is developed or the capsule is disassembled.

Three zirconium-clad powdered UO_2 fuel samples and three zirconium-clad pelleted UO_2 samples were subjected to transient irradiations in transparent capsules. These tests were run to obtain additional information on the modes of fuel failure and extent of metal-water reactions obtained with these types of fuel elements (see Progress Report for August 1968, ANL-7487, p. 110).

---

*Stone, J. P., et al., J. Chem. Eng. Data 11, 321 (1966).

Neutron radiographs were made of seven groups of experimental capsules from EBR-II.

The extensive core-loading changes required for various experiments result in certain fuel elements being transferred frequently between the reactor and storage. A plan to inspect these elements visually when radiation levels and program requirements permitted was recently initiated. During this reporting period a small puncture was detected in the fuel cladding near the bottom of a fuel element which was being transferred from storage to the reactor. This puncture was apparently caused by some sharp object being forced against the cladding during a fuel-handling operation. It is not clear, however, whether the reactor had been operated with this defective element in the core. Since this element had been in and out of the reactor many times in the past two years, an attempt was made to correlate reactor-cooling-system filter-radiation levels with the presence or absence of this element, but no correlation was found. This type of cladding failure has always been considered possible, and no significant safety hazards would be associated with operation of the reactor with a fuel element having such a defect. However, the defective element was returned to storage and will not be used in the reactor.

2. Development of Automatic Power Level Control System (J. F. Boland)

Last Reported: ANL-7548, p. 131 (Jan 1969).

The purchase order for the hydraulic control-rod-drive system was placed with MTR Systems Corporation; delivery is scheduled for September 1969. Specifications for the stored-program digital-controller equipment to program the hydraulic control-rod-drive system were sent to vendors, and bids are due by May 1, 1969.

C. Chemical Reaction--Research and Development--Chemical and Associated Energy Problems (Thermal)

1. Analysis of Loss-of-coolant Accidents (J. C. Hesson)

Last Reported: ANL-7527, pp. 134-135 (Dec 1968).

The work on analyses-of-coolant-accidents, which included calculational studies and simulation experiments, has been completed. The calculational studies resulted in the CHEMLOC-II computer program that was discussed previously (see Progress Report for December 1967, ANL-7403, pp. 152-156) and is described in a topical report.* The simulation experiments, which included steam oxidation and hydriding tests, also have been

*Hesson, J. C., Anderson, J. L., and Ivins, R. O., CHEMLOC-II: A Computer Program Describing the Core Heating and Cladding-Steam Reaction for a Water-cooled Power Reactor Following a Loss of Coolant, ANL-7361 (April 1968).

reported (see Progress Reports for September 1968, ANL-7500, pp. 131-133, and for December 1968, ANL-7527, pp. 134-135); a topical report on the experimental work is being prepared.

2. Pressure Generation due to Particle-Water Energy Transfer (R. O. Ivins)

a. Swinging-arm Heat-transfer Study

Last Reported: ANL-7500, pp. 133-135 (Sept 1968).

To analyze adequately the consequences of an accident in a water-cooled thermal reactor in which hot fuel materials are dispersed into the water coolant, knowledge is needed of the manner in which large amounts of energy are transferred from these particles to the coolant. Experiments are continuing to study the forced-convection transient heat transfer from spheres in water. In the experiments, heated silver, stainless steel, and platinum spheres are propelled through water at atmospheric pressure by means of a motor-driven swinging arm (see Progress Report for August 1967, ANL-7371, p. 111). The temperature of the sphere is monitored continuously by a thermocouple attached to the sphere through the arm. The rate of heat transfer from the sphere to water is calculated using the time-averaged bulk temperature of the sphere (the arithmetic average temperature before entering and after leaving the water).

Results for 1/2-in.- and 1/4-in.-dia silver spheres were reported previously (see Progress Reports for March 1968, ANL-7438, p. 132, for June 1968, ANL-7460, p. 128, and for September 1968, ANL-7500, p. 133). It has not been possible to obtain heat-transfer data at sphere temperatures above 900°C with silver and stainless steel because of the low melting point of silver and silver solder. Therefore, to extend the sphere temperature range, 1/4-in.-dia platinum spheres (m.p. ~1775°C) have been used. These spheres were mounted (welded) on 1/16-in.-dia platinum-sheathed tungsten-rhenium alloy thermocouples.

Tests were conducted at water temperatures of 23, 32, 45, 58, 70, and 85°C at sphere velocities of about 2.5, 5.4, and 10 ft/sec and at average sphere temperatures up to 1575°C. Figure IV.C.1 shows the results for water temperatures of 23 and 58°C. These tests with the platinum sphere show that, in the film-boiling region, the heat-transfer rates increase with increasing sphere velocities and decrease at increasing water temperatures. In the nucleate boiling region (sphere temperatures $< \sim 400$°C), the results agree with those obtained previously with silver spheres. Figure IV.C.1 indicates that, in water at 24°C, heat-transfer rates in the film-boiling region continue to decrease with increasing temperature at sphere velocities less than ~5 ft/sec. In the case of water at 58°C, this effect is observed at sphere velocities up to 10 ft/sec.

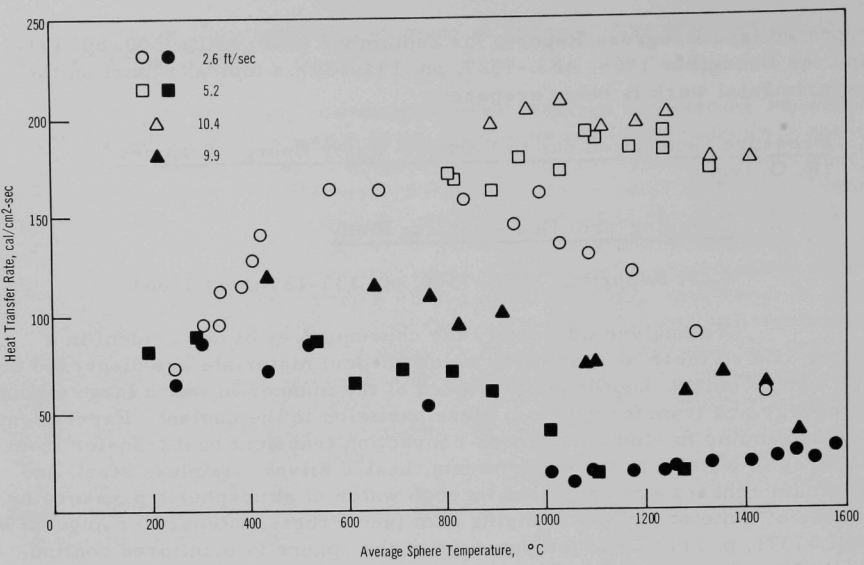

Fig. IV.C.1. Heat Flux from 1/4-in.-dia Platinum Sphere on Swinging Arm (straight-arm experiments). Open symbols are for water at 24°C; solid symbols are for water at 58°C.

D. Effluent Control--Research and Development--Gaseous Effluent Studies--Plutonium Volatility Safety

1. Filtration Studies (formerly Plutonium Hexafluoride Safety) (R. W. Kessie)

Last Reported: ANL-7527, pp. 138-139 (Dec 1968).

The volatility of PuF_6, combined with the high toxicity of plutonium, requires that a high degree of cleanup be provided for the off-gas from an enclosure in the event of an accidental release of PuF_6 in the enclosure. An experimental study to obtain data on the filtration of PuO_2F_2 aerosol by high-efficiency filters* has been completed. In the procedure used, a stream of PuF_6 was continuously mixed with air of controlled moisture content at ~25°C to form PuO_2F_2, and the aerosol was passed through one, two, or three 10-cm-dia filters in series for 1 hr.

The five independent variables of major significance in the study and their ranges are as follows: the three reactant gas partial pressures in the

*The individual filters were each pretested with a heterogeneous DOP aerosol. All filters had a DOP penetration between 1.4×10^{-4} and 2.7×10^{-4} at an air velocity through the medium of 2.5 cm/sec and a DOP penetration between 0.6×10^{-5} and 1.9×10^{-5} at a velocity of 0.75 cm/sec.

air mixture before reaction, p_{PuF_6} (1.56×10^{-4} to 2.105 Torr), p_{H_2O} (0.28 to 5.45 Torr), and p_{F_2} (9.36×10^{-7} to 34.8 Torr); the average reaction time t before filtration (1.98 to 225 sec); and the gas velocity v incident on the surface of the filter medium (0.248 to 2.52 cm/sec).

The total range of plutonium penetration (based on the quantity of PuF_6 introduced during the experiment) of high-efficiency filters in series for all 36 experiments is as follows:

	Plutonium Penetration		
No. of Filters	Minimum	Maximum	Maximum for $\frac{v p_{PuF_6}}{p_{H_2O}} < 0.1 \frac{cm}{sec}$
1	2×10^{-10}	2×10^{-1}	1×10^{-6}
2	1×10^{-12}	1×10^{-2}	6×10^{-10}
3	$<5 \times 10^{-14}$	3×10^{-11}	1×10^{-11}

The high maximum penetration of both the first and second filters is due to incomplete hydrolysis of PuF_6. The third filter has a very high effectiveness for removing plutonium despite small excesses of PuF_6 over H_2O. Penetration of both the first and second filters is most significantly affected by the value of $v p_{PuF_6} / p_{H_2O}$.

The major effects of the variables studied were determined by making an empirical correlation of the results to find functions that give the best fit to the experimental data while using the fewest number of arbitrary coefficients. The plutonium penetration of two filters in series, P_2, is best correlated by the following relation:

$$\ln P_2 = -23.45 - 2.81 \frac{p_{F_2} \ln p_{H_2O}}{t p_{H_2O}} - 0.264\, p_{PuF_6} (\ln p_{F_2})(\ln t)^2 v (\ln v).$$

The geometric standard deviation between the calculated values obtained from the above relation and the experimental values was 4. The experimental reproducibility was better than a factor of 4.

A much more complicated expression was found for the plutonium penetration of the first filter, but this did not correlate as well with results as did the relation for the first two filters, even though experimental reproducibility for penetration of the first filter was better than that for the first two filters. The incompleteness of the correlation indicates the complexity of the processes involved. Model studies may have to be used to obtain a more significant functional relationship.

PUBLICATIONS

The Ignition of Irradiated Uranium
D. F. Fischer and J. G. Schnizlein
J. Nucl. Mater. 28, 124-128 (1968)

Violently Sprayed Sodium-Air Reaction in an Enclosed Volume
T. S. Krolikowski
ANL-7472 (September 1968)

B